Spring 2012

Effect of side edge distance and concrete materials on corrosion in precast prestressed concrete panels

Dayi Zhang

Department:

EFFECT OF SIDE EDGE DISTANCE AND CONCRETE MATERIALS ON CORROSION IN PRECAST PRESTRESSED CONCRETE PANELS

by

DAYI ZHANG

A THESIS

Presented to the Faculty of the Graduate School of the

MISSOURI UNIVERSITY OF SCIENCE AND TECHNOLOGY

In Partial Fulfillment of the Requirements for the Degree

MASTER OF SCIENCE IN CIVIL ENGINEERING

2011

Approved by

Dr. Lesley Sneed, Advisor
Dr. Jeffery Volz
Dr. Roger LaBoube

ABSTRACT

This study involved the spalling problem found in some partial-depth precast prestressed bridge decks in the state of Missouri. Recently, panels of several bridges have exhibited corrosion of the prestressing steel tendons causing concrete spalling at the edges of panels. Some of the exposed tendons are corroded to the point of rupture. The effect of factors, namely concrete side edge distance and concrete material type, on steel corrosion in chloride-contaminated reinforced concrete was investigated in this study. Wet-dry cycle tests and accelerated corrosion tests were carried out on sixty-three specimens designed with three different side edge distances and three different concrete mixture types. Visual inspection and gravimetric study were performed on all test specimens. For specimens subjected to wet-dry cycle test, corrosion potential measurement, electrical resistivity measurement, and chloride content analysis were also conducted. For specimens subjected to accelerated corrosion test, time from corrosion initiation to corrosion cracking was used to verify the effectiveness of various models in predicting cracking time with low impressed current. Findings indicate that, for specimens of constant thickness, concrete deterioration and tendon corrosion decreased as the side edge distance increased. In addition, experimental results showed little difference in deterioration levels between specimens of concrete with fibers and the control specimens with normal concrete. Higher levels of deterioration were found in specimens with corrosion inhibitor compared to the control specimens with normal concrete.

ACKNOWLEDGEMENTS

I am very grateful to my advisor, Dr. Lesley Sneed, who gave me the opportunity to work on this research project and helped me through the completion my Master's degree. Her support and guidance played a very important role in the progress of my research and study.

In addition, I would like to thank the Missouri Department of Transportation (MoDOT) and the National University Transportation Center at Missouri S&T for providing funding for this study.

I would also like to thank my committee members, Dr. Volz and Dr. LaBoube, for all of their instruction and time and with this study.

In addition, I would like to extend my recognition to Dr. You, Dr. Belarbi, Issa Issa, Kandi Wieberg and Adam Morgan who assisted with my research.

Finally, I would like to give special thanks to my parents for their constant support and encouragement. Their belief in me was the motivation for all the work I did.

TABLE OF CONTENTS

LIST OF ILLUSTRATIONS

Page

LIST OF TABLES

Page

NOMENCLATURE

Symbol	Description
A	Surface area in cm^2
C	Cover to the reinforcement (mm)
D	Diameter of reinforcing bars (mm)
D’	The density of the corroding metal
ΔD	Change in diameter of the bar
E_c	Elastic modulus of concrete
E_{ef}	Effective elastic modulus of concrete that is equal to $E_c/(1+\phi_{cr})$
F	Faraday’s constant (96490 C/mol)
i	Current density ($\mu A/cm^2$)
i_{cor}	Corrosion rate (10^{-4} $g/cm^2/day$)
i_{corr}	Corrosion rate (mA/cm^2)
I	Corrosion current in A
j_r	Rate of rust production
K	Constant=8.76×10^7 for desired units of micrometres per year
Δm	Mass loss of steel (g)
M	Atomic mass of Fe (56g/mol)
S	Bar spacing
t_{cr}	Time from corrosion initiation to corrosion cracking
T	Time of exposure in s
T’	Time of exposure in hours
T_{cr}	Propagation period
T_0	Initiation period
W	Mass loss in grams
ρ_r	Density of steel
ρ_{st}	Density of rust products
ρ_{cor}	Function of the mass densities of steel and rust
ψ	Function of C, D, and δ_0 $\psi=(D+2\delta_0)/ 2C(C+D+2\delta_0)$
ϕ_{cr}	Concrete creep coefficient

ν	Poisson's ratio of concrete (0.18)
δ_0	Thickness of the porous zone

1. INTRODUCTION

Precast-prestressed concrete panels are very popular in bridge construction to accelerate the construction of concrete bridge decks. The Missouri Department of Transportation (MoDOT) has 10,335 structures in their bridge inventory, 1,712 of which consist of precast-prestressed 3.0-3.5 in. thick deck panels that serve as stay-in-place (SIP) formwork for a 5.0-5.5 in. thick cast-in-place (CIP) slab. The precast-prestressed concrete (PPC) panels also serve a structural entity in the bridge deck. Traditionally, these SIP panels are reinforced with low-relaxation, seven-wire steel prestressing strands oriented perpendicular to the traffic direction along with mild steel temperature reinforcement in the traffic direction.

Recently, some bridges with this PPC deck panel system in the MoDOT inventory have been observed to experience rusting of embedded steel reinforcement and concrete spalling. The plausible seasons for this spalling problem observed in those bridges in service likely include corrosion of the steel reinforcement in the panels due to use of deicing salts, permeability/cracking of the panels, and inadequate concrete cover. Corrosion of steel reinforcement can be detrimental since it can result in shorter life spans for the deck panels. This is explained in Chapter 2 of this thesis.

Since the use of SIP deck panels has proven to be a very cost-effective practice for concrete bridge deck construction in Missouri, it is motivated to investigate the corrosion problem of embedded steel prestressing reinforcement in concrete and study more durable alternatives for using these panels in new construction.

1.1. PARTIAL-DEPTH PRECAST PRESTRESSED CONCRETE PANELS AS STRUCTURAL FORMWORK FOR BRIDGE DECKS

Spalling problems associated with partial-depth precast concrete deck panels are the focus of this research study. Therefore, the main features of this system are described and discussed in detail in this section.

A type of bridge deck that is commonly used in Missouri during the past 30 years consists of a 3.0 to 3.5 in. thick precast-prestressed concrete panel performing as

formwork and that is composite with a cast-in-place toppping slab. The panels are placed adjacent to each other along the direction of traffic flow, and pretensioned strands located at mid-depth are oriented in the bridge transverse direction. The adjacent panels are not connected to one another at the transverse joints (perpendicular to the traffic direction). The prestressing strands in the panels serve as the bottom layer of reinforcement in the bridge deck which resists positive moment. Cast-in-place concrete deck (typically 4.5 in. thick) is placed on top of the SIP panels after panels are in place. The top layers of mild steel reinforcement are placed in the CIP panels for the negative moment regions. Mild reinforcement is also present in both the SIP panels and CIP topping in the longitudinal direction of the bridge to resist shrinkage and temperature stresses as well as negative moment in the bridge girder.

Wieberg (2010) concluded that “Based on the results from the first bridge inspections in St. Louis, spalling in the PPC panels is the result of the penetration of water and chlorides through the reflective cracking in the CIP topping, to the interface between the CIP topping and the PPC panels, then through the PPC panels to the prestressing tendons located near the panel joints”. According to this, effect of side edge distance was evaluated in this study.

1.2. PROBLEM DESCRIPTION

It was recently observed that some bridges within Missouri with the panel system described in Section 1.1 have experienced rustings of embedded steel reinforcement and concrete spalling issues at the bottom of panel joints. Fig 1.2 illustrates examples of the steel reinforcement rusting and concrete spalling observed. As shown in Fig 1.2, rusting of embedded steel tendon can be seen through the concrete cover. At the panel joint locations, reinforcement is exposed and ruptured at some locations due to the corrosion. Concrete spalling is also observed in the figure.

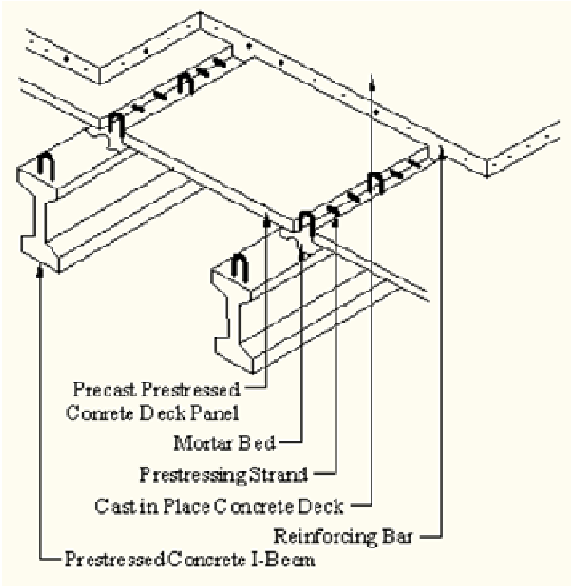

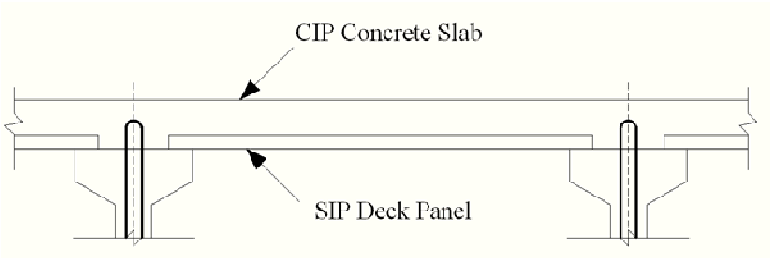

Figure 1.1. Typical partial-depth precast prestressed concrete deck panel (Sprinkel 1985)

Figure1.2. Spalled sections of concrete at various panel joints

1.3. SCOPE AND OBJECTIVES

The work included in this thesis is a portion the MTI/MoDOT Collaborative Structures Research program (2008-2010) Project 1B: Spalling Solution of Precast-Prestressed Bridge Decks. The objective of this thesis work was to evaluate the influence of side edge distance and concrete materials on the spalling behavior of the PPC panels. To achieve this objective, the scope of this thesis work included the following:

1. Literature review was conducted on the deterioration of steel in concrete and techniques to monitor corrosion (Chapter 2).
2. Experimental investigation was performed on sixty-three reinforced concrete specimens subjected to wet-dry cycle test and accelerated corrosion test to investigate the influence of various parameters on the specimen durability. Visual inspection, corrosion potential measurement, electrical resistivity measurement, chloride content analysis, and gravimetric study were conducted (Chapter 3).
3. For specimens subjected to wet-dry cycle test, analysis was made based on visual inspection, corrosion potential measurement, electrical resistivity measurement, chloride content analysis, and gravimetric study to evaluate the effect of different test variables on the possibility and degree of corrosion (Chapter 4).
4. For specimens subjected to accelerated corrosion test, time-to-corrosion cracking determined from visual inspection was compared with models from the literature to study the effectiveness of low impressed current technique in simulaing chloride induced corrosion of steel in reinforced concrete structures (Chapter 4).

2. BACKGROUND

As introduced in Chapter 1, partial-depth precasted-prestressed concrete bridge deck panels are widely used in bridge construction in Missouri. Recently, some bridges with this type of deck system have exhibited significant deterioration, including rust, cracks, and concrete spalling. To gain a better understanding of the entire deterioration process, extensive literature review was conducted and categorized in Sections 2.1 through 2.4. Section 2.1 discusses the mechanism of corrosion of reinforcing steel in concrete, as well as the function of different components in the electrochemical process. Section 2.2 describes various non-destructive techniques to monitor corrosion of steel in concrete, providing methods to evaluate the possibility, rate, and degree of the corrosion. Section 2.3 explains five models to predict the time to corrosion cracking, that can be used to predict the corrosion service life of reinforced concrete structures and to determine whether repair or rehabilitate is needed. Section 2.4 discusses alternate concrete materials investigated in this research in an attempt to improve the corrosion behavior of the concrete deck panels.

2.1. DETERIORATION OF STEEL IN CONCRETE

Corrosion of prestressing steel in prestressed concrete structures can lead to the loss of load-bearing capacity of structures through debonding between reinforcement and concrete, loss of reinforcement cross-section, cracking, and spalling of concrete. The partial-depth precast concrete bridge deck in Fig 1.2 shows the problems observed. The following sections describe the mechanism of electrochemical corrosion (Section 2.1.1), the passivity phenomenon (Section 2.1.2), electrolytic characteristics of concrete (Section 2.1.3), and the principles of steel corrosion in the concrete (Section 2.1.4).

2.1.1. Mechanism of Electrochemical Corrosion. It is generally accepted that the mechanism of steel reinforcing corrosion is electrochemical in nature (ACI 222R-01). The alkaline environment of concrete results in formation of a protective film of iron oxides at the steel-to-concrete interface to prevent corrosion of the steel reinforcement.

This passivity of the steel can be broken by carbonation or chloride attack (details are discussed in Sections 2.1.2 and 2.1.3). Thus, corrosion will start after the damage of the passive film as long as a basic corrosion cell is present. Expansive corrosion product (rust) is formed that occupies several times the volume of the original steel. The expansive corrosion products create tensile stress in the concrete surrounding the corroding steel bar that can result in cracking and spalling of the concrete.

In the electrochemical corrosion process, two reactions occur at the metal-liquid interface: the electron producing reaction, which is an anodic reaction (oxidation), and the electron consuming reaction, which is a cathodic reaction (reduction). For a basic corrosion cell, there are four essential components for a basic corrosion cell (Liu 1996) described in Sections 2.1.1.1 through 2.1.1.4.

2.1.1.1. Anode. The anode usually loses electrons from electrically neutral metal atoms to form discrete ions. The corrosion reaction of a metal M is usually expressed by the simplified equation: $M \rightarrow MZ^{+} + ze^{+}$. For iron, z equals two.

2.1.1.2. Cathode. The cathode reaction consumes the electrons produced by the anode process. There are two basic reactions at the cathode which depend on the pH of the solution:

$$pH < 7: 2H^{+} + 2e^{-} \rightarrow H_2 \quad (2.1)$$

$$pH > 7: 2H_2O + O_2 + 4e^{-} \rightarrow 4OH^{-} \quad (2.2)$$

2.1.1.3. Electrolyte. The electrolyte refers to the conductive solution in which cations move from anodic to cathodic regions and anions move in the opposite direction.

2.1.1.4. Electrical connection. The anode and cathode must be connected electrically to ensure current occurs.

2.1.2. Passivity. Passivity is the phenomenon in which insoluble corrosion product (e.g. rust) forms a protective film on the surface of the metal. Passivity can be divided into two types, which are chemical passivity and mechanical passivity. Chemical passivity is due to an invisible thin but dense and semiconducting oxide film on the metal surface, effecting electrode potential of the metal significantly. Mechanical passivity is

due to the precipitation of solid salts on the metal surface, effecting corrosion rate by porous and usually non-conducting salt layer.

The maintenance of passivity needs certain electrochemical environmental conditions (Liu 2006). Breakdown of the passive film will initiate the corrosion of the metal with the presence of a basic corrosion cell described in section 2.1.1. Passivity is usually destroyed by changes of the electrochemical environmental conditions or mechanical forces such as chloride ions.

2.1.3. Concrete as an Electrolyte. Generally, concrete of appropriate mixture proportion, compacting, and curing can provide an excellent protective environment for steel reinforcement. The physical protection is provided by the concrete cover blocking the access of aggressive species. Chemical protection is provided by concrete's high alkalinity solution due to the presence of sodium and potassium oxides in the pore structure of the cement paste matrix, as well as calcium hydroxide produced in the hydration reactions of cement components (Liu 1996).

The pH of concrete influences significantly the corrosion of steel in concrete. Generally, the lower the pH of concrete, the higher the probability of corrosion occurrence (Bhaskara 1987). For different pH values of concrete, the rate of corrosion occurrence changes as follows (Bhaskara 1987):

- $pH > 10$: no corrosion
- $4 < pH < 10$: corrosion rate is constant
- $pH < 4$: corrosion rate is rapid

The range of high pH values of typical concrete (12.5-13.5) lies within the pH domain in which insoluble oxides of iron are thermodynamically stable (Liu 1996). This leads to the passivity on the metal surface in which significant corrosion is hindered due to the formation of a protective surface film on the anode.

Unfortunately, due to the porous structure of concrete and existing microcracks, which are hard to avoid completely, the ingress of aggressive species occurs causing the breakdown of the passive film. The most common causes of passive film breakdown are incorporation of chloride ions in the film and neutralization of the pore solution by atmospheric carbonation (CO_2) (Liu 1996).

Carbonation can also reduce the pH of concrete (Klieger 1994). The reason is that carbon dioxide in the atmosphere participates in carbonation reaction which dissolves calcium hydroxide in the pore water. The carbonation reaction is a rather slow process, so the corrosion of steel reinforcement due to carbonation is normally observed only when the concrete cover is very thin, or when the concrete is of poor quality (Sorensen 1982).

Sections 2.1.3.1 through 2.1.3.3 describe properties of Portland cement concrete, concrete constituents, and water in the concrete that are relevant to the electrolytic behavior of concrete.

2.1.3.1. Portland cement concrete. Portland cement concrete is a very commonly used engineering material in the building construction industry. It is economical in terms of cost and less energy input than other materials in production, and it is convenient as well in terms of ready availability. Portland cement is the most widely used hydraulic cement, which primarily consists of hydraulic calcium silicates, aluminates, and ferroaluminates (Zemajtis 1998). Generally, the term aggregate refers to material of granular shape, such as sand, gravel, or crushed stone. Elements of portland cement concrete can be easily formed into a variety of shapes and sizes which feature excellent resistance to water and fire. Due to the much lower tensile strength of portland cement concrete compared with its compressive strength, about 10 percent, reinforcing steel is embedded to control cracking resulting from tensile stresses. Due to the properties of the material itself, creep and shrinkage are two factors that need to be taken into account during the design process.

2.1.3.2. Concrete constituents. Concrete is a highly heterogeneous and complex structure, that contains a heterogeneous distribution of different types and amounts of solid phases, pores, and microcracks (Mehta 1993). In addition, the structure of concrete is also subject to changes with time, environmental humidity, and temperature. Solid phase and pore systems are described in Section 2.1.3.2.1 and 2.1.3.2.2, respectively.

2.1.3.2.1. Solid phase. Solid phase refers to hydrated cement paste (HCP), aggregate, and transition zone - a layer between the aggregate and cement paste. The transition zone is about 20 μm thick and is more porous than the bulk paste. Among the solid components of concrete, the transition zone has the greatest contribution to concrete properties (e.g. strength, elastic modulus, and permeability). At early ages, ettringite and

calcium hydroxide are major constituent of the transition zone causing this layer weak and porous. After mineral admixtures are added into concrete, calcium hydroxide further reacts with the incorporated materials and forms calcium silicate hydrate (CSH), which increases zone thickness, makes it denser, and thus less permeable (Zemajtis 1998).

2.1.3.2.2. Pore system. The pore system in the HCP can be classified into four catagories depending on their sizes: entrapped air voids (1000 – 5000μm), entrained air voids (50-1000 μm), capillary voids (0.01-1μm), and interparticle spaces (0.001-0.003 μm).

The structure, pore size distribution and pore connectivity in the concrete cement phase determine the availability of oxygen and moisture at the steel surface, both of which are necessary for the maintenance of a passive film (Liu 1996). They also control the diffusion rate of chloride ion and carbon dioxide which, as mentioned in Section 2.1.1, are the two most deleterious factors in the corrosion of embedded steel in concrete. The typical sizes of both the solid phase and the voids contained in hydrated cement paste are shown in Figure 2.1 (Mehta 1993).

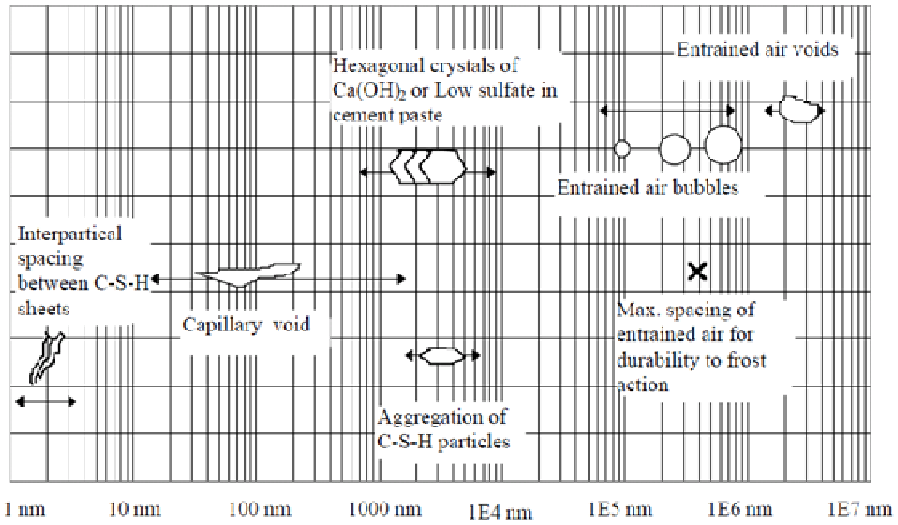

Figure 2.1. Dimensional range of solids and pores in a hydrated cement paste (Mehta 1993)

The size of interlayer space (gel pore) is too small to have an adverse affect on the permeability of the hydrated cement paste, and water in these small voids are held by hydrogen bonding. It is the capillary pore system that is the major cause of the diffusion and permeation processes, and therefore, the corrosion.

Pore size distribution depends primarily on the water-to-cement ratio (w/c) and on the degree of cement hydration. The mercury intrusion technique is used to test several hydrated cement paste specimens. Figure 2.2 shows the typical pore size distribution plots (Mehta 1980).

It is generally known that small pores, less than 50 nm, mainly effect drying shrinkage and creep. Large pores, greater than 50 nm, which develop with increasing w/c, can reduce concrete strength and increase permeability. It has been shown that for well-cured laboratory specimens with w/c greater than 0.5, the permeability of concrete will increase exponentially (Jones 1992).

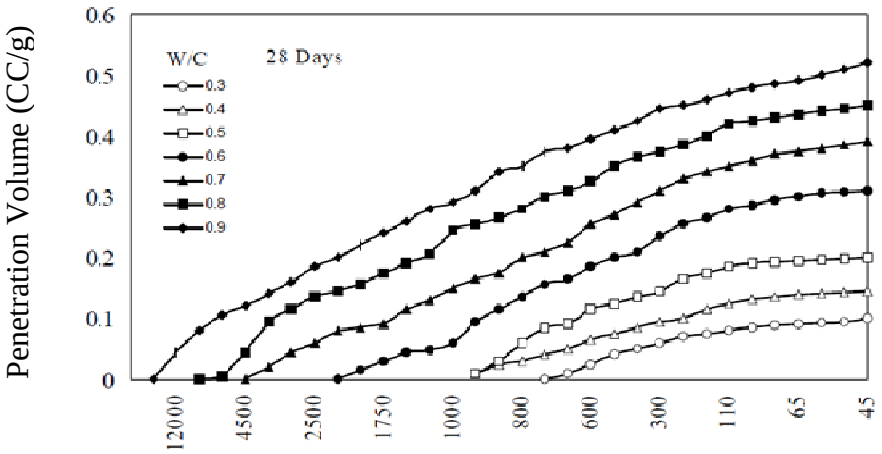

a. Different w/c at 28 days

Figure 2.2. Pore size distribution in hydrated cement pastes (Mehta 1980)

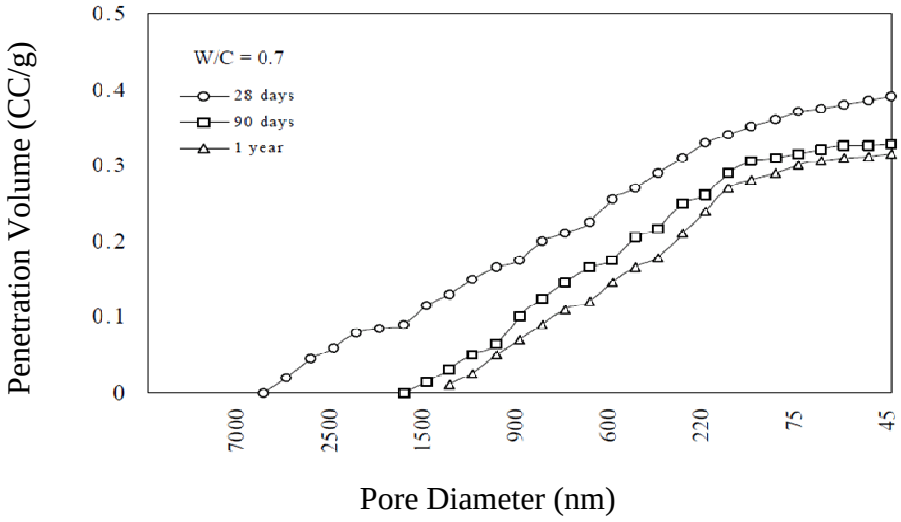

b. Different Ages with w/c=0.7

Figure 2.2. (Continued) Pore size distribution in hydrated cement pastes (Mehta 1980)

2.1.3.3. Water in the concrete. A large amount of water can exist in the hydrated cement paste, depending on the environmental humidity, porosity and pore size distribution of the hydrated cement paste. This water, or rather pore water solution in the hydrated cement paste, can be classified into different forms based on how difficult it can be removed from concrete. For the water in the hardened cement paste, it can exist in the following forms discussed in Section 2.1.3.3.1 through 2.1.3.3.4. Transportation of water in concrete is discussed in Section 2.1.3.3.5.

2.1.3.3.1. Capillary water. The capillary water refers to water existing in capillaries 5 nm in diameter or larger.

2.1.3.3.2. Adsorbed water. Absorbed water exists close to the solid surface and is positioned by attractive forces. Most portion of adsorbed water will be lost when the paste is dried to about 30% relative humidity. Depending on the surface energy of the solid, water adsorption is not limited to a mono-layer adsorption model, but follows a multilayer model.

2.1.3.3.3. Interlayer water. Interlayer is a monomolecular water layer that is laid between the layers of calcium silicate hydrate structure which is held by hydrogen bonding. This water is lost only with very strong drying (i.e. below 11% relative humidity).

2.1.3.3.4. Chemically combined water. Chemically combined water exists as a part of the cement hydration products in the form of hydrates and is not lost with drying.

2.1.3.3.5. Transport of water in concrete. Permeability can be defined as the ease with which a gas or fluid can flow through a solid. For concrete, permeability is directly determined by the continuity of the pore system (Section 2.1.3.2.2).

The concrete porous structure system filled with air and pore water solution allows the ingress for deleterious substances and an electrolyte. The water movement is determined by cracking and the HCP properties in mature concrete. Although aggregate is usually less permeable than HCP, its presence in concrete generates low density transition zones which makes concrete more permeable. Furthermore, the movement of water in HCP also depends on changes in pore structure resulting from continued hydration, as well as changing solubility of its constituents. The analysis of mechanisms of mass transfer in concrete is very complicated because of the complexity of concrete pore structure, variation in mixture proportioning and curing, or continued hydration (Klieger 1994).

2.1.4. Principles of Steel Corrosion in Concrete. Corrosion of steel in concrete is an electrochemical process as discussed in Section 2.1.1. The corroding system consists of an anode in which steel is corroded, a cathode (graphite rods in the case of this study as discussed in Chapter 3), an electrolyte (e.g. 5% sodium chloride solution), and an electrical conductor as connector. The potential difference between anode and cathode is the driving electrical force for steel corrosion. (In the case of this study, a power supply enlarges the potential as discussed in Section 3.4.2.)

As the passive film is degraded by chloride ions attacks or carbonation, the metallic Fe at the anode is oxidized to ferrous ions Fe^{2+} as shown in Eq 2.3:

$$Fe \rightarrow Fe^{2+} + 2e^{-} \qquad (2.3)$$

The electrons released by anode are transferred to the cathodic area. Reduction reaction occurs on cathode as indicated in Eq 2.4:

$$O_2+2H_2O+4\ e^- \rightarrow 4OH^- \quad (2.4)$$

Figure 2.3 illustrates the reaction on anode and cathode reflected by the Eq. 2.3 and Eq. 2.4.

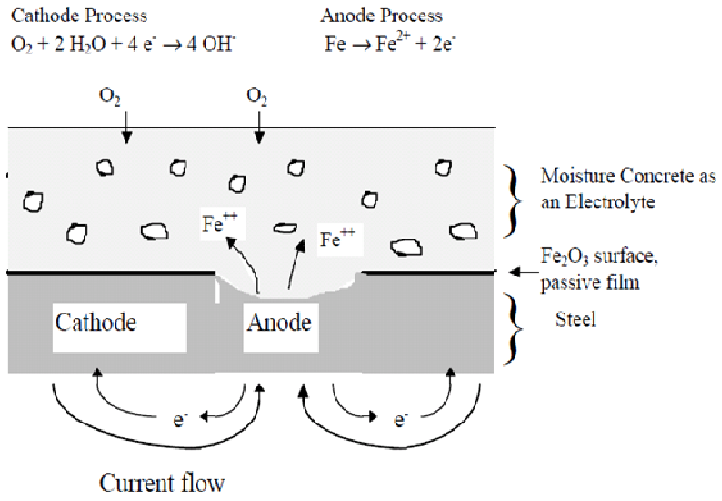

Figure 2.3. Mechanism of corrosion of steel in concrete
(Mehta 1993)

The hydroxyl ions OH^- that arrive at the anodic area electrically neutralize the Fe^{2+} ions to generate ferrous hydroxide which dissolves in pore water to form solution of ferrous hydroxide (Bazant 1979) shown in Eq 2.5:

$$\text{Anode: } Fe^{2+} + 2OH^- \rightarrow Fe(OH)_2 \quad (2.5)$$

The product ferrous hydroxide further reacts with available oxygen and water and forms water insoluble red rust as indicated in Eq 2.6:

$$\text{Anode: } 4Fe(OH)_2 + O_2 + 2H_2O \rightarrow 4Fe(OH)_3 \quad (2.6)$$

Red rust is not the only product of corrosion of steel in concrete. Other products include compounds such as black rust, Fe_3O_4, green rust, $FeCl_2$, and other ferric and ferrous oxides, hydroxides, chlorides, and hydrates. Several factors contribute to their

composition such as availability of pore water, pH and composition of the solution, and oxygen supply.

Corrosion products are deleterious to concrete because they occupy much larger volume than the steel bar. The black rust volume is twice as large as that of steel, and red rust volume is four times as large (Bazant 1979). The increase in volume causes tensile stresses in surrounding concrete which can cause cracking and spalling of the cover concrete.

As the concentration of solution increases, ferrous corrosion products form an acid solution with chlorides which further enhances corrosion by neutralizing the alkaline concrete environment. In addition, ferrous chloride, which are more soluble than the oxides, move away from the reinforcing steel and expose new surface areas to the corrosive environment.

2.2. CORROSION MONITORING TECHNIQUES

Corrosion of steel embedded in concrete cannot be visually observed until the deterioration causes external signs such as rust, cracks, or spalling. In order to predict the corrosion service life of reinforced concrete structures and to determine whether it is needed to repair or rehabilitate the concrete element, it is necessary to use non-destructive techniques to evaluate the corrosion level or to measure the corrosion rate of the reinforcement.

Due to the special electrolytic characteristics of concrete structures, it is difficult to develop corrosion monitoring devices applied to the reinforced structures for accurate assessment (Liu 1996). However, there are several electrochemical techniques that can be used to monitor corrosion of steel in concrete successfully, such as corrosion potential (Section 2.2.1) and linear polarization techniques (Section 2.2.2). In addition, chloride content measurement techniques (Section 2.2.3) and gravimetric techniques (Section 2.2.4) are two effective methods to evaluate the corrosion damage and corrosion rate, respectively.

2.2.1. Corrosion Potential. As described in Section 2.1.1, corrosion is an electrochemical process. Electrical potential is generated by the process of corrosion, and

the half-cell provides a method of measuring these electrical potentials. The method and equipment are explained and illustrated in ASTM C 876-09. The measurement of the free corrosion potential of the reinforcement can determine the voltage difference between the steel and reference electrode in contact with the concrete, which is shown by Figures 2.4 and 2.5.

Guidance on interpretation of half-cell results and the relationship to potential for corrosion from half-cell surveys is given in ASTM C 876-09 and is summarized in Table 2.1. As can be seen, the more negative the reading, the greater the probability of corrosion.

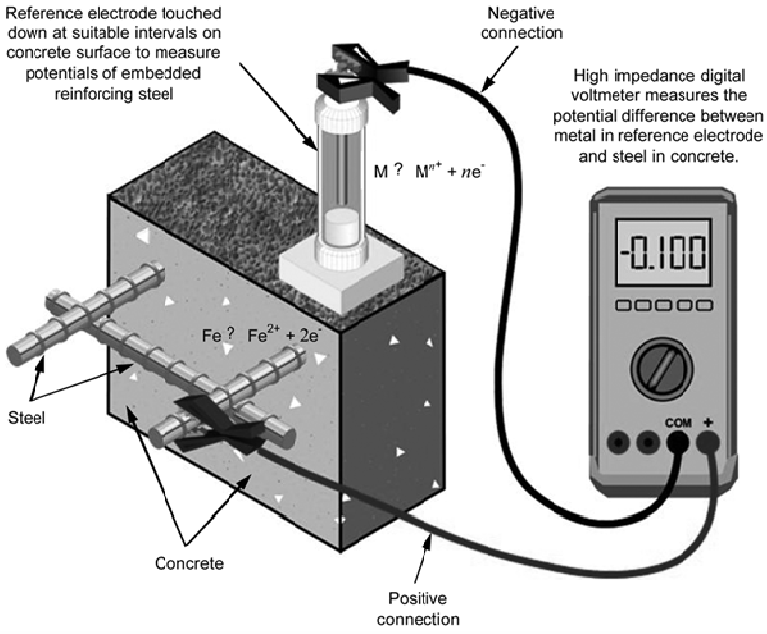

Figure 2.4. Reference electrode circuitry (ASTM C 876-09)

2.2.2. Linear Polarization Technique. The linear polarization technique is a non-destructive method for assessing the instantaneous corrosion current density. It has been widely used in monitoring corrosion of laboratory specimens, as well as field structures (Zemajtis 1998). The name linear polarization refers to the linear regions of the

polarization curve (current vs. potential curve), in which slight changes in current applied to corroding metal in an ionic solution can cause corresponding changes in the potential of the metal.

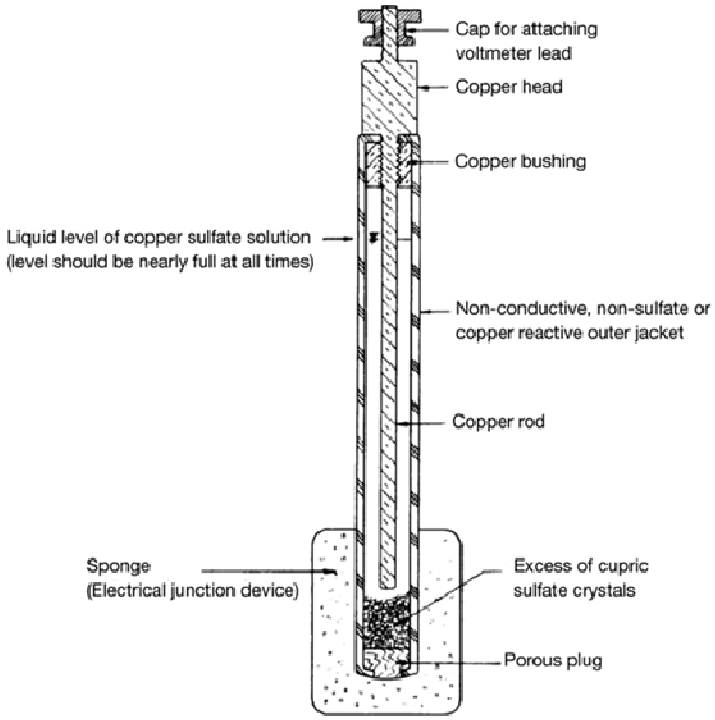

Figure 2.5. Copper-copper sulfate half cell circuitry (ASTM C 876-09)

Table 2.1. Interpretation from results from half-cell potential surveys (according to ASTM C876-09)

E_{corr} (Cu/ $CuSO_4$)	Probability of corrosion
>-0.20V	Greater than 90% probability of no corrosion
-0.35 to -0.20 V	Corrosion activity uncertain
<-0.35V	Greater than 90% probability of active corrosion

Stern and Geary showed that for a simple corroding system, a few millivolts around the corrosion potential, the polarization curve may be considered quasi-linear (Stern and Geary 1957). Corrosion current density is directly proportional to the instantaneous rate of metal loss. Usually, the corrosion current density is referred to as the corrosion rate.

3LP is one of the most common devices, which are based on the linear polarization method, to determine the corrosion rate of steel in concrete. This device is shown in Figure 2.6.

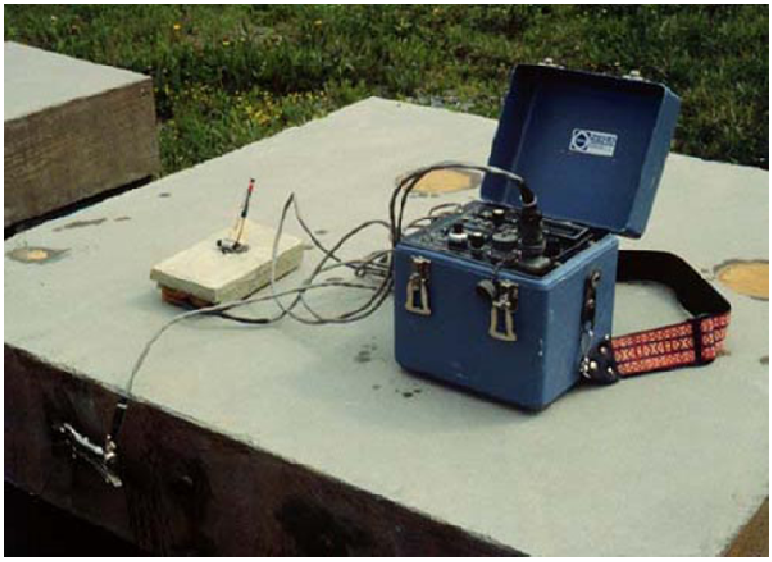

Figure 2.6. 3LP device (Zemajtis 1998)

The name “3LP” refers to “three electrode linear polarization” technique. The three electrodes are: counter, working, and reference electrodes. The counter electrode applies a cathodic current to the steel reinforcement, which is called the working electrode. A third electrode, the reference electrode, monitors the corresponding change in potential of steel/concrete surface due to applied current. Given the Stern-Geary relationship, corrosion current can be determined. Then the corrosion current density or

corrosion rate can be estimated by dividing the current by the area of steel that was polarized.

Corrosion current density measurements are very susceptible to several variable field conditions including concrete temperature, moisture, and oxygen content. The manufacturer's interpretation of measured corrosion current density, corrosion rate, using the 3LP device is given in Table 2.2.

Table 2.2. Manufacturer's data interpretation for the 3LP device (Zemajtis 1998)

i_{corr}	Interpretation
<0.21 mA/cm^2	No damage expected
0.21-1.07 mA/cm^2	Damage possible in 10-15 years
1.07-10.07 mA/cm^2	Damage possible in 2-10 years
> 10.7 mA/cm^2	Damage possible in less than 2 years

2.2.3. Chloride Content Measurement Techniques. Measuring the chloride content of the concrete at the depth of reinforcement is another method to estimate the potential of corrosion damage induced by chloride. ASTM C 1218-08 provides a standard test method for water-soluble chloride in mortar and concrete. ASTM C 1152-04 presents a standard test method for acid-soluble chloride in mortar and concrete.

The chloride content can be expressed in terms of percent chloride by the mass of cement weight (% in weight of cement) or in terms of pounds of chloride per cubic yard of concrete (kilogram of chloride per cubic meter of concrete). The results of chloride content may be used to determine whether the level of chloride ions of a site is high enough to initiate corrosion of the reinforcement. If above the corrosion threshold value, the higher the chloride ion concentration, the greater the active corrosion (Clear 1989). Table 2.3 provides guidelines for interpretation of chloride content measurements (Newhouse 1993).

Table 2.3. Recommended action for chloride content measurements (Newhouse 1993)

Chloride Concentration	Recommendation
<0.59 kg/m^3	Leave intact
0.59-1.19 kg/m^3	Questionable area
> 1.19 kg/m^3	Remove concrete below bar level or replace entire section

Samples for measuring chloride concentration are collected as pulverized concrete at several average depths. Evaluating the chloride content at different depths provides important information for the chloride amount required to initiate corrosion. The collection apparatus used is an impact drill with 29 mm (1-1/8 in) hollow diameter bit, 2.3 times the maximum aggregate size, connected to a vacuum collection unit (Cady and Gannon 1992). Figure 2.7 shows such a setup with a portable power generator for the vacuum and the drill operation.

Figure 2.7. Sampling for chloride concentrations – collection apparatus: impact drill with hollow drill bit, powder concrete collection unit, and vacuum (Zemajtis 1998)

Figure 2.8. Powder concrete collection unit (Zemajtis 1998)

2.2.4. Gravimetric Study. Gravimetric technique is a destructive method to obtain the corrosion rate. Reinforcement bar should be weighed before and after being introduced in the concrete specimens. Detailed descriptions on preparing, cleaning and evaluating the specimens are well documented in ASTM G 1-03.

The average corrosion rate can be obtained as an expression of the loss of steel mass (gravimetric loss) as shown in Eq 2.7:

$$\text{Corrosion rate} = (K \times W) / (A \times T' \times D') \qquad (2.7)$$

In Eq 2.7, K is a constant=8.76×10^7 for desired units of micrometres per year (see ASTM G1-03 for more values for different corrosion rate units desired), W is mass loss in grams, A is the surface area in cm^2, T' is time of exposure in hours, and D is the density of the corroding metal (D'=7.86 g/cm^3 for carbon steel). Instantaneous corrosion rates cannot be measured by this technique, but only a mean value during the period of test.

Although this method is very time-consuming and only applicable to laboratory studies, it is a useful tool and accurate method to quantify corrosion attack on specimens in laboratory experiments (Liu 1996).

2.3. MODELS TO ESTIMATE TIME FROM CORROSION INITIATION TO CONCRETE CRACKING

Prediction of time to corrosion cracking is a key element in evaluating the service life of corroding reinforced concrete, because the end of functional service life is often defined by appearance of the first corrosion crack where rehabilitation of a corroding structural element is required (EI Maaddawy and Soudki 2007). Sections 2.3.1 through 2.3.4 describe four models for prediction of time from corrosion initiation to corrosion cracking. In addition, based on those four models, Section 2.3.5 explains a modified model for a more accurate prediction of time to corrosion cracking.

2.3.1. Bazant's Mathematical Models. Bazant proposed a simplified analytical model to estimate the time to corrosion cracking of concrete cover (Bazant 1979). Basic assumptions are included as follows: 1) penetration of oxygen and chloride ions through concrete cover is quasi-stationary and one dimensional; 2) steady-state of corrosion producing expansive rust layer begins at the time of depassivation; 3) the model is based on red rust which has the most significant influence for cracking concrete, assuming that $\rho_r=\rho_{st}/4$, where ρ_r and ρ_{st} are the density of rust products and steel, respectively.

Bazant's model expression for time to corrosion cracking is shown by Eq. 2.8:

$$t_{cr} = \rho_{cor}\frac{D\cdot\Delta D}{S\cdot j_r} \tag{2.8}$$

In Eq 2.8, S is the bar spacing, D is the diameter of the bar, ΔD is the change in diameter of the bar, j_r is the rate of rust production, and ρ_{cor} is a function of the mass densities of steel and rust, $\rho_{cor} =[(1/\rho_r) - (0.523/\rho_{st})]^{-1}\pi/2$.

According to Bazant's models, the time from corrosion initiation to cracking is a function of corrosion rate, cover depth, spacing, and certain mechanical properties of concrete such as tensile strength, modulus of elasticity, Poisson's ratio, and creep coefficient. A sensitivity analysis of Bazant's theoretical equations demonstrates that for those parameters, corrosion rate is the most significant parameter in determining the time to cracking of the cover concrete (Liu 1996).

Bazant's model, however, has never been consistent well with experimental and field results (Liu 1996). In addition, Bazant's model assumes that all corrosion products contribute to pressure on the surrounding concrete which would underestimate the time to

corrosion cracking since some of them fill the porous zone or move away from the steel-to-concrete interface (EI Maaddawy and Soudki 2007).

2.3.2. Tuutti's Model. According to Tuutti's conceptual model (Tuutti 1980), the service life of corroded reinforced concrete structures can be divided into two stages. As shown by Figure 2.9, the first is initiation period T_0 which corresponds the time required for CO_2 or Cl^- to penetrate to the steel-to-concrete interface and start the corrosion. The second stage is the propagation period, T_{cr}, which represents the time between corrosion initiation and corrosion cracking.

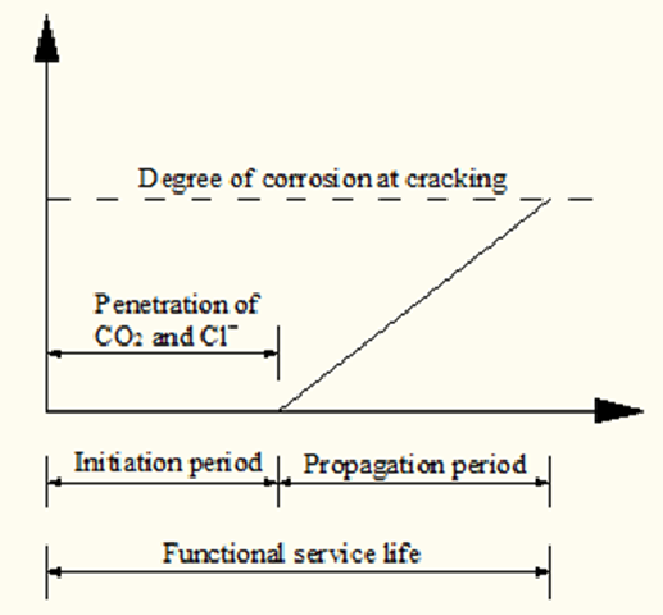

Figure 2.9. Service life model of corroded structures (Tuutti 1980)

Researchers concluded that Tuutti's model underestimates the time to corrosion cracking compared with times obtained from field and laboratory observations because it includes the same assumption as Bazant's model (Section 2.3.1) that all corrosion products create expansive pressure on the concrete.

2.3.3. Cady-Weyers' Deterioration Model. Cady and Weyers proposed their deterioration model (Cady and Weyers 1984) to estimate the service life of concrete bridge components in salt-induced corrosive environment. As illustrated in Figure 2.10,

three distinct phases are taken into account in the model: diffusion, corrosion and deterioration. The first phase, diffusion, represents the time for chloride ions to penetrate the concrete cover and to initiatite corrosion. The second phase, corrosion, describes the time from initiation of corrosion to first cracking of the concrete cover. The third phase, deterioration, is defined as the time for corrosion damage to a certain level for necessary repair or rehabilitation.

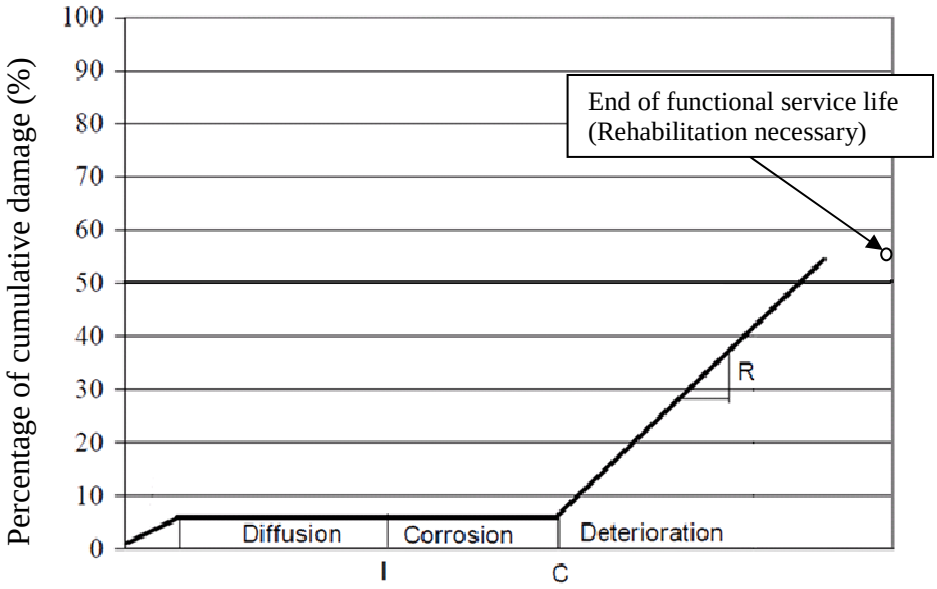

Figure 2.10. Cady-Weyers' corrosion-deterioration model for concrete bridge (adapted from Cady and Weyers 1984)

The corrosion rate is the key to predicting the time to cracking. The corrosion rate is mainly controlled by the rate of oxygen diffusion to the cathode, resistivity of the pore solution, and temperature (Liu 1996).

2.3.4. Morinaga's Empirical Equation. Morinaga proposed an empirical equation based on field and laboratory data to calculate the time from corrosion initiation to corrosion cracking (Morinaga 1988). Assuming that cracking of concrete will first

occur when there is a certain quantity of corrosion products forming on the reinforcement, the equation is shown in Eq 2.9:

$$\mathbf{t_{cr}} = \frac{\mathbf{0.602D(1+\frac{2C}{D})^{0.85}}}{\mathbf{i_{cor}}} \quad (2.9)$$

In Eq. 2.9, t_{cr} is the time from corrosion initiation to corrosion cracking (days), i_{cor} is the corrosion rate (10^{-4} g/cm^2/day), C is the cover to the reinforcement (mm), and D is the diameter of reinforcing bar (mm).

Morinaga's empirical equation does not consider the mechanical properties of concrete which would be influential (EI Maaddawy and Soudki 2007).

2.3.5. Modified Model by EI Maaddawy and Soudki. After anyalyzing and considering the primary deficiencies of previous models described by Sections 2.3.1 through 2.3.4, EI Maaddawy and Soudki proposed a modified model to predict time from corrosion initiation to corrosion cracking. The accuracy of the model was validated by experimental data (EI Maaddawy and Soudki 2007). For this modified model, the concrete around a corroding steel reinforcing bar is assumed to be a thick-walled cylinder with a wall thickness equal to the thinnest concrete cover, and it is assumed that the concrete around a corroding steel reinforcing cracks when the tensile stresses in the circumstantial direction at every part of the ring reaches the tensile strength of the concrete (EI Maaddawy and Soudki 2007).

Figure 2.11 shows the modified service life model. Propagation period T_{cr} is divided into two different periods. The first is free expansion period T_{free} which represents the time for corrosion products to fell the porous zone around the corroding steel bar. The second period encompasses the time in which the stress increases.

Faraday's law can be used to predict the actual steel mass loss at certain current density.

$$\Delta\mathbf{m} = \frac{\mathbf{MIT}}{\mathbf{zF}} \quad (2.10)$$

In Eq. 2.10, Δm is the mass loss of steel (g), M is the atomic mass of Fe (56 g/mol), I is the corrosion current (A), T is the time (s), F is Faraday's constant (96490 C/mol), and z is the valence (Fe=2).

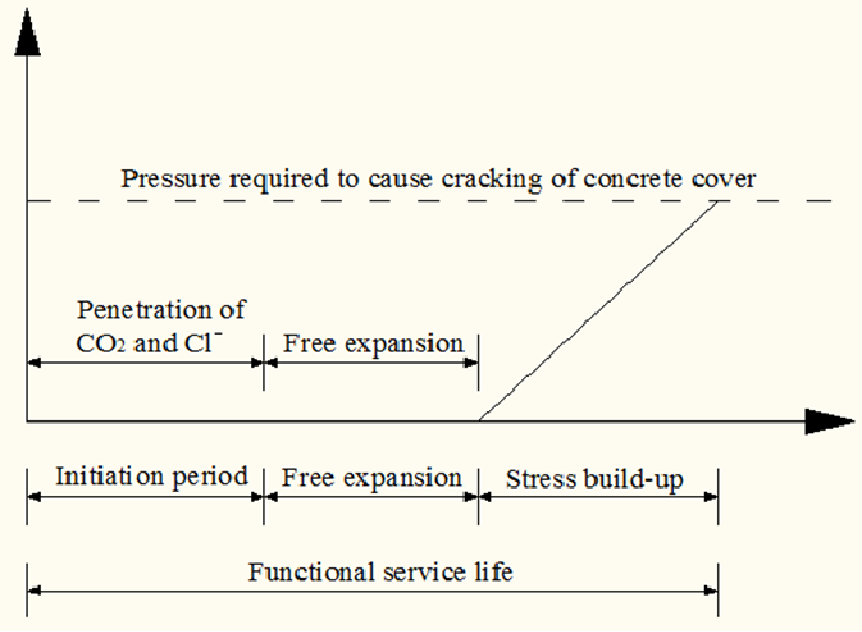

Figure 2.11. Modified service life model (EI Maaddawy and Soudki 2007)

Combined with other expressions (EI Maaddawy and Soudki, 2007) results in the final equation as shown in Eq 2.11 which gives the time from corrosion initiation to corrosion cracking T_{cr}:

$$T_{cr} = \left[\frac{7117.5(D+2\delta_0)(1+\nu+\psi)}{iE_{ef}}\right] + \left[\frac{2Cf_{cf}}{D} + \frac{2C\delta_0 E_{ef}}{(1+\nu+\psi)(D+2\delta_0)}\right] \quad (2.11)$$

In Eq.2.11, C is the thinnest concrete cover, D is the diameter of the steel reinforcing bar (mm), $\psi=(D+2\delta_0)/2C(C+D+2\delta_0)$, E_{ef} is the effective elastic modulus of concrete that is equal to $E_c/(1+\phi_{cr})$, E_c is the elastic modulus of concrete, ϕ_{cr} is the concrete creep coefficient (2.35 as per the CSA Standard A23.3-94), ν is Poisson's ratio of concrete (0.18), and i is the current density ($\mu A/cm^2$).

The thickness of the porous zone δ_0 is usually between 10 μm and 20 μm (Thoft-Christensen 2000). So the lower and upper bonds for the time from corrosion initiation to corrosion cracking will be approximated with δ_0 equal to 10 μm and 20 μm, respectively (EI Maaddawy and Soudki 2007).

2.4. ALTERNATE CONCRETE MATERIALS

Various alternate concrete materials have been developed to improve the performance of conventional concrete in terms of durability. Corrosion inhibiting admixture and fiber-reinforced concrete (FRC) are two types of materials used in this experimental study as discussed in Chapter 3. These materials are described in Sections 2.4.1 and 2.4.2, respectively.

2.4.1. Corrosion Inhibitor Admixtures. Corrosion inhibitor admixtures are widely used to reduce corrosion rate of reinforcing steel in concrete. The principle of corrosion inhibitors is based on the mutual dependence of anodic and cathodic reactions, which states that corrosion can be retarded by reducing the corrosion rate of only one of the half-cell reactions.

The corrosion inhibiting reaction is affected by many factors, including solubility, precipitation, dispersion, chloride to inhibitor ratio (anodic inhibitors only), chemical composition of cement, curing conditions, molecular structure, pH of pore solution and temperature (Mehta 1984). The effectiveness, or corrosion inhibition efficiency, of a corrosion inhibitor is influenced by many factors, including but not limited to: fluid composition, quantity of water, and flow regime.

Types of inhibitors are: anodic, cathodic, and mixed which are discussed in Sections 2.4.1.1 through 2.4.1.3.

2.4.1.1. Anodic inhibitor. Anodic inhibitors keep reacting with the corrosion products (e.g. rust) and form passive film on the surface of steel reinforcement until all the surface of reinforcement is covered. Thus, the reaction on the anode expressed by Eq. 2.3 can be retarded. Effective inhibition can be provided only when the quantity of the inhibitor is sufficient. Therefore, anodic inhibitors are said to be “dangerous” because when used in not enough quantity, they may cause the corrosion rate to increase (Zemajtis 1998).

2.4.1.2. Cathodic inhibitor. Cathodic inhibitors delay the cathodic reaction (see Eq. 2.1 and Eq 2.2) by reacting with the hydroxyl ions to precipitate insoluble compounds on the cathode site so the access of oxygen can be prevented. In contrast, cathodic inhibitors are said to be “safe” because the active cathode area is reduced regardless of the quantity of inhibitor used.

2.4.1.3. Mixed inhibitor. Mixed inhibitor also effects the corrosion by formation of a passivation layer on the surface of the material which prevents access of the corrosive species to the metal, excluding either the oxidation or reduction part of the corrosion system, or scavenging the dissolved oxygen.

2.4.2. Fiber-Reinforced Concrete (FRC). Fiber reinforced concrete (FRC) is concrete containing fibrous material that increases its structural integrity and enhances mechanical properties. FRC contains short discrete fibers that are uniformly distributed and randomly oriented. A thin and short fiber (short hair-shaped glass fiber for instance) can reduce cracking effectively while the concrete stiffens during the first hours after placing the concrete, but it cannot increase the concrete tensile strength. However, a larger size fiber (for example, 1 mm diameter and 45 mm length) can also increase the concrete tensile strength when the modulus of elasticity of the fiber is higher than the matrix (concrete or mortar binder). Thus, geometry of fiber such as shape, dimension, and length is a very important factor to influence the mechanical properties of FRC. The adoption of FRC to precast-prestressed panels can be an alternative way to make a corrosion-resistant system. Some research has indicated that using fibers has limited impact, abrasion, brittle, and shatter resistance in concrete.

Fibers types include steel, glass, synthetic, and natural materials. Table 2.3 shows the mechanical properties of some fiber types that may be used in FRC (ACI 549.2R 2004).

The fiber type used this study is synthetic fiber (see Section 3.2.2.3). Synthetic fibers specifically engineered for concrete are manufactured from man-made material that can withstand the long-term alkaline environment of concrete. Synthetic fibers are added before or during the mixing of concrete. Synthetic fibers benefit the concrete in both the plastic and hardened state. Synthetic fibers can reduce plastic settlement cracks, reduce platic shrinkage cracks, lowered permeability, increase impact and abrasion resistance, and provide impact shatter resistance (NRMCA 1994).

The mechanical blocking action of synthetic fibers can inhibit the growth of micro shrinkage cracks at early age, when stress exceeds the strength of the concrete at a specific time due to volume changes in concrete. The uniform distribution of fibers

throughout the concrete discourages the development of large capillaries by lowering the permeability of water migration (NRMCA 1994).

Due to the property of synthetic fibers to enhance the overall integrity of the concrete structure, the early age concrete benefits of synthetic fibers continue to contribute to the hardened concrete by reducing the permeability and increasing the resistance to shattering abrasion and impact forces (NRMCA 1994).

Table 2.4. Mechanical properties of various fibers (ACI 549.2R 2004)

	Tensile strength (MPa)	Modulus of elasticity (GPa)	Tensile strain (%) (max-min)	Fiber diameter (mm)	Adhesion to matrix (relative)	Alkali resistance (relative)
Asbestos	600-3600	69-150	0.3-0.1	0.02-30	Excellence	Excellent
Carbon	590-1800	28-520	2-<1	7-18	Poor to good	Excellent
Aramid	2700	62-130	4-3	11-12	Fair	Good
Polypropylene	200-700	0.5-9.8	15-10	10-150	Poor to good	Excellent
Polyamide	700-1000	3.9-6	15	10-50	Good	No
Polyester	800-1300	Up to 1.5	20-8	10-50	Fair	No
Rayon	450-1100	Up to 11	15-7	10-50	Good	Fair
Polyvinyl alcobol	1150-1470	21-36	15	4-14	Good	Good
Polyacrylonitrile	850-1000	17-18	9	19	Good	Good
Polvethvlene	400	2-4	400-100	40		Excellent
Polyethylene pulp						
Oriented	-	-	-	1-20	Good	Excellent
Carbon steel	3000	200	2-1	50-85	Excellent	Excellent
Stainless steel	3000	200	2-1	50-85	Excellent	Excellent
AR glass	1700	72	2	12-20	Excellent	Good

3. EXPERIMENTS

3.1. OBJECTIVE

As discussed in Chapter 2, chloride induced corrosion of reinforcing steel is the primary cause for deterioration of concrete in bridge decks. For the bridges investigated in this research, the use of deicing salt was suspected to be the main source of chlorides necessary for the corrosion to take place. Figure 3.1 illustrates the three phase corrosion phases involved. The 1st phase, diffusion, is defined as the period for chloride ions or carbonation to penetrate through the concrete cover to the steel reinforcement surface to initiate corrosion. The 2nd phase, corrosion, describes the time from corrosion initiation to first cracking of corrosion cover. Prediction of this time to corrosion cracking is important for evaluating the service life of corroding reinforced concrete structures, since the appearance of the first corrosion cracking is a key sign marking the end of the functional service life where repair or rehabilitation is required. The 3rd phase, deterioration, is defined as the time for the corrosion damage to reach a certain level, in this case, concrete spalling.

As described in Chapter 1, this study was aimed at investigating ways to reduce the corrosion-induced spalling of PPC panels in new construction. In order to investigate the effects of potentially significant variables on the three phases of the corrosion process, experimental tests including wet-dry cycle tests and accelerated corrosion tests were designed and carried out. This chapter describes the experiments performed including the test variables, test specimen construction, and test methods. Results are presented and analyzed in Chapter 4.

3.2. TEST VARIABLES

The goal of the experiments conducted was to investigate the effects of the parameters considered, including side edge distance to reinforcement and concrete admixture, on the process of corrosion initiation, and time from corrosion initiation to corrosion cracking.

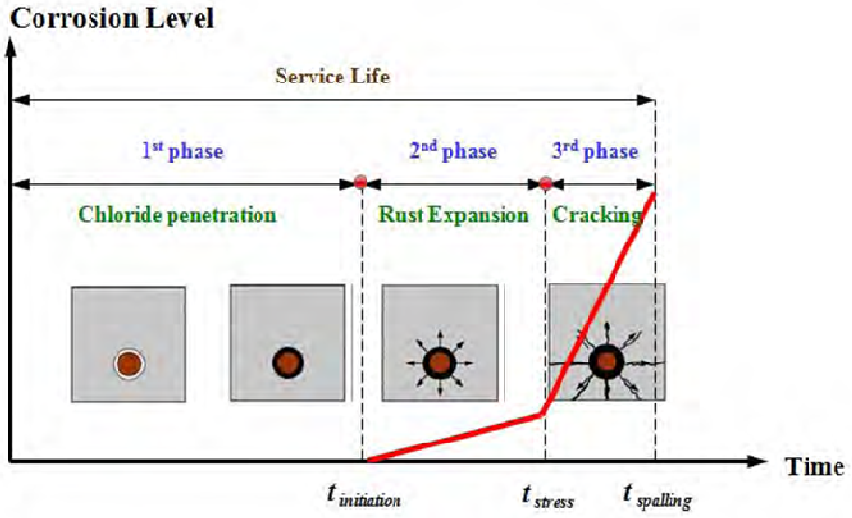

Figure 3.1. Corrosion process as a function of time (Sneed et al 2010)

Table 3.1. Specimen ID for wet-dry cycle test specimens

Side cover	**Concrete type + 0% NaCl**		
	Normal concrete	Corrosion inhibitor	FRC
	Designation	Designation	Designation
1.5 in.	SP1-NC-1	SP1-CI-1	SP1-FRC-1
	SP1-NC-2	SP1-CI-2	SP1-FRC-2
	SP1-NC-3	SP1-CI-3	SP1-FRC-3
2.5 in.	SP2-NC-5	SP2-CI-5	SP2-FRC-5
	SP2-NC-6	SP2-CI-6	SP2-FRC-6
	SP2-NC-7	SP2-CI-7	SP2-FRC-7
3.5 in.	SP3-NC-9	SP3-CI-9	SP3-FRC-9
	SP3-NC-10	SP3-CI-10	SP3-FRC-10
	SP3-NC-11	SP3-CI-11	SP3-FRC-11

Table 3.2. Specimen ID for accelerated corrosion test specimens

Side cover	**Concrete type + 3% NaCl**		
	Normal concrete	Corrosion inhibitor	FRC
	Designation	Designation	Designation
1.5 in.	SP1-NC-13	SP1-CI-13	SP1-FRC-13
	SP1-NC-14	SP1-CI-14	SP1-FRC-14
	SP1-NC-15	SP1-CI-15	SP1-FRC-15
	SP1-NC-16	SP1-CI-16	SP1-FRC-16
2.5 in.	SP2-NC-17	SP2-CI-17	SP2-FRC-17
	SP2-NC-18	SP2-CI-18	SP2-FRC-18
	SP2-NC-19	SP2-CI-19	SP2-FRC-19
	SP2-NC-20	SP2-CI-20	SP2-FRC-20
3.5 in.	SP3-NC-21	SP3-CI-21	SP3-FRC-21
	SP3-NC-22	SP3-CI-22	SP3-FRC-22
	SP3-NC-23	SP3-CI-23	SP3-FRC-23
	SP3-NC-24	SP3-CI-24	SP3-FRC-24

A total of sixty-three specimens were included in this study. Specimen ID was assigned and labeled according to side edge distance and type of concrete. Content of NaCl is not labeled in the specimen ID since it was held constant in each test type. For all of the specimens subjected to wet-dry cycle test, the NaCl content was 0%, and for all the specimens subjected to accelerated corrosion test, the NaCl content was 3%. Specimens are numbered in the form of “SP side edge distance – concrete type – specimen number”. In the first term, SP 1, 2, or 3 corresponded to the side edge distance of 1.5 in., 2.5 in., or 3.5 in., respectively. Side edge distance was measured from side face of specimen to the centerline of reinforcement. In the second term, normal concrete, fiber reinforced concrete, or concrete containing corrosion inhibitor were labeled as NC, FRC, or CI, respectively. The third term represents the specimen number within the set of duplicate test specimens. Specimens are shown in Tables 3.1 and 3.2. Test variables are discussed in Sections 3.2.1 and 3.2.2.

3.2.1. Side Edge Distance. The partial depth precast prestressed panels investigated in this study had a thickness of 3 in., which is consistent with current MoDOT specifications for SIP panels (MoDOT). Thus, this dimension was held constant

per the direction of the MoDOT. As a result, the top and bottom edge distance to reinforcement remained constant. Side edge distance to reinforcement, however, could be modified by specifying different minimum side cover requirements for the panels. Thus the effect of varying the side edge distance in a 3 in. thick specimen was investigated in this study. The increase in side edge distance was expected to increase the length of the 1st and 3rd phase of the corrosion process (Figure 3.1) resulting in an increase in $t_{spalling}$ by prohibiting chloride penetration and horizontal crack propagation. Three side edge distances were considered: 1.5 in., 2.5 in., and 3.5 in. Figures 3.2 through 3.4 show dimensions of the profile and the cross-section of the specimens with those three side edge distances, respectively.

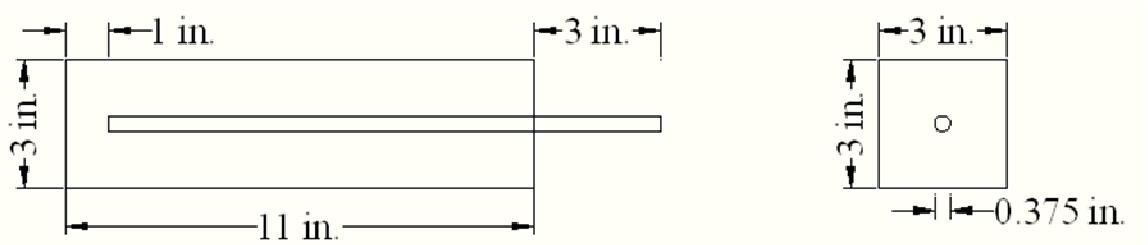

Figure 3.2. Specimens with side edge distance of 1.5 in.

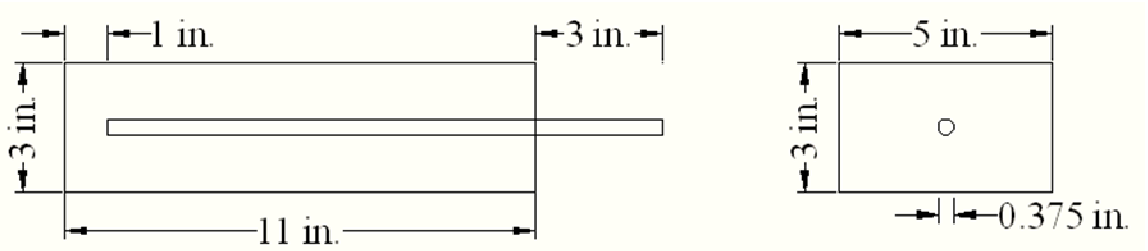

Figure 3.3. Specimens with side edge distance of 2.5 in.

3.2.2. Concrete Admixture. The addition of various admixtures (i.e. fibers and corrosion inhibitor) was examined to investigate the potential durability benefits relative

to the control condition (normal concrete). Such benefits may include reduction in crack propagation by retarding embedded steel corrosion or increasing the tensile strength of concrete.

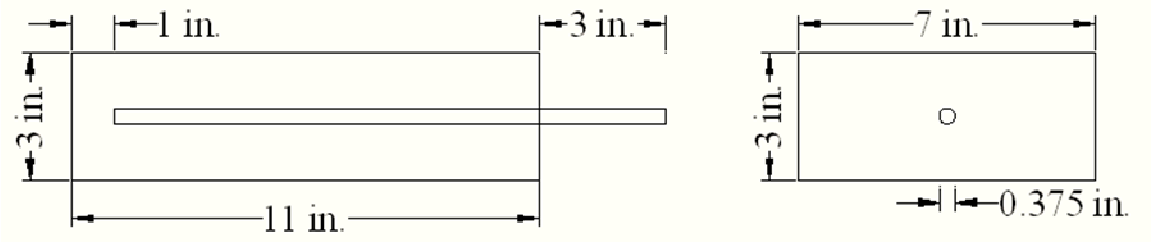

Figure 3.4. Specimens with side edge distance of 3.5 in.

3.2.2.1. Normal concrete. Specimens without corrosion inhibitor and polymer fibers added in the mixture are termed “normal concrete” and serve as the control specimens.

3.2.2.2. Corrosion inhibitor. As introduced in the Chapter 2, corrosion inhibitors, which are organic compounds, can function by forming an impervious film on the metal surface or by interfering with reactions of either the anode or cathode. It was expected that the addition of corrosion inhibitor would be mostly effective in preventing deleterious factors from destroying the passive film, retarding the initial corrosion, and resulting in a longer 1st phase (i.e. increase in $t_{initiation}$ in Figure 3.1).

3.2.2.3. Synthetic fibers. The addition of polypropylene fibers was expected to be more effective in the 2nd and 3rd phases of the corrosion process in Figure 3.1 by increasing the concrete tensile strength when the modulus of elasticity of the fiber is higher than the matrix (concrete or mortar binder). Thus, service life can be increased by longer 2nd phase before cracking occurs due to tensile failure of concrete. In addition, fibers also lower the permeability of concrete and thus reduce bleeding of water, which helps to delay corrosion problems by reducing the 1st phase. Concrete with fibers is referred to as fiber-reinforced concrete (FRC).

3.3. TEST SPECIMEN CONSTRUCTION

3.3.1. Construction Procedure. All specimens for the wet-dry cycle test and accelerated corrosion test were constructed at Coreslab Structures precast concrete plant in Marshall, MO on December 28 and 29, 2009.

All specimens were 11 in. long and 3 in. high with different widths to accommodate a variation in side edge distance to the centerline of the reinforcement (1.5 in., 2.5 in., and 3.5 in.) as shown in Figure 3.4. Specimen height was consistent with the MoDOT specified panel thickness (3 in.). Specimen length (11 in.) was consistent with the standard specimen size prescribed by ASTM G 109-07. Specimens were formed using custom built plywood formwork. Reinforcement was supported from the soffit using plastic bar supports as shown in Figure 3.5.

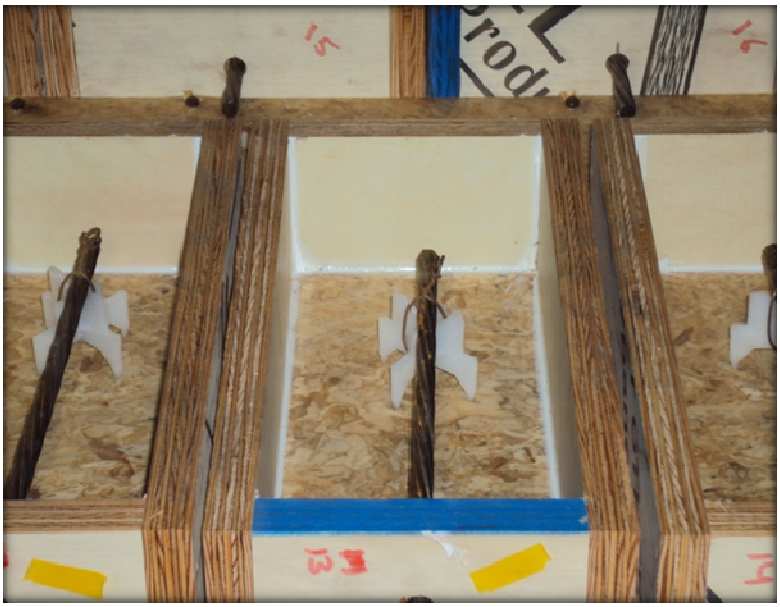

Fig 3.5. Specimens before concrete placement

3.3.2. Test Specimen Materials. The materials used to construct the test specimens are described in the following sections.

3.3.2.1. Cement. Ashgrove Type III Porland Cement was used with w/c ratio of 0.341. This type of cement provides a higher early strength required in some applications and is excellent for use in cold weather conditions.

3.3.2.2. Aggregate. Limestone was used for coarse aggregate with a ratio of 2.1 lb per pound of cement. Kaw sand was used for fine aggregate with a ratio of 1.7 lb per pound of cement.

3.3.2.3. Additives. Glenium 7700 ready-to-use high-range water-reducing admixture was added with a ratio of 0.11 oz per pound of cement. MB-VR standard neutralized Vinsol* Resin admixture were used by 0.05 oz per pound of cement.

3.3.2.4. Reinforcement. Reinforcement consisted of ASTM A 416-10 standard Grade 270 seven-wire strand prestressing tendons with diameter of 3/8 in.

3.3.2.5. Sodium chloride. Sodium chloride of technical grade purchased from CQ Concepts was added to specific specimens with a ratio of 3% by volume with mixing water.

3.3.2.6. Corrosion inhibitor. Unicore Type M. Corrosion Inhibitor was used in specific specimens by 0.01 oz per pound of water.

3.3.2.7. Polypropylene fibers. MasterFiber F70-C Fibrillated Microsynthetic Fiber was used in specific specimens by 1.5 lb/yd^3.

3.4. TEST METHODS

Of the total sixty-three test specimens, twenty-seven were subjected to wet-dry tests and the remaining thirty-six were subjected accelerated corrosion tests using potentiostatic approach. These tests methods and evaluation techniques are described in Sections 3.4.1 and 3.4.2, respectively.

3.4.1. Wet-dry Cycle Test. The wet-dry cycle test was conducted in the Civil Engineering Materials Laboratory in Butler-Carlton Hall at Missouri S&T from January 27, 2010 to August 3, 2010. Twenty-seven test specimens were kept indoors and were exposed to the wet-dry cycle test. As discussed in Section 3.2, the content of NaCl was excluded from the inventory of parameters to investigate how chloride ions penetrate the

concrete cover at different times, considering the effects of only the geometrical conditions (i.e. side edge distance) and different concrete materials.

Each cycle was one week in duration and was divided into two stages. In the first stage that lasted four days, the specimens were submerged into a wetting solution at a level of 9 in. from the bottom of a specimen, as shown in Fig. 3.6. The wetting solution used was 5% sodium chloride by weight. In the second stage, which lasted three days, specimens were subjected to drying in an oven under a temperature of 104^{o}F, which corresponds to the average highest temperature in Missouri during the summer. This test setup was developed based on experimental works by Hamid (2004). Waterproof epoxy coatings (Fosroc-Nitoflor FC 140 and Duromar 2510) were used to coat both the top and bottom surface of the test specimens to promote uniform chloride penetration within the immersed portion of the specimens.

Visual inspection, corrosion potential measurement and electrical resistivity measurement were conducted during the interim between the two stages. In addition, chloride content analysis was carried out every two months to investigate the penetration of chloride ions through concrete cover. Procedures are discussed in Sections 3.4.1.1 through 3.4.1.5.

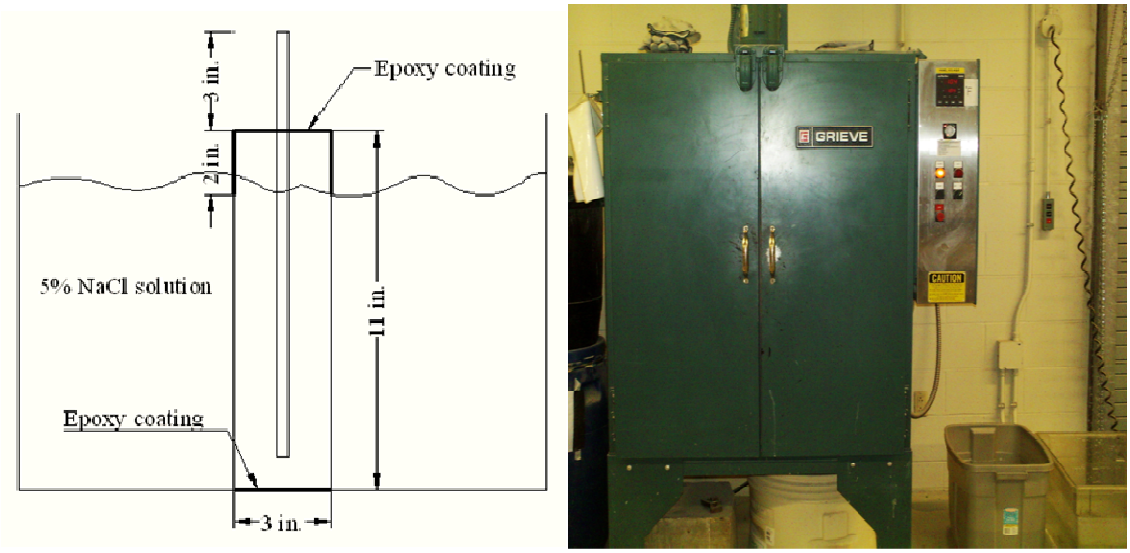

Figure 3.6. Wet-dry cycle test

3.4.1.1. Visual inspection. Visual inspection was carried out during six months of wet-dry cycle test to examine and note locations of efflorescence, rust, and cracks.

3.4.1.2. Corrosion potential measurement. Based on the method specified by ASTM C 876-09, a CANIN^{+} corrosion analyzing instrument was used with a copper/copper sulfate half-cell rod as the reference electrode to investigate and assess the corrosion of steel in the concrete specimens by measuring the half-cell potential. Figure 3.7 shows the instruments used and the locations of the probe for the measurements. Measurements were conducted every two weeks before all specimens were transferred from the dry cycle to wet cycle, and Table 2.1 was used to interpret the results.

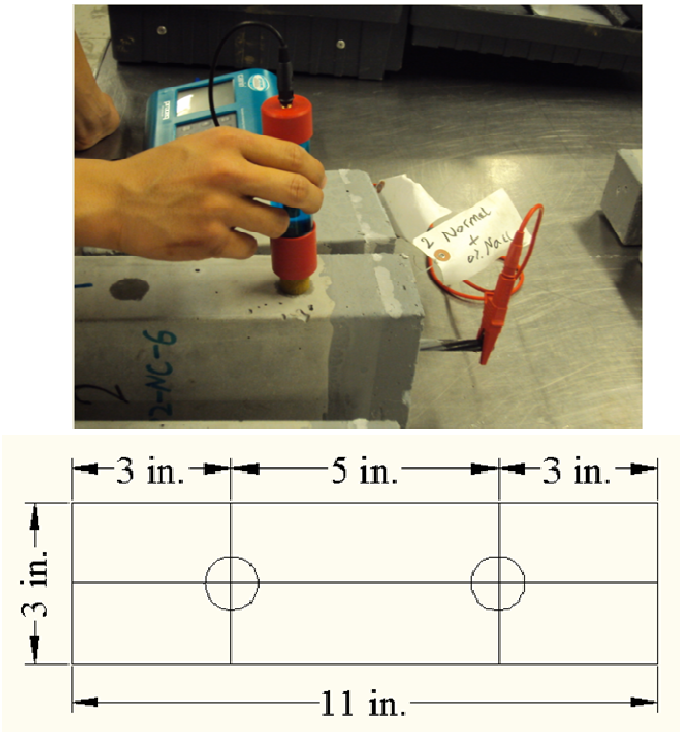

Figure 3.7. Corrosion potential measurement

3.4.1.3. Electrical resistivity measurement. The CANIN^{+} corrosion analyzing instrument discussed in Section 3.4.1.2 was also used to evaluate the corrosion level of steel in concrete by displaying and processing the electrical resistivity measured by a

four-point Wenner probe shown in Figure 3.8. Location of the probe was set at the geometric center of the side surface with thicker concrete cover.

Figure 3.8. Electrical resistivity measurement (Proceq SA 2007)

Measurements were conducted every two weeks together with corrosion potential measurements as discussed in Section 3.4.1.2. Table 3.3 was used to interpret the measurement results. The increase of electrical resistivity can be related to an accelerated corrosion activity between measurements.

Table 3.3. Interpretation from results from Electrical Resistivity

Electrical resistivity (kΩ-cm)	Probability of corrosion
>20	Low
10-20	Low to moderate
5-10	high
<5	Very high

3.4.1.4. Chloride content analysis. When the chloride concentration reaches a threshold value, corrosion can be initiated. Sohanghpurwala (2006) reported this

threshold value as 0.025% to 0.033% of concrete weight, while Smith and Virmani (2000) proposed a threshold value of 0.71 kg/m^3 (1.2 lb/yd^3). Table 2.3 presents the recommended action for chloride content measurements.

As introduced in Chapter 2, there are two main types of chloride ion tests. The first is the acid soluble test, which is used to determine the total chloride content in the concrete. The second is the water soluble test, which is used to provide the chloride ion content in the pore water. In this investigation, the water soluble chloride content analysis method was used to measure the chloride content at different depths as specified by ASTM C 1218-08.

In case of absence of an initial corrosion record, the chloride profile (chloride concentration variation with depth) can provide important information about the diffusion rate of chloride ion. Measuring the chloride at different depths provides important information for availability of chloride amount required to initiate corrosion and source of chloride in the concrete. In this investigation, the chloride content measurement was made every two months at different locations including 0.5 in. from the surface, mid-distance between the surface and steel location, and at the steel location.

The chloride content tests for two months samples were conducted by MoDOT. For samples taken at four months and six months, the tests were conducted in the Engineering Research Lab of Missouri S&T. Equipment from Germann Instruments Inc. was used. The rapid chloride test water-soluble (RCTW) method was carried out according to the instruction and maintenance manual. Chloride content was measured by collecting concrete powder samples at different depths. Figure 3.9 shows the position of concrete blocks cut from the specimens. Epoxy coating was applied on the cut surface before the next test cycle to prevent chloride from penetrating the concrete surface at the cut location during later test.

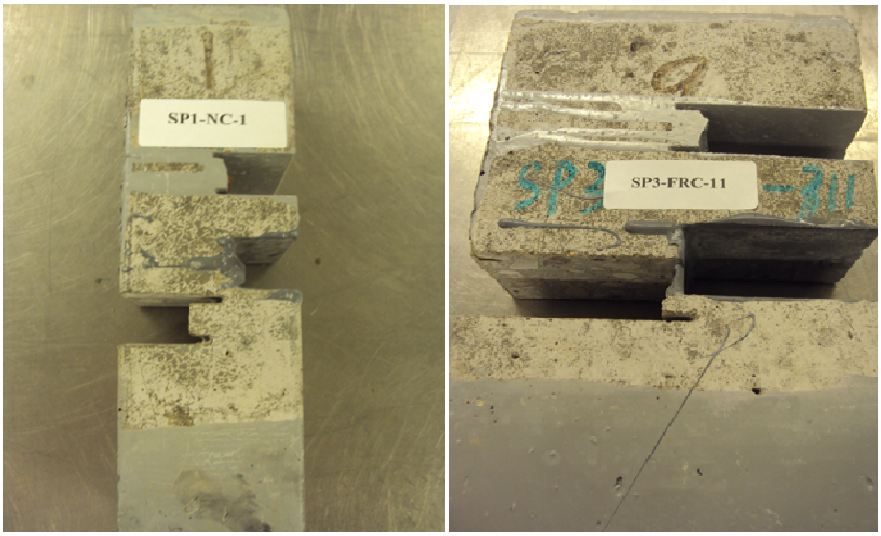

Figure 3.9. Specimens after cut of concrete block

3.4.1.5. Gravimetric study. The gravimetric method was applied to specimens subjected to wet-dry cycle test with the precision to tenth. The gravimetric method requires measuring the weight of the steel tendon before concrete casting and after test. According to ASTM G 1-03, the mass loss was used to assess the corrosion damage by corrosion rate. See Section 2.2.4 for detailed method.

3.4.2. Accelerated Corrosion Test. Accelerated corrosion by means of impressed current, which is widely used in concrete durability testing, was planned and carried out. Accelerated corrosion testing was performed on thirty-six specimens containing 3% NaCl in the concrete mixture submerged in a 5% NaCl solution. The addition of the 3% NaCl can provoke and accelerate the corrosion, since no time is needed for chloride ingress. Therefore, observed times to corrosion cracking are times from corrosion initiation to corrosion cracking.

The corrosion process was accelerated by inducing an impressed current of 0.4 mA into the specimens. Embedded steel tendons performed as an anode, and 0.5 in. diameter graphite rods were used as a cathode as shown in Figure 3.10. In addition, all specimens were connected to one power supply in parallel as shown in Figure 3.11. Typical current densities range from 200 to 3,000 $\mu A/cm^2$ (1,290 to 19,355 $\mu A/in^2$) based on the study by Tamer and Khaled (2003). In this study, however, a much lower current

density was applied corresponding to 4.78 μA/cm^2. This was due to an initial calculation error, however it allowed the unique opportunity to evaluate the behavior or the specimens under low current density, which has not been reported in the literature. In this test, epoxy coating (Fosroc-Nitoflor FC 140 and Duromar 2510) was applied only to the bottom surface of the test specimen to prohibit the chloride ingress from the bottom surface as well as to promote of chloride ingress through the side surfaces. Visual inspection and gravimetric study methods were applied which are explained in Sections 3.4.2.1 and 3.4.2.2.

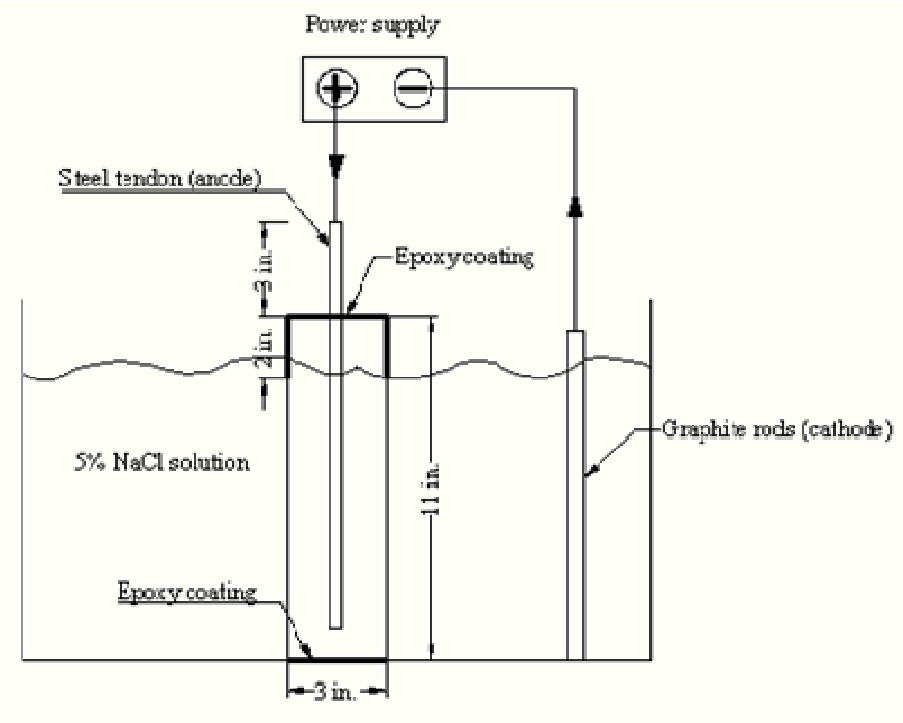

Figure 3.10. Accelerated corrosion test schematic

3.4.2.1. Visual inspection. Of the thirty-six specimens subjected to the accelerated corrosion test, eighteen of them were subjected to accelerated corrosion test for six months. The other eighteen were subjected to accelerated corrosion test for twelve

months. Visual inspection was conducted on all thirty-six specimens very two or three days to record the occurrence and propagation of cracking and concrete deterioration.

Figure 3.11. Accelerated corrosion test experimental setup

3.4.2.2. Gravimetric study. The gravimetric study method was applied to the accelerated corrosion test specimens according to ASTM G 1-03. Mass loss of the steel reinforcement was obtained by measuring the weight of the steel tendon before concrete casting and after entire testing to the precision of hundredth. Of the thirty-six specimens subjected to accelerated corrosion test, eighteen of them were subjected to impressed current for six months before the gravimetric study. The other eighteen specimens were subjected to impressed current for twelve months before the gravimetric study.

4. DISCUSSION OF RESULTS

In this chapter, results of the experiments described in Chapter 3 are presented and discussed. Section 4.1 presents the results of the visual inspection for both the wet-dry cycle test and the accelerated corrosion test. In Section 4.2, gravimetric study results are presented for the wet-dry cycle test and accelerated corrosion test. Corrosion potential measurements are discussed in Section 4.3. Electrical resistivity measurements are discussed in Section 4.4. Chloride content measurements are discussed in Section 4.5.

4.1. VISUAL INSPECTION

Visual inspection was conducted on specimens subjected to the wet-dry cycle test at the end of six months of the entire testing period as discussed in Section 3.4.1.1. It was also carried out on specimens subjected to accelerated corrosion test after testing periods of six months and twelve months as discussed in Section 3.4.2.1. Results of visual inspection based on those two tests are discussed in Sections 4.1.1 and 4.1.2, respectively.

4.1.1. Wet-dry Cycle Test. After six months of the wet-dry cycle test, visual inspection was conducted to observe the concrete deterioration. The main types of concrete deterioration observed were efflorescence, rust, and cracking.

Table 4.1 summarizes the deterioration observed in specimens with 1.5 in. side edge distance. All test specimens showed efflorescence on the surface due to the salt solution as shown in Figure 4.1. Rust was also observed in most of the specimens on both cross section surface and side surface with lesser concrete cover, while cracks were observed in all specimens mostly on side surface with lesser concrete cover with the exception of those specimens with normal concrete. Figure 4.2 shows the rust and cracks on specimen SP1-FRC-1.

Table 4.1. Visual inspection results of specimens subjected to wet-dry cycle test with 1.5 in. side edge distance

Specimen designation	Concrete deterioration		
	Efflorescence	Rust	Cracks
SP1-NC-1	X		
SP1-NC-2	X	X	
SP1-NC-3	X	X	
SP1-CI-1	X	X	X
SP1-CI-2	X	X	X
SP1-CI-3	X	X	X
SP1-FRC-1	X	X	X
SP1-FRC-2	X	X	X
SP1-FRC-3	X	X	X

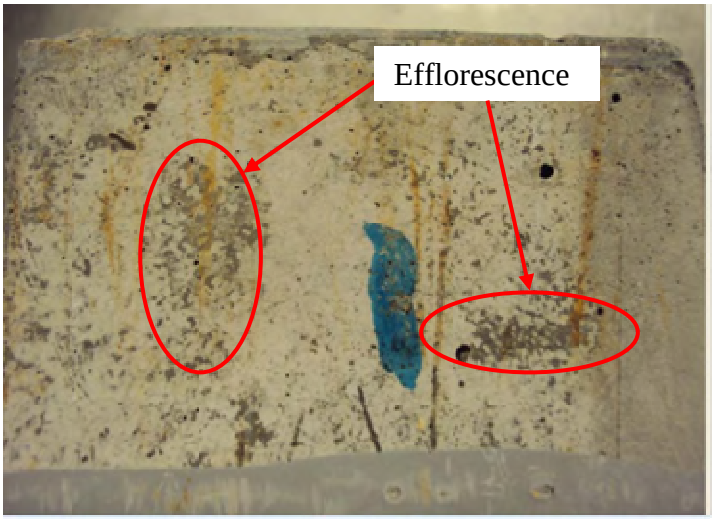

Figure 4.1. Efflorescence on specimen SP1-NC-2

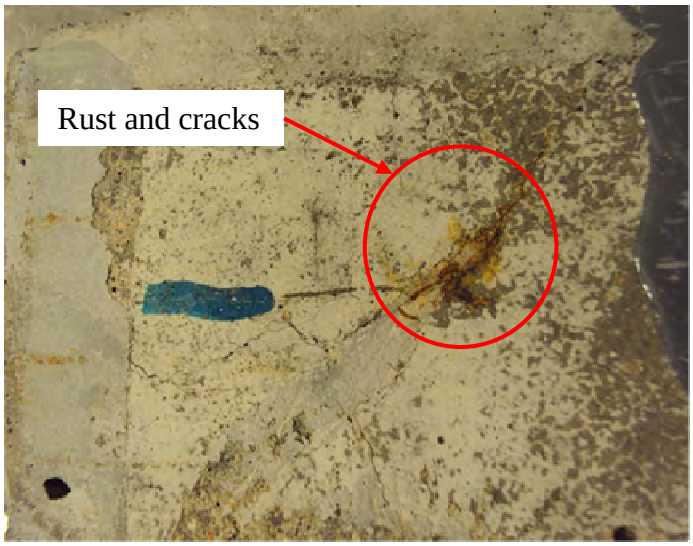

Figure 4.2. Rust and cracks on specimen SP1-FRC-1

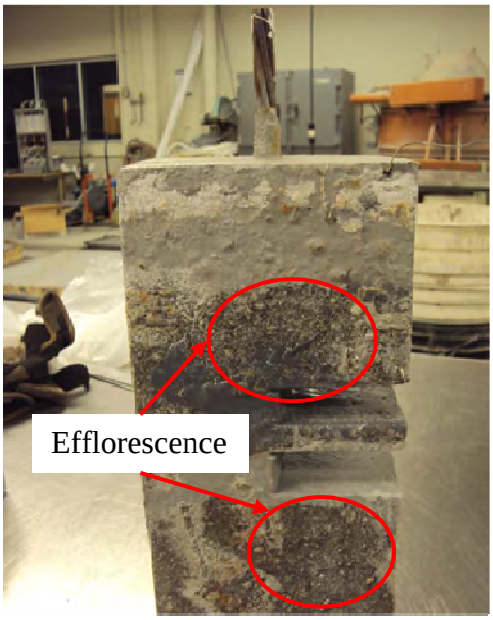

Figure 4.3. Efflorescence on specimen SP2-NC-5

Table 4.2 summarizes the deterioration observed in specimens with 2.5 in. side edge distance. Similar to the test specimens with 1.5 in. side edge distance, all specimens showed efflorescence at the surface as shown in Figure 4.3. Rust and cracks were

observed only in two of the specimens containing corrosion inhibitor. Cracking observed in SP2-CI-7 was similar to that observed in the test specimens with 1.5 in. side edge distance as shown in Figure 4.2.

Table 4.2. Visual inspection results of specimens subjected to wet-dry cycle test with 2.5 in. side edge distance

Specimen designation	Concrete deterioration		
	Efflorescence	Rust	Cracks
SP2-NC-5	X		
SP2-NC-6	X		
SP2-NC-7	X		
SP2-CI-5	X	X	
SP2-CI-6	X		
SP2-CI-7	X	X	X
SP2-FRC-5	X		
SP2-FRC-6	X		
SP2-FRC-7	X		

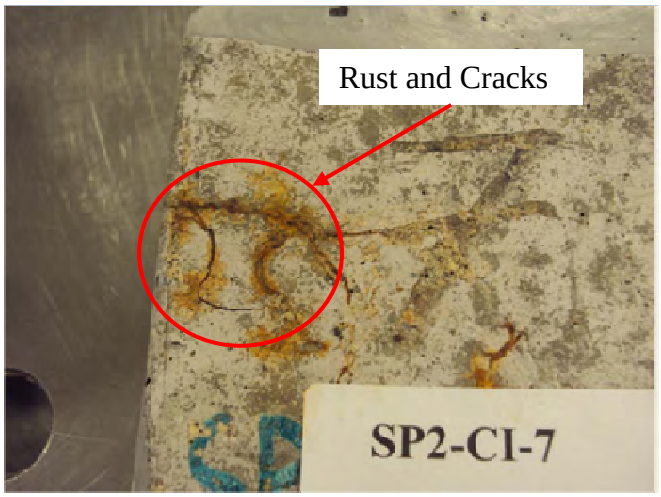

Figure 4.4. Rust and cracks on specimen SP2-CI-7

As shown in Table 4.3, specimens with side edge distance of 3.5 in. showed results similar to the specimens with 2.5 in. side edge distance. Efflorescence was observed in all specimens as shown in Figure 4.5. Only specimens containing corrosion inhibitor showed rust and cracks as shown in Figure 4.6.

Table 4.3. Visual inspection results of specimens subjected to wet-dry cycle test with 3.5 in. side edge distance

Specimen designation	Concrete deterioration		
	Efflorescence	Rust	Cracks
SP3-NC-9	X		
SP3-NC-10	X		
SP3-NC-11	X		
SP3-CI-9	X	X	X
SP3-CI-10	X	X	
SP3-CI-11	X		
SP3-FRC-9	X		
SP3-FRC-10	X		
SP3-FRC-11	X		

Based on observations from all wet-dry test specimens, it is apparent that increasing of side edge distance enhanced significantly the durability of the specimens in terms of much less rust and fewer cracks. Also, the addition of corrosion inhibitor and fibers influenced the environmental response of the concrete. According to Tables 4.2 and 4.3, FRC showed similar response to the normal concrete specimens, while the specimens with corrosion inhibitor showed more deterioration than the normal concrete specimens. Comparison between specimens with corrosion inhibitor and FRC specimens shows that FRC showed better environmental performance, since rust and cracks occurred only in specimens with corrosion inhibitor. These different performances can be attributed to the inherent material characteristics. Corrosion inhibitor changes the

chemical composition of the concrete, while the addition of fibers changes the mechanical properties of the concrete.

Figure 4.5. Efflorescence on specimen SP3-CI-10

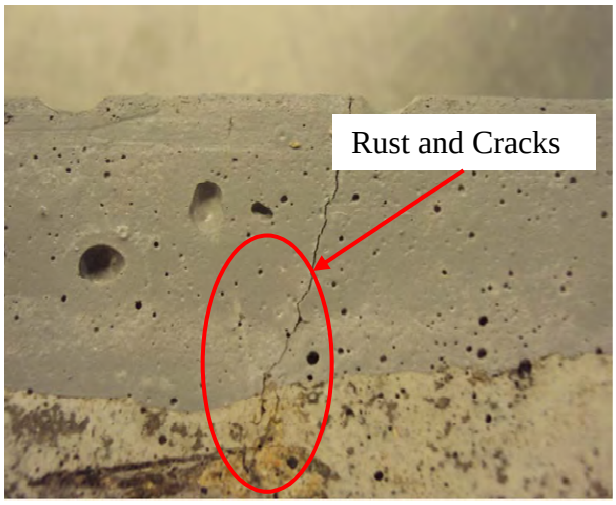

Figure 4.6. Rust and cracks on specimen SP3-CI-9

4.1.2. Accelerated Corrosion Test. As described in Section 3.4.2, specimens subjected to accelerated corrosion test contained Nacl in the concrete mixture and were

subjected to a very low impressed current of 0.4 mA. Based upon visual inspection, concrete deterioration observed in the accelerated corrosion test specimens was much more severe than those specimens subjected to wet-dry cycle test discussed in Section 4.1.1. Results of the visual inspection after six and twelve months are discussed in Sections 4.1.2.1 and 4.1.2.2, respectively.

4.1.2.1. Specimens after six months. Table 4.4 summarizes the visual inspection results for specimens with 1.5 in. side edge distance. The table shows that all specimens exhibited deterioration including rust (Figure 4.7), cracking (Figure 4.8), and some specimens exhibited loose concrete (Figure 4.9). Rust was observed on four side surfaces of all specimens since the depths of concrete cover of each side surface are the same. Loose concrete was only observed on one specimen with corrosion inhibitor and one FRC specimen.

Table 4.4. Visual inspection results of the specimens with 1.5 in. side edge distance subjected to accelerated corrosion test for six months

Specimen designation	Concrete deterioration		
	Rust	Cracks	Loose concrete
SP1-NC-13	X	X	
SP1-NC-14	X	X	
SP1-CI-13	X	X	
SP1-CI-14	X	X	X
SP1-FRC-13	X	X	X
SP1-FRC-14	X	X	

Table 4.5 summarizes the visual inspection results of the specimens with 2.5 in. side edge distance. Rust was observed in all specimens on the surface with lesser concrete cover with respect to the steel tendon (i.e. the short direction of the cross-section). Figure 4.10 shows the rust on side surface of specimen SP2-CI-17 with lesser

concrete cover. Cracks were observed in only three specimens, and all of them occurred on bottom surface in the short direction of the cross-section as shown in Figure 4.11.

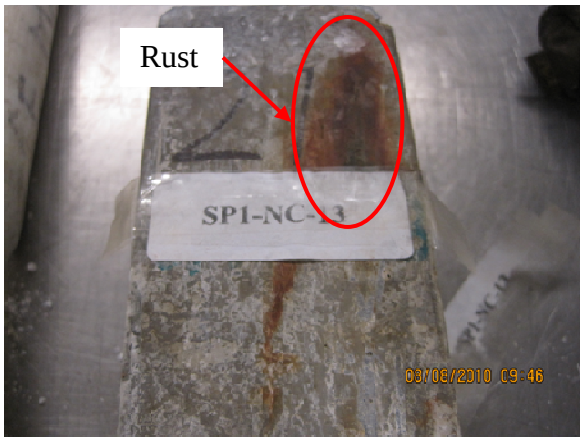

Figure 4.7. Rust on specimen SP1-NC-13

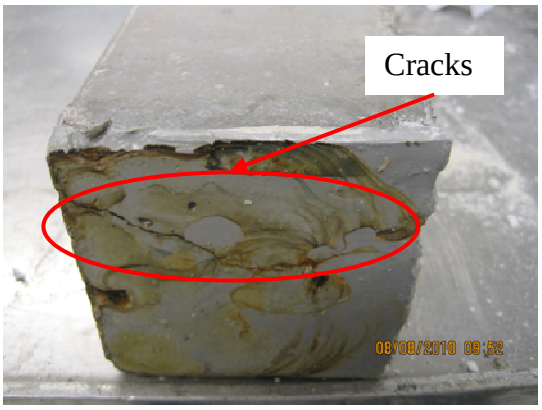

Figure 4.8. Cracks on specimen SP1-CI-13

Similar to the results of the 1.5 in. side edge distance specimens, based upon the comparison among specimens with 2.5 in. side edge distance, it is difficult to distinguish the effects of different concrete material type on the deterioration because specimens showed almost the same deterioration level. It is apparent, however, that increasing of the

side edge distance prohibited the propagation of corrosion-induced cracks to the side surface with greater concrete cover (i.e. the long direction of the cross-section).

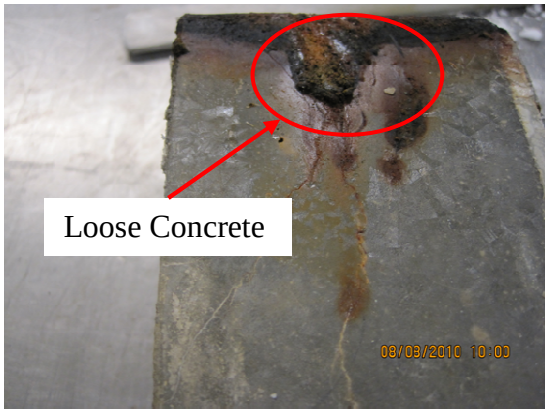

Figure 4.9. Loose concrete on specimen SP1-CI-14

Table 4.5. Visual inspection results of the specimens with 2.5 in. side edge distance subjected to accelerated corrosion test for six months

Specimen designation	Concrete deterioration		
	Rust	Cracks	Loose concrete
SP2-NC-17	X	X	
SP2-NC-18	X		
SP2-CI-17	X	X	
SP2-CI-18	X		
SP2-FRC-17	X	X	
SP2-FRC-18	X		

Table 4.6 summarizes the visual inspection results for test specimens with 3.5 in. side edge distance. Rust and cracks were observed only in test specimens with normal concrete, while no deterioration was observed in specimens containing corrosion inhibitor and fibers. Rust and cracks are shown in Figures 4.12 and 4.13 respectively.

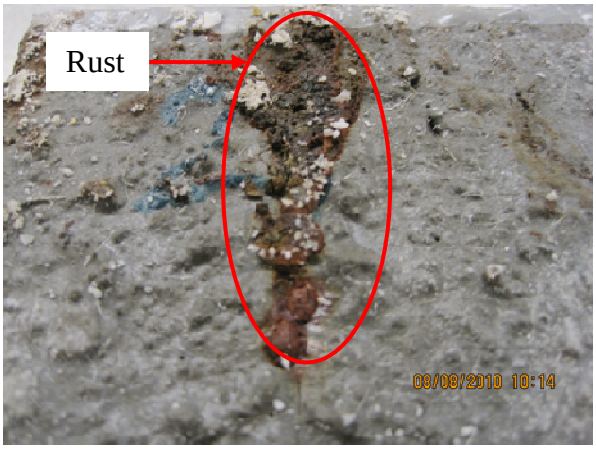

Figure 4.10. Rust on specimen SP2-CI-17

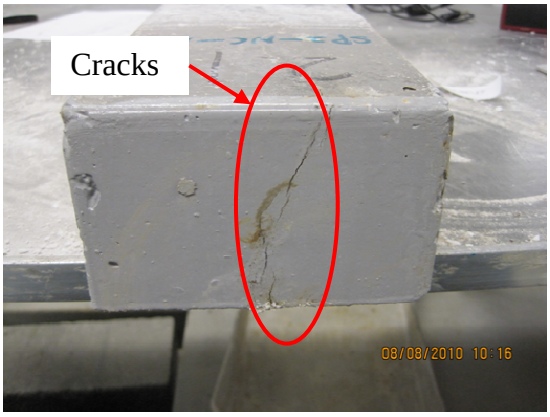

Figure 4.11. Cracks on specimen SP2-CI-17

Compared with the results of specimens with 1.5 and 2.5 in. side edge distance, it is apparent that increasing edge distance significantly improves the durability of concrete, especially on the side surface with greater concrete cover (i.e. long direction of the cross-section).

Table 4.6. Visual inspection results of the specimens with 3.5 in. side edge distance subjected to accelerated corrosion test for six months

Specimen designation	Concrete deterioration		
	Rust	Cracks	Loose concrete
SP3-NC-21	X	X	
SP3-NC-22	X		
SP3-CI-21			
SP3-CI-22			
SP3-FRC-21			
SP3-FRC-22			

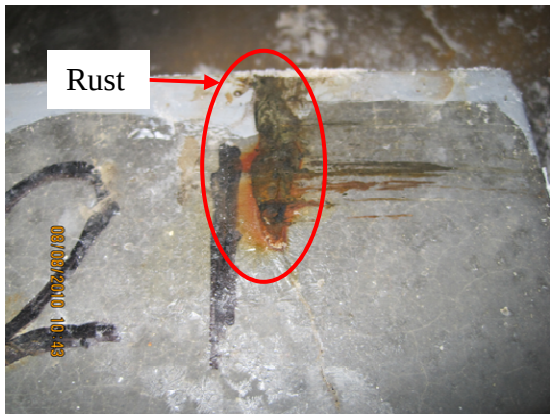

Figure 4.12. Rust on specimen SP3-NC-21

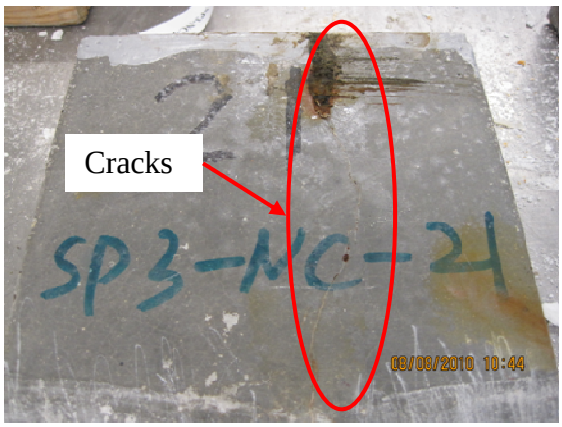

Figure 4.13. Cracks on specimen SP3-NC-21

4.1.2.2. Specimens after twelve months. Visual inspection of specimens at twelve months shows generally much more deterioration than those of six months as described in Section 4.1.2.1.

Table 4.7 summarizes the visual inspection results for test specimens with 1.5 in. side edge distance. Rust and cracks occurred on all the specimens. Loose concrete occurred only on one specimen with corrosion inhibitor and one FRC specimen. Rust, cracks, and loose concrete are shown in Figures 4.14, 4.15 and 4.16, respectively.

Compared with the normal concrete, specimens with corrosion inhibitor and FRC specimens showed more severe problem of loose concrete. In addition, for all specimens, longitudinal cracks were observed extending from the tendon to all the four side surfaces.

Table 4.7. Visual inspection results of the specimens with 1.5 in. side edge distance subjected to accelerated corrosion test for twelve months

Specimen designation	Concrete deterioration		
	Rust	Cracks	Loose concrete
SP1-NC-15	X	X	
SP1-NC-16	X	X	
SP1-CI-15	X	X	X
SP1-CI-16	X	X	
SP1-FRC-15	X	X	
SP1-FRC-16	X	X	X

Table 4.8 shows the results of visual inspection for the specimens with 2.5 in. side edge distance. Rust and cracks are all shown to a high degree on side surface with lesser concrete cover (i.e. short direction of the cross-section). Only one specimen SP2-CI-19 exhibited loose concrete. Rust, cracks and loose concrete are shown in Figures 4.17, 4.18 and 4.19, respectively. No specimens with 2.5 in. side edge distance showed any cracks throughout the side surface with lesser concrete cover (i.e. short direction of the cross-section) with the exception of specimens SP2-CI-20.

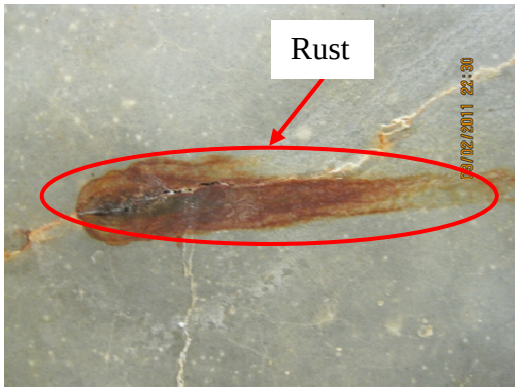

Figure 4.14. Rust on specimen SP1-CI-15

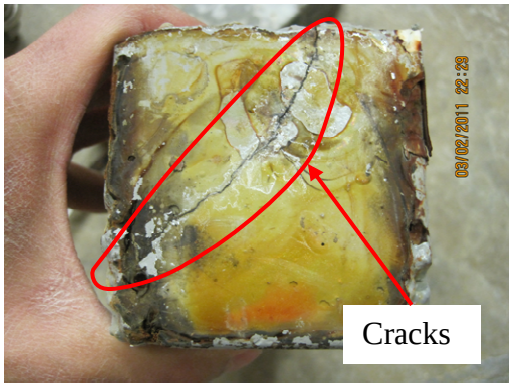

Figure 4.15. Cracks on specimen SP1-NC-16

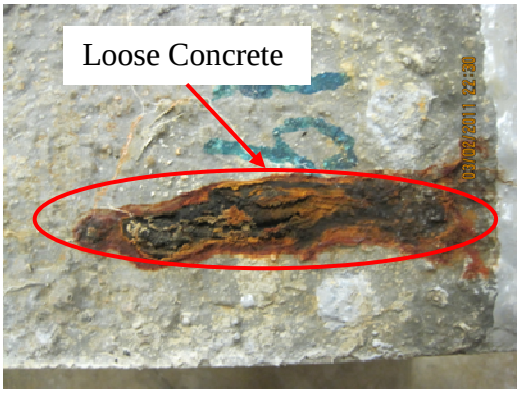

Figure 4.16. Loose concrete on specimen SP1-CI-15

Table 4.8. Visual inspection results of the specimens with 2.5 in. side edge distance subjected to accelerated corrosion test for twelve months

Specimen designation	Concrete deterioration		
	Rust	Cracks	Loose concrete
SP2-NC-19	X	X	
SP2-NC-20	X	X	
SP2-CI-19	X	X	X
SP2-CI-20	X	X	
SP2-FRC-19	X	X	
SP2-FRC-20	X	X	

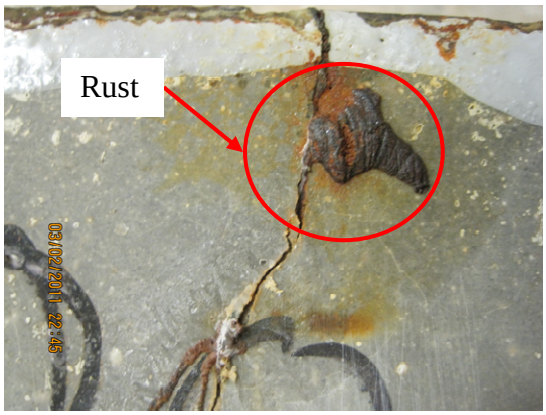

Figure 4.17. Rust on specimen SP2-CI-19

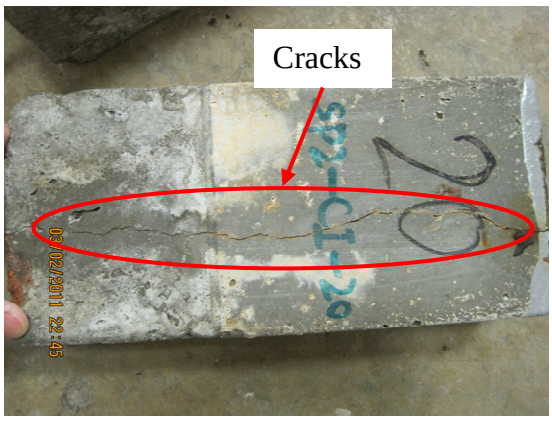

Figure 4.18. Cracks on specimen SP2-CI-20

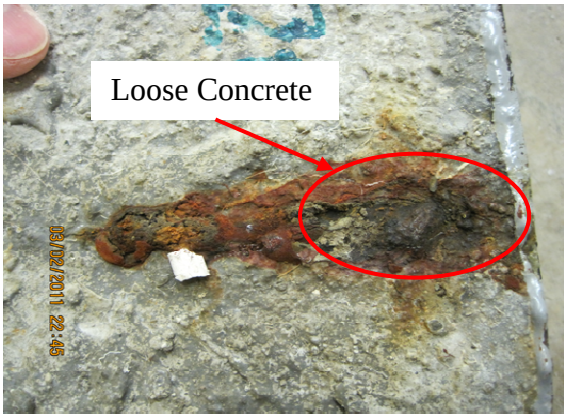

Figure 4.19. Loose concrete on specimen SP2-CI-19

Table 4.9 summarizes the visual inspection results of the specimens with 3.5 in. side edge distance. Rust and cracks were observed on two side surfaces with lesser concrete cover (i.e. short direction of the cross-section) in every specimen and almost the same level of severeness. Figures 4.20 and 4.21 show the rust and cracks, respectively. No specimens exhibited loose concrete. In addition, according to visual observation, the occurrence of rust and propagation of cracks were inhibited significantly on the side surfaces with greater concrete cover (i.e. long direction of the cross-section).

Table 4.9. Visual inspection results of the specimens with 3.5 in. side edge distance subjected to accelerated corrosion test for twelve months

Specimen designation	Concrete deterioration		
	Rust	Cracks	Loose concrete
SP3-NC-23	X	X	
SP3-NC-24	X	X	
SP3-CI-23	X	X	
SP3-CI-24	X	X	
SP3-FRC-23	X	X	
SP3-FRC-24	X	X	

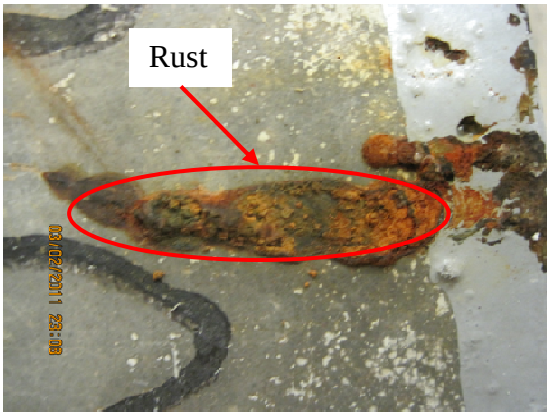

Figure 4.20. Rust on specimen SP3-CI-24

Figure 4.21. Cracks on specimen

4.2. GRAVIMETRIC STUDY

Gravimetric study was performed on all wet-dry cycle test specimens to evaluate the corrosion rate by obtaining the steel mass loss (Section 3.4.1.5). Gravimetric study was also conducted on the accelerated corrosion specimens to evaluate test variables (i.e. concrete material type and side edge distance) and to assess the effectiveness of low impressed current technique to simulate corrosion of steel reinforcement embedded in concrete (Section 3.4.2.2). Results are presented and discussed in Sections 4.2.1 and 4.2.2, respectively.

4.2.1. Wet-dry Cycle Test. All specimens subjected to the wet-dry cycle test were prepared, cleaned and evaluated for gravimetric study according to ASTM G 1-03, Method C3.5. As introduced in Section 2.1.6, corrosion rate can be expressed in the following equation:

Corrosion rate = (K ×W) / (A×T×D)

where K is a constant=8.76×10^7 for desired units of micrometers per year, W is mass loss in grams, A is the surface area in cm^2, T is time of exposure in hours, and D is the density of the corroding metal (D=7.86 g/cm^3 for carbon steel). As introduced in Section 2.2.4, no instantaneous corrosion rates can be measured by this technique, but only a mean value during the period of test.

For specimens subjected to wet-dry cycle test, Table 4.10 shows the average mass loss of specimens with same concrete material type and side edge distance. Results of Table 4.10 can be reflected by a chart in Figure 4.22. More information about initial and measured mass of the reinforcement steel can be obtained in Table A.1.

As shown in Figure 4.22, for specimens with side edge distances of 1.5 in. and 2.5 in., specimens with normal concrete show higher corrosion rate than specimens with the other two types of concrete material. In addition, for specimens with normal concrete, corrosion rate decreases with the increase of the side edge distance. However, no other obvious trends can be found from the chart.

Results of gravimetric study on specimens subjected to wet-dry cycle test indicate that six months may be a too short period to cause a significant corrosion on specimens.

Table 4.10. Mass loss and corrosion rate for specimens subjected to wet-dry cycle test

Specimens ID	Reinforcement mass loss/ initial mass (%)	Average reinforcement mass loss/ initial mass (%)	Reinforcement corrosion rate (μm/year)	Average reinforcement corrosion rate (μm/year)
SP1-NC-1	0.63	0.85	4234.03	5645.37
SP1-NC-2	1.90		12702.09	
SP1-NC-3	0.00		0.00	
SP1-CI-1	0.35	0.45	2352.24	2979.50
SP1-CI-2	0.00		0.00	
SP1-CI-3	0.99		6586.27	
SP1-FRC-1	0.00	0.00	0.00	0.00
SP1-FRC-2	0.00		0.00	
SP1-FRC-3	0.00		0.00	
SP2-NC-5	0.14	0.68	940.90	4547.66
SP2-NC-6	0.99		6586.27	
SP2-NC-7	0.92		6115.82	
SP2-CI-5	0.28	0.09	1881.79	627.26
SP2-CI-6	0.00		0.00	
SP2-CI-7	0.00		0.00	
SP2-FRC-5	0.28	0.52	1881.79	3449.95
SP2-FRC-6	0.63		4234.03	
SP2-FRC-7	0.64		4234.03	
SP3-NC-9	0.64	0.42	4234.03	2822.69
SP3-NC-10	0.63		4234.03	
SP3-NC-11	0.00		0.00	
SP3-CI-9	0.64	0.21	4234.03	1411.34
SP3-CI-10	0.00		0.00	
SP3-CI-11	0.00		0.00	
SP3-FRC-9	0.35	0.54	2352.24	3606.77
SP3-FRC-	0.63		4234.03	
SP3-FRC-	0.64		4234.03	

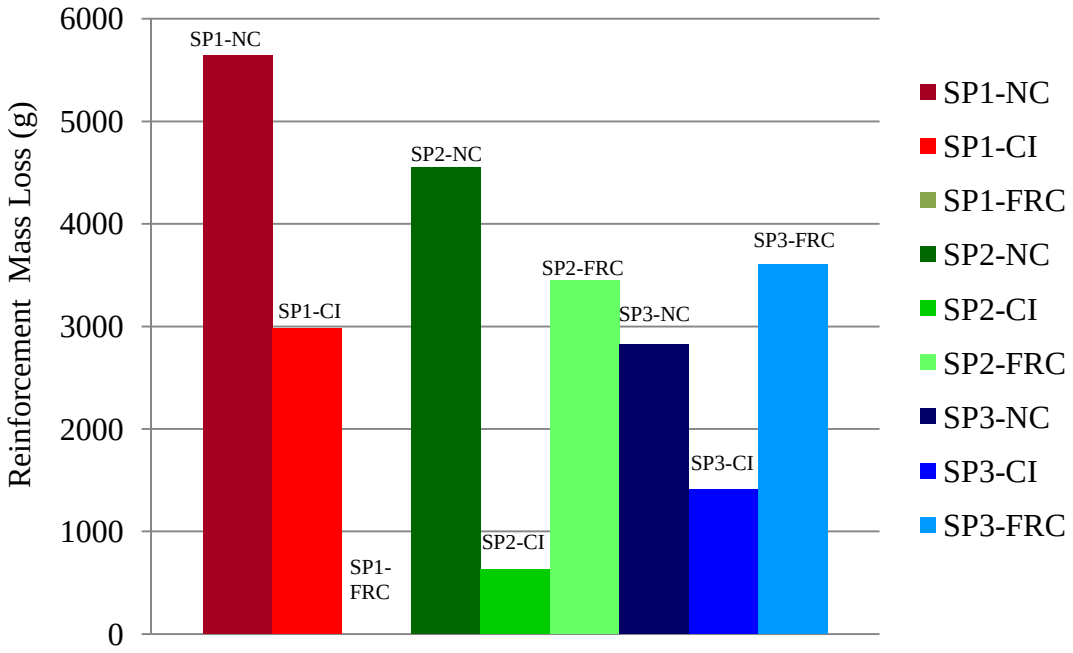

Figure 4.22. Average corrosion rate of specimens subjected to wet-dry cycle test

4.2.2. Accelerated Corrosion Test. All specimens subjected to the accelerated corrosion test were prepared, cleaned and evaluated for gravimetric study according to ASTM G 1-03, Method C 3.5.

In Tables 4.11 and 4.12, degree of corrosion is presented by the average reinforcement mass loss/ initial mass loss of specimens with same side edge distance and concrete material type. In addition, average measured mass loss/ predicted mass loss based on Faraday's law (Eq 2.10) for impressed current of 0.4 mA are also shown, for testing periods of six and twelve months, respectively. Results of Tables 4.11 and 4.12 can be reflected by chart in Figures 4.23 and 4.24, respectively. More information about initial and measured mass of the reinforcement steel is provided in Tables B.1 and B.2.

Table 4.11. Measured mass loss/ initial mass of reinforcement in specimens with sodium chloride content of 3% subjected to impressed current of 0.4 mA for six months

Specimens ID	Average reinforcement mass loss/ initial mass (%)	Average predicted mass/ initial mass (%)	Average measured mass loss/ predicted mass loss
SP1-NC-13	1.44	1.31	1.09
SP1-NC-14			
SP1-CI-13	2.42	1.33	1.82
SP1-CI-14			
SP1-FRC-13	1.76	1.32	1.34
SP1-FRC-14			
SP2-NC-17	1.94	1.33	1.46
SP2-NC-18			
SP2-CI-17	1.29	1.32	0.97
SP2-CI-18			
SP2-FRC-17	3.88	1.33	2.92
SP2-FRC-18			
SP3-NC-21	0.80	1.32	0.60
SP3-NC-22			
SP3-CI-21	0.48	1.33	0.36
SP3-CI-22			
SP3-FRC-21	1.92	1.31	1.46
SP3-FRC-22			

Table 4.12. Measured mass loss/ initial mass of reinforcement in specimens with sodium chloride content of 3% subjected to impressed current of 0.4 mA for twelve months

Specimens ID	Average reinforcement mass loss/ initial mass (%)	Average predicted mass/ initial mass (%)	Average measured mass loss/ average predicted mass loss
SP1-NC-15	2.56	2.64	0.97
SP1-NC-16			
SP1-CI-15	1.58	2.63	0.60
SP1-CI-16			
SP1-FRC-15	1.80	2.66	0.68
SP1-FRC-16			
SP2-NC-19	1.00	2.65	0.38
SP2-NC-20			
SP2-CI-19	2.41	2.65	0.91
SP2-CI-20			
SP2-FRC-19	1.23	2.66	0.46
SP2-FRC-20			
SP3-NC-23	1.53	2.63	0.58
SP3-NC-24			
SP3-CI-23	1.11	2.65	0.42
SP3-CI-24			
SP3-FRC-23	1.87	2.63	0.71
SP3-FRC-24			

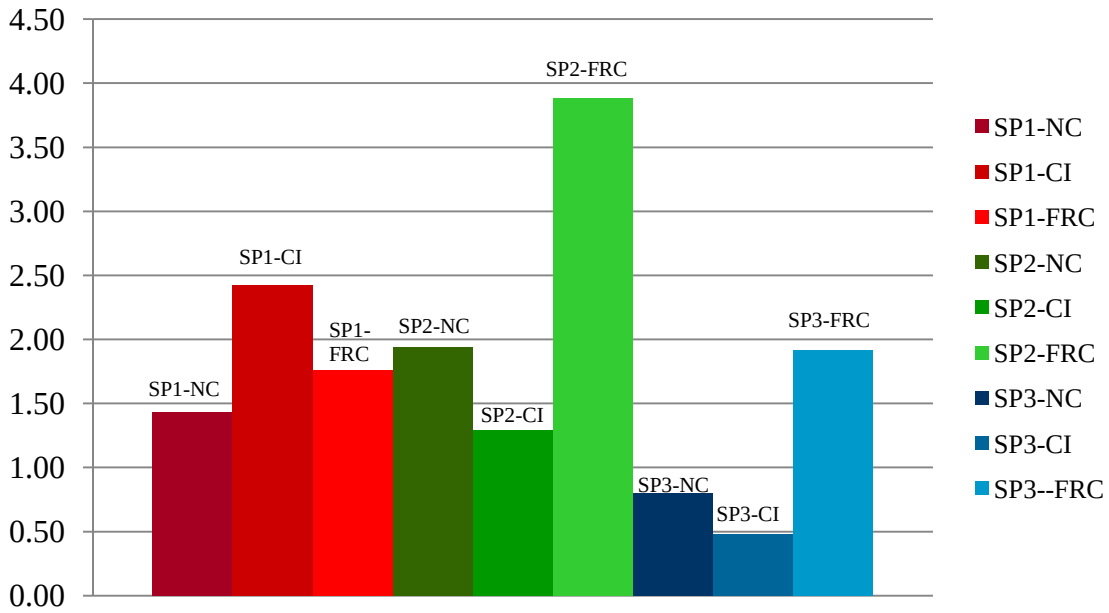

Figure 4.23. Average measured mass/ initial mass of reinforcement in specimens subjected to accelerated corrosion test for six months

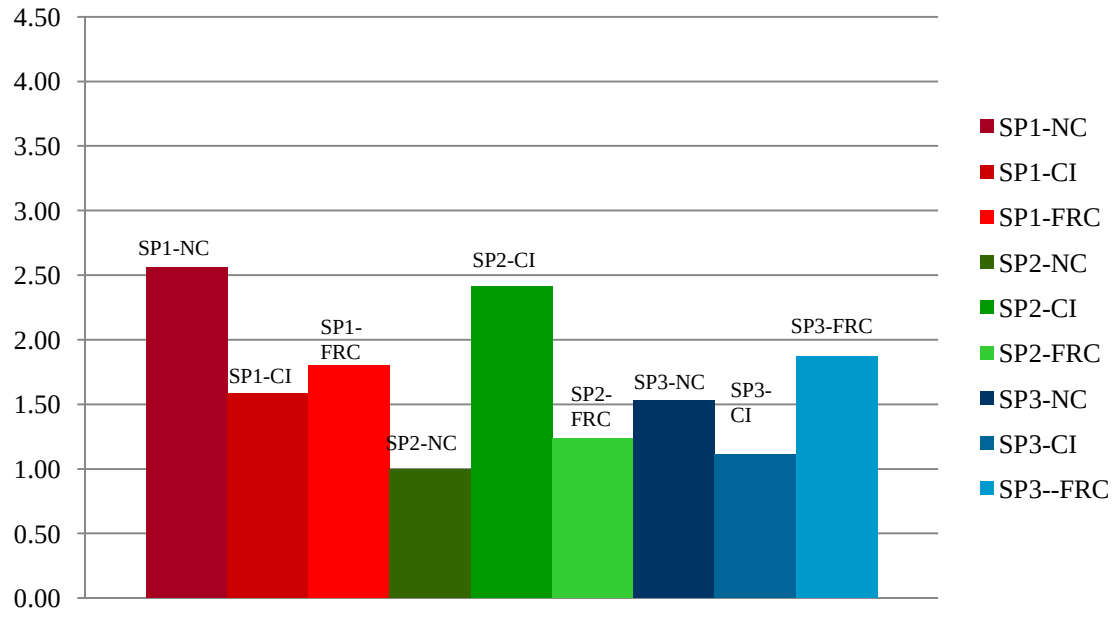

Figure 4.24. Average measured mass loss/ initial mass of reinforcement in specimens subjected to accelerated corrosion test for twelve months

As shown in Figures 4.23 and 4.24, specimens after test for twelve months generally show a higher degree of corrosion than those after test for six months.

Tables 4.11 and 4.12 show the difference between measured mass loss and predicted mass loss reflect by the ratio of average measured mass loss and average predicted mass loss. Even though Faraday's law tends to overestimate the actual mass loss of steel, since it treats the current as fully effective which is not realistic, for those ratios of measured mass loss and predicted mass loss less than 1, results show that Faraday's law predicted much more than the measured mass loss with the impressed current technique. In addition, there are also ratios of average measured mass loss and average predicted mass loss much larger than one. The reason for the relatively large difference between measured and predicted mass loss can be attributed to the low current density 4.78 $\mu A/cm^2$, which is much lower than the effective range of the applied impressed current densities, 200 $\mu A/cm^2$-300 $\mu A/cm^2$ that has been proven by other tests using impressed current technique to simulate corrosion of steel reinforcement in concrete (Tamer and Khaled 2003). However, considering the different various factors complicating the corrosion process, Faraday's law can still give a reasonable approximation of the mass loss due to corrosion, even though the prediction is not so accurate when the specimens are subjected to a small impressed current value.

4.3. CORROSION POTENTIAL MEASUREMENT

As discussed in Section 3.4.1.2, corrosion potential measurement was conducted every two weeks on concrete specimens subjected to wet-dry cycle test based on the method specified by ASTM C 876-09. Table 2.1 was used to interpret the measurement results.

In the following Figures 4.25 and 4.26, each curve represents the average measurement result of the three specimens with the same concrete material type and side edge distance. For example, in Figure 4.25a, curve SP1-NC represents the average the measurement result of SP1-NC-1, SP1-NC-2, and SP1-NC-3.

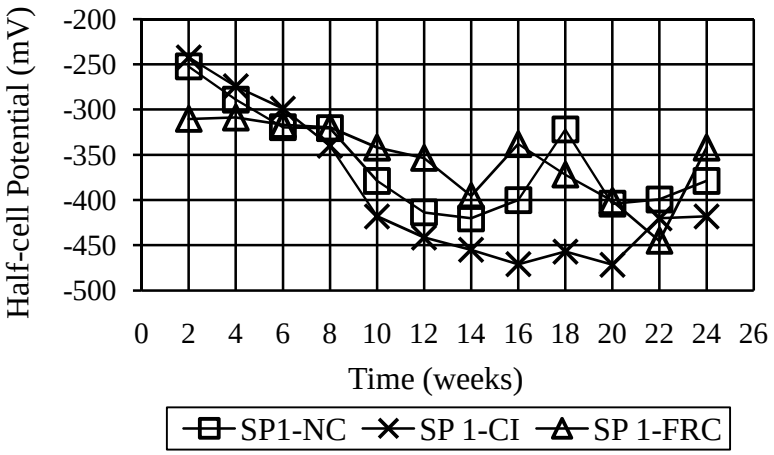

a. 1.5 in. side edge distance

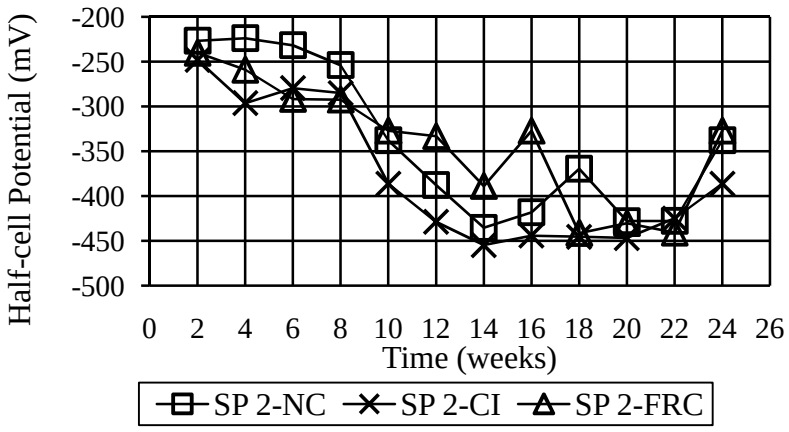

b. 2.5 in. side edge distance

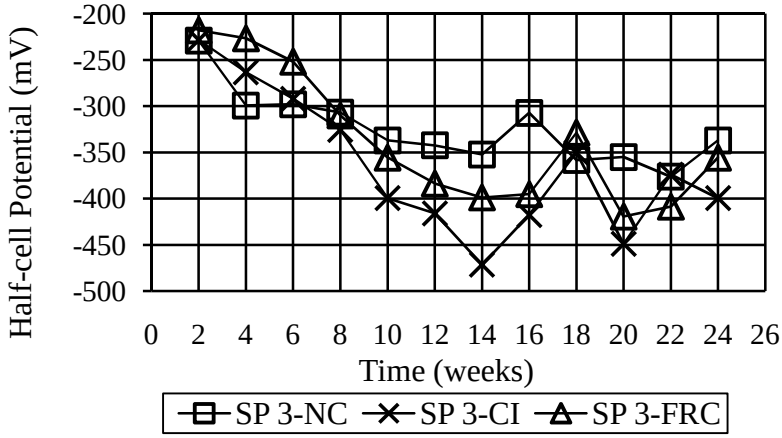

c. 3.5 in. side edge distance

Figure 4.25. Corrosion potential vs. time curve for specimens with different concrete materials

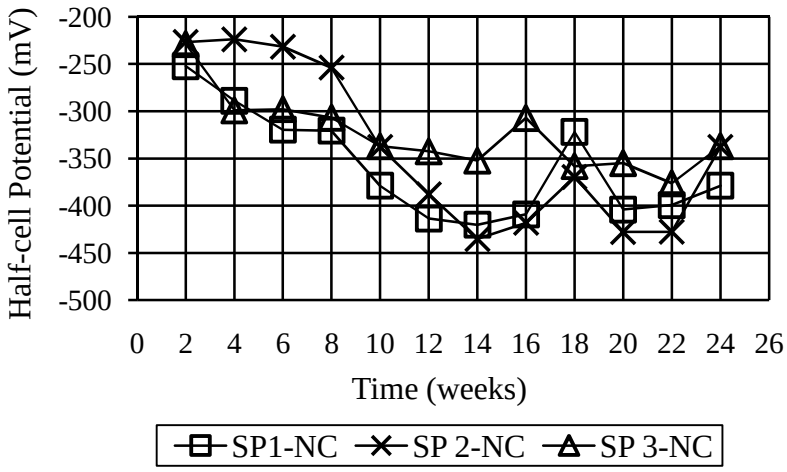

a. Normal Concrete

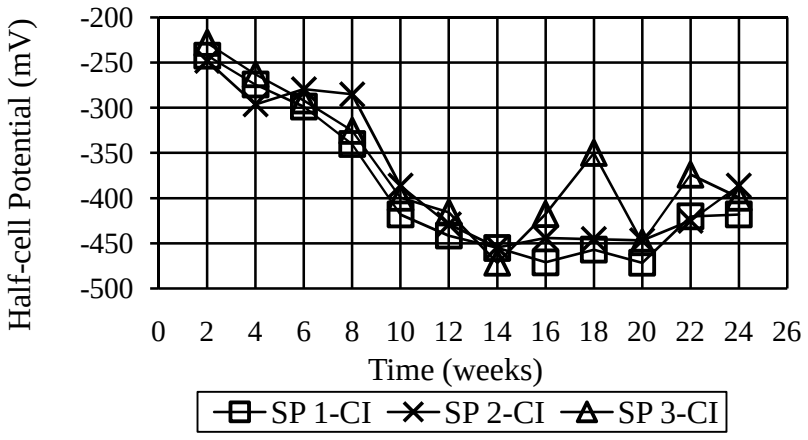

b. Concrete with Corrosion Inhibitor

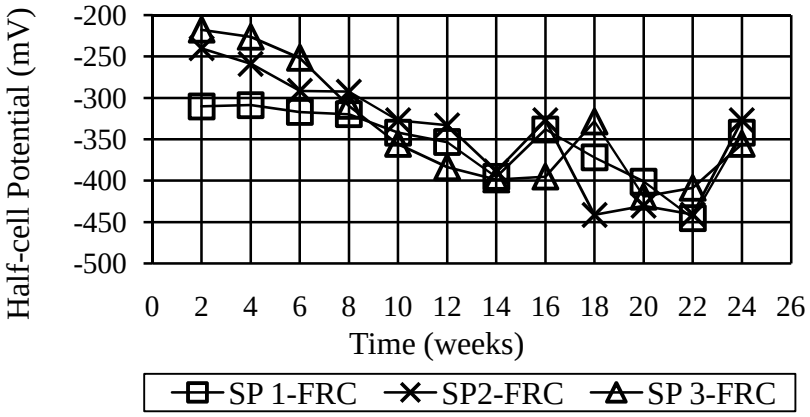

c. Concrete with Fibers

Figure 4.26. Corrosion potential vs. time curve for specimens with different side edge distance

Figure 4.25 shows the relationship between corrosion potential and time for test specimens constructed with the same side edge distance and different concrete type. Irrespective of material properties, all test specimens showed values lower than -200 mV, since the first measurement, which corresponds to a lower limit corrosion probability of at least 50%. Irrespective of side edge distance, specimens containing corrosion inhibitor show the largest (i.e. most negative) corrosion potential values, indicating the highest probability of corrosion compared with specimens with the other two types of concrete material.

Almost all the specimens showed increasing corrosion possibility up to 90% by the fourteenth week. However, fluctuations in the data occurred to some extent from the fourteenth week on. This may be due to the measurement environment with higher temperature and moisture content in the summer. At the end of the testing period, all of them showed lower corrosion possibility than that of fourteenth week. However, that did not make the corrosion possibility much lower than 90%.

Figure 4.26 shows the relationship between corrosion potential and time for test specimens constructed with the same concrete property and different side edge distances. Irrespective of concrete property, specimens with 1.5 in. side edge distance showed higher corrosion possibility than the others generally. However, specimens with 2.5 in. side edge distance do not always show higher possibility than those with 3.5 in. side edge distance. In addition, for specimens with corrosion inhibitor in concrete, all three side edge distances showed nearly the same corrosion possibility with the exception of results of eighteenth week, indicating that the factor of side edge distance had the least influence on specimens with corrosion inhibitor.

4.4. ELECTRICAL RESISTIVITY MEASUREMENT

As discussed in Section 3.4.1.3, the electrical resistivity measurement was conducted every two weeks together with the corrosion potential measurement to investigate and assess the corrosion of steel in specimens subjected to wet-dry cycle test. Table 3.3 was used to interpret the measurement results.

In the following Figures 4.27 and 4.28, each curve represents the average measurement result of the three specimens with the same concrete material type and side

edge distance. For example, in Figure 4.27a, curve SP1-NC represents the average the measure result of SP1-NC-1, SP1-NC-2 and SP1-NC-3. Some data at the fourth, eighth, and sixteenth week are not included since they are too high to be reasonable. Those results are attributed to the sawing operation when samples were cut for chloride content analysis discussed in Section 3.4.1.4. Curves including all the data are included in Figures C.1 and C.2.

Figure 4.27 shows the relationship between electrical resistivity and time for test specimens constructed with the different concrete property and same side edge distance. It can be seen that none of the specimens exhibited a very high possibility (electrical resistivity less than 5 kΩ-cm) of corrosion after six months of testing. Irrespective of side edge distance, specimens with normal concrete show an overall better performance than the others. FRC specimens show a general higher possibility of corrosion than specimens with other concrete types.

Figure 4.28. shows specimens with 1.5 in. side edge distance were the only specimens that showed a high possibility (electrical resistivity larger than 5 kΩ-cm and less than 10 kΩ-cm) of corrosion. Generally, possibility of corrosion of all specimens decreases with the increasing of the side edge distance indicating specimens of larger side edge distance have better resistance to corrosion.

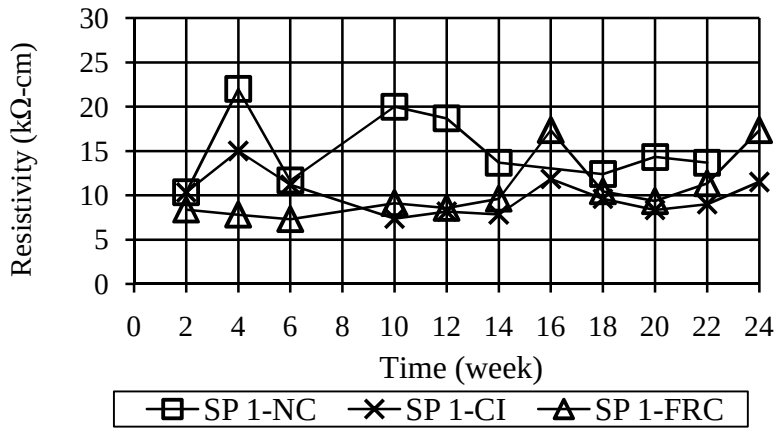

a. 1.5 in. side edge distance

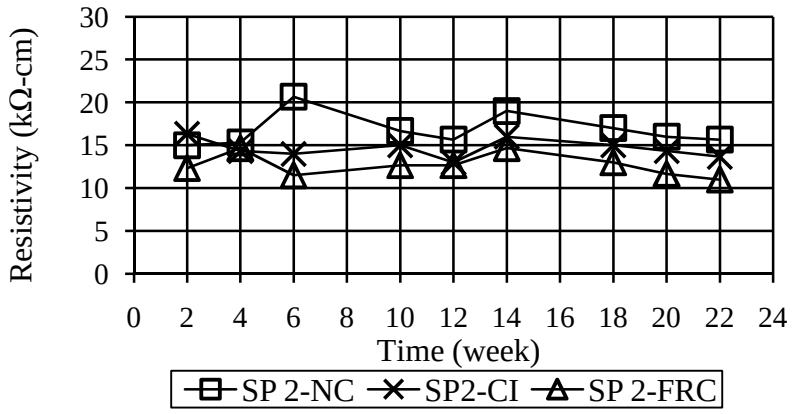

b. 2.5 in. side edge distance

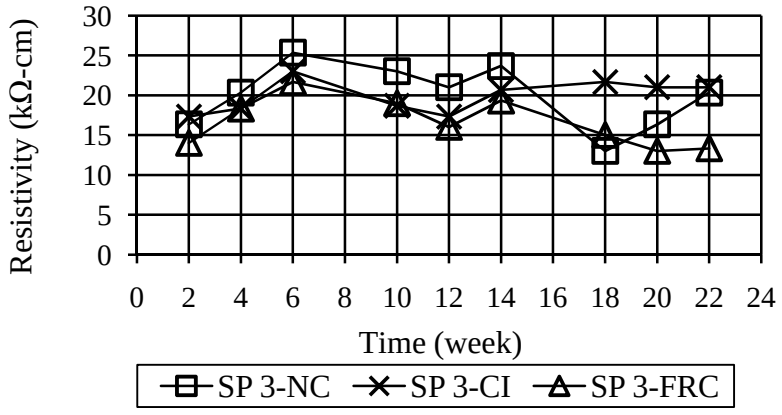

c. 3.5 in. side edge distance

Figure 4.27. Electrical resistivity vs. time curve for specimens with different side edge distances

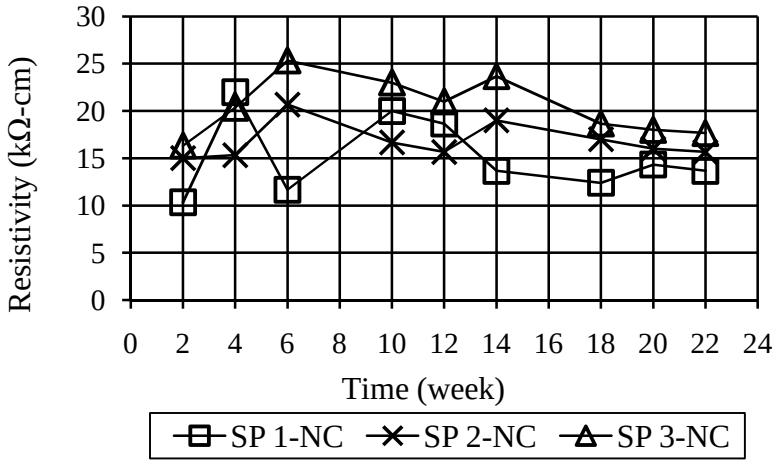

a. Normal Concrete

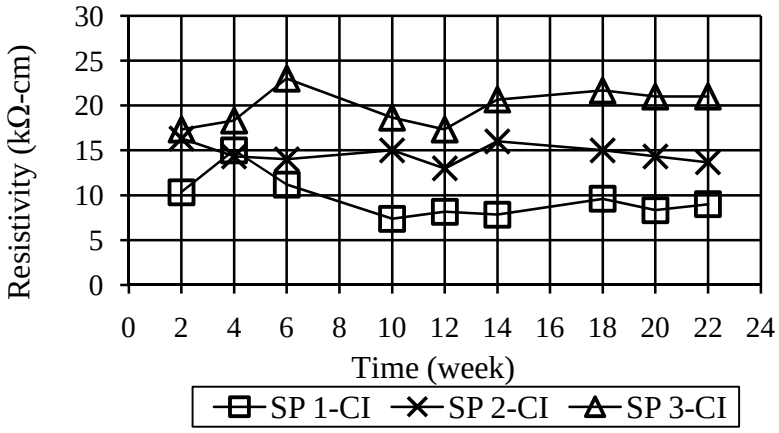

b. Concrete with Corrosion Inhibitor

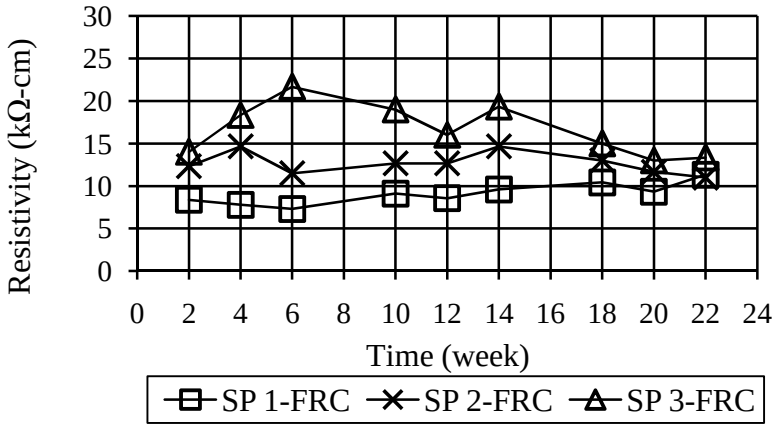

c. Concrete with Fibers

Figure 4.28 Electrical resistivity vs. time curve for specimens with different concrete materials

4.5. CHLORIDE CONTENT MEASUREMENT

As discussed in Section 3.4.1.5, the water soluble chloride content analysis was used every two months to measure the chloride content of specimens subjected to wet-dry cycle test at different depths including 0.5 in. from the surface, mid-distance between the surface and steel location, and at the steel location. From the data collected, the chloride content at different times was examined to determine whether the chloride content is enough to initiate corrosion of the reinforcement.

Figures 4.29 through 4.31 show the measured chloride content of specimens at different locations at two months, four months, and six months, respectively. The chloride ion content test performed at two months was conducted by MoDOT and is presented by Figure 4.29. Chloride contents at different distances from the exposed surface were evaluated as parts per million (ppm) of chloride. ACI 222R specifies that at least 330 ppm of chloride in concrete is required to initiate corrosion in concrete. So from Figure 4.29, data collected at the steel location of all specimens exceeded the threshold value of corrosion initiation at two months. In addition, for normal concrete and FRC specimens, specimens with larger side edge distance have less content of chloride ions at the steel location, which is not the case for specimens with corrosion inhibitor. This also indicates that corrosion inhibitor is not effective to reduce corrosion in this study.

Four-month and six-month chloride tests were conducted at Missouri S&T using rapid chloride test equipment. The unit of measurement used in this chloride test was percentage of chloride by concrete weight. The threshold range for corrosion initiation is 0.025%. In general, measured chloride content increased with increasing time for given depth.

Generally, increase of side edge distance can retard the penetration of chloride in concrete. Specimens with concrete containing corrosion inhibitor showed relatively higher chloride content than the other two types of specimens with respect to each side edge distance. This result is consistent with observation of the corrosion potential test discussed in Section 4.3.

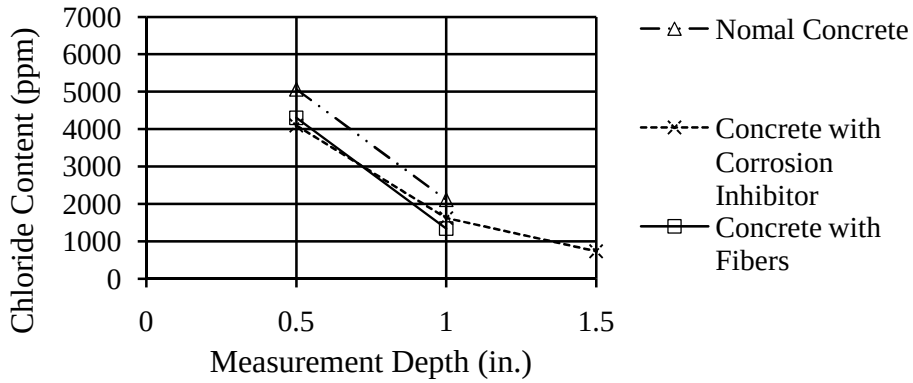

a. 1.5 in. side edge distance

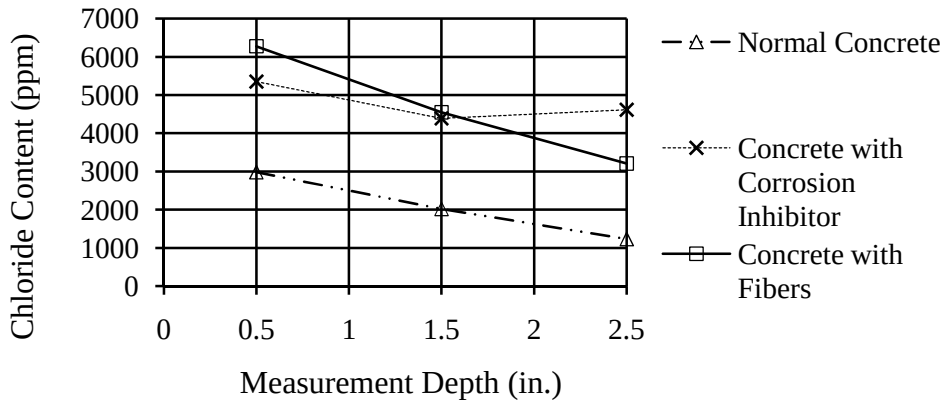

b. 2.5 in. side edge distance

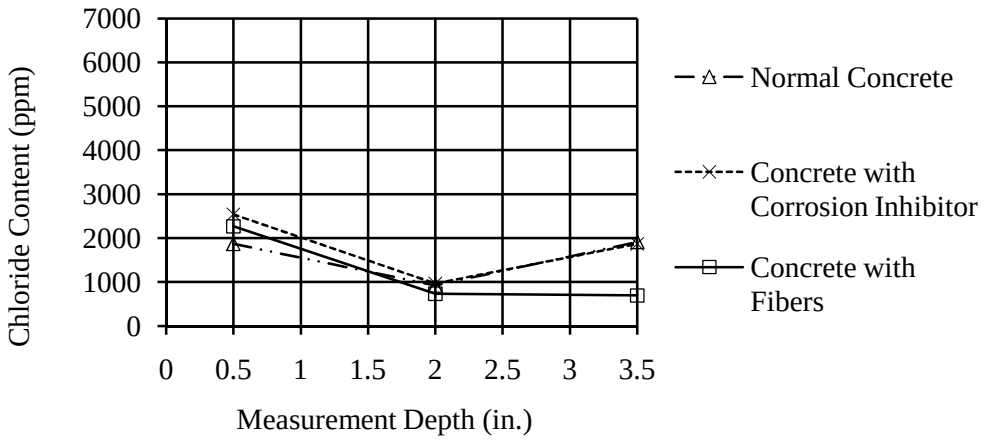

c. 3.5 in. side edge distance

Figure 4.29. Chloride content profiles for two months

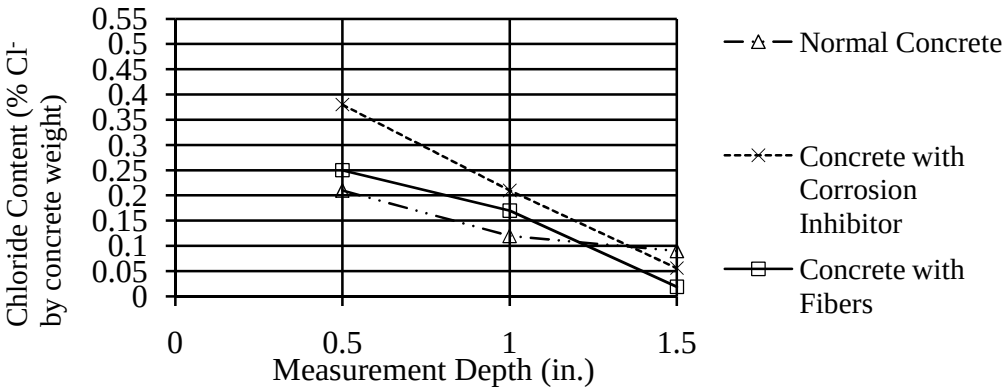

a. 1.5 in. side edge distance

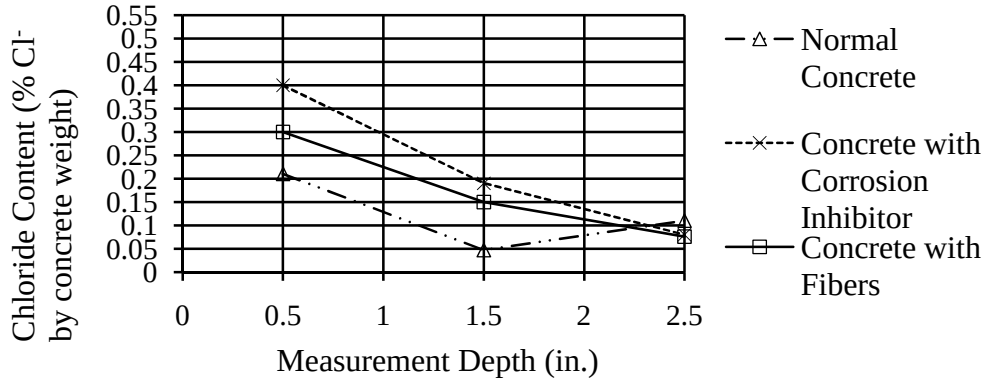

b. 2.5 in. side edge distance

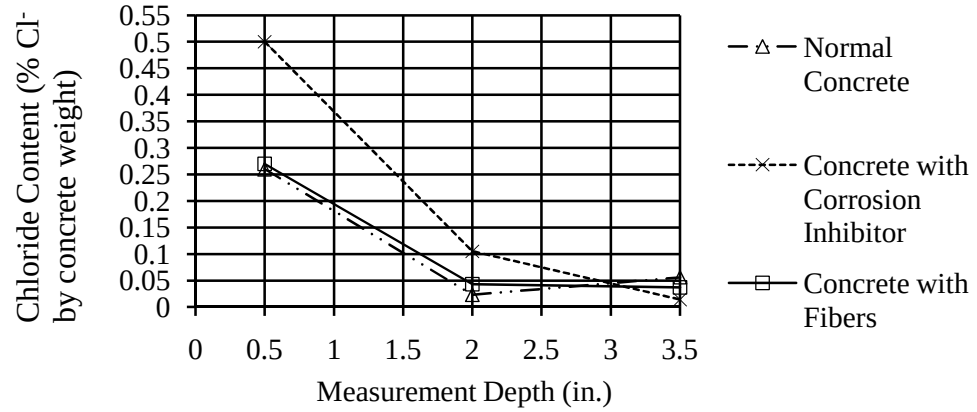

c. 3.5 in. side edge distance

Figure 4.30. Chloride content profiles for four months

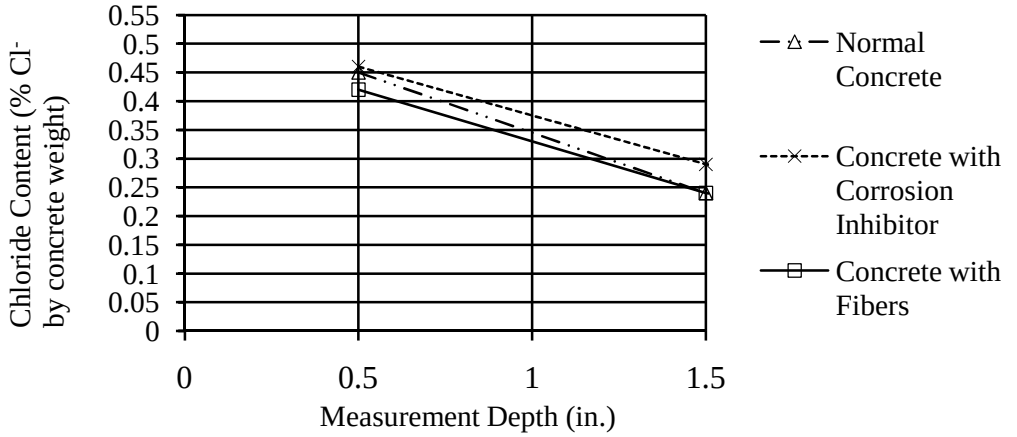

a. Normal Concrete

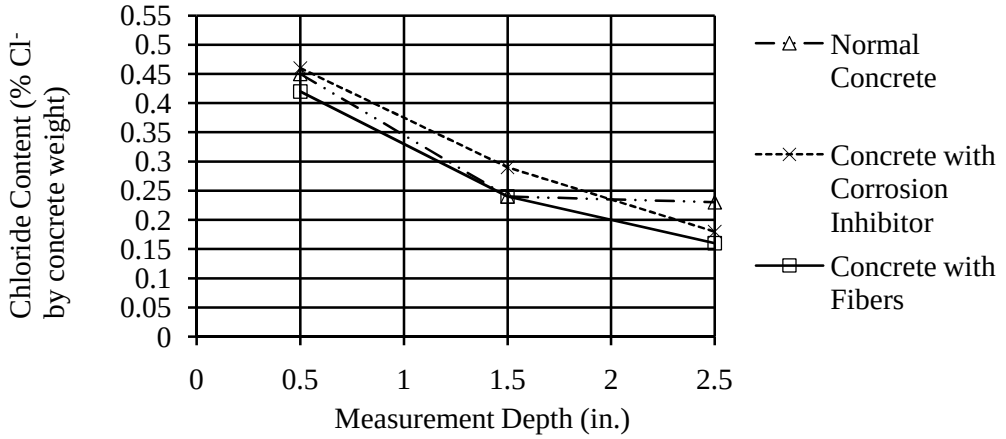

b. Concrete with Corrosion Inhibitor

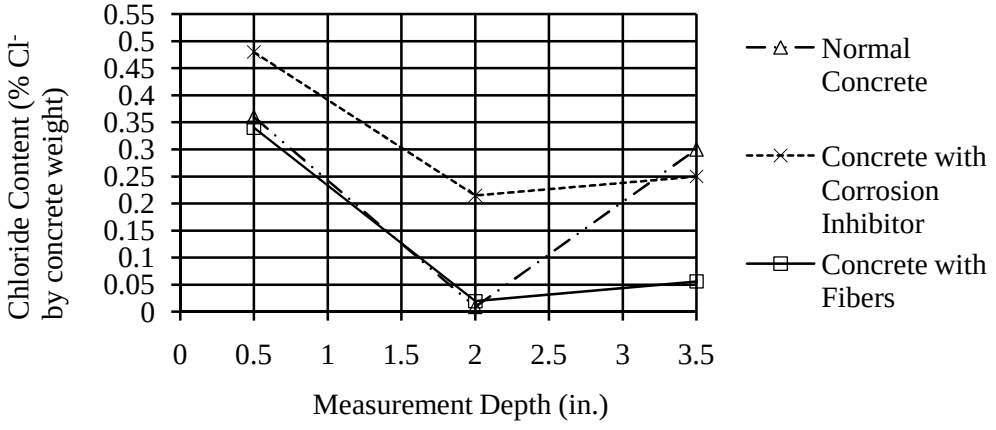

c. Concrete with Fibers

Figure 4.31. Chloride content profiles for six months

4.6. COMPARISON BETWEEN TEST RESULTS AND EI MAADDAWY AND SOUDKI'S MODEL FROM CORROSION INITIATION TO CRACKING

As introduced in Section 2.3.6, EI Maaddawy and Soudki's model can be used to predict the time from corrosion initiation to corrosion cracking by Eq. 2.11. Tables 4.14 through 4.16 show the ratios of the observed to predicted time to corrosion cracking for specimens subjected to accelerated corrosion test, which can assess the effectiveness model in predicting the time of corrosion cracking subjected to low impressed current of 0.4 mA.

Table 4.13. Specimens of normal concrete

Specimens ID	Observed time to cracking (hours)	Time to cracking predicted by EI Maaddawy and Soudki's model (2006) (hours)	Observed time to cracking/ predicted time to cracking
SP1-NC-13	3024	1920-2640	1.15-1.58
SP1-NC-14	1344	1920-2640	0.51-0.70
SP1-NC-15	1344	1920-2640	0.51-0.70
SP1-NC-16	1388	1920-2640	0.53-0.72
SP2-NC-17	2800	1920-2640	1.06-1.46
SP2-NC-18	3024	1920-2640	1.15-1.58
SP2-NC-19	5592	1920-2640	2.12-2.91
SP2-NC-20	2280	1920-2640	0.86-1.19
SP3-NC-21	2880	1920-2640	1.09-1.50
SP3-NC-22	X	1920-2640	X
SP3-NC-23	5184	1920-2640	1.96-2.70
SP3-NC-24	5808	1920-2640	2.20-3.03

Table 4.14. Specimens of concrete with corrosion inhibitor

Specimens ID	Observed time to cracking (hours)	Time to cracking predicted by EI Maaddawy and Soudki's model (2006) (hours)	Observed time to cracking/ predicted time to cracking
SP1-CI-13	3024	1920-2640	1.15-1.58
SP1-CI-14	768	1920-2640	0.29-0.40
SP1-CI-15	1320	1920-2640	0.50-0.69
SP1-CI-16	1320	1920-2640	0.50-0.69
SP2-CI-17	1584	1920-2640	0.60-0.83
SP2-CI-18	X	1920-2640	X
SP2-CI-19	4968	1920-2640	1.88-2.59
SP2-CI-20	2280	1920-2640	0.86-1.19
SP3-CI-21	2880	1920-2640	1.09-1.50
SP3-CI-22	X	1920-2640	X
SP3-CI-23	2280	1920-2640	0.86-1.19
SP3-CI-24	4896	1920-2640	1.85-2.55

Table 4.15. Specimens of concrete with fibers

Specimens ID	Observed time to cracking (hours)	Time to cracking predicted by EI Maaddawy and soudki's model (2006) (hours)	Observed time to cracking/ predicted time to cracking
SP1-FRC-13	1080	1920-2640	0.41-0.56
SP1-FRC-14	2880	1920-2640	1.09-1.50
SP1-FRC-15	4584	1920-2640	1.74-2.39
SP1-FRC-16	2880	1920-2640	1.09-1.50
SP2-FRC-17	3024	1920-2640	1.15-1.58
SP2-FRC-18	3024	1920-2640	1.15-1.58
SP2-FRC-19	5184	1920-2640	1.96-2.70
SP2-FRC-20	2880	1920-2640	1.09-1.50
SP3-FRC-21	X	1920-2640	X
SP3-FRC-22	2880	1920-2640	1.09-1.50
SP3-FRC-23	4480	1920-2640	1.70-2.33
SP3-FRC-24	2880	1920-2640	1.09-1.50

Note: Boxes with X indicate that specimens did not exhibit cracking until being broken for measuring mass loss.

Considering the complication of corrosion process, Tables 4.14 through 4.16 show that the use of EI Maaddawy and Soudki's Model can give a reasonable prediction of time from corrosion initiation to corrosion cracking.

In addition, comparison of Table 4.14 with Tables 4.13 and 4.15 shows that specimens containing corrosion inhibitor did not perform better than the other specimens in terms of time to corrosion cracking.

5. CONCLUSIONS AND RECOMMENDATION FOR FUTURE STUDY

This research study involved spalling problems associated with partial-depth precast concrete deck panels in the MoDOT bridge inventory. As described in Chapter 1, this study was aimed at investigating ways to reduce the corrosion-induced spalling of PPC panels in new construction. The objective of this thesis work was to evaluate the influence of side edge distance and concrete materials on the corrosion-induced spalling behavior of the PPC panels.

Experimental investigation of the effect of factors including concrete side edge distance and concrete material type on steel corrosion in chloride contaminated reinforced concrete was carried out. Section 3.4 discussed two test methods, the wet-dry test and accelerated corrosion test, carried out on a total of sixty-three specimens. Test variables included side cover (measured to centerline of reinforcement, 1.5 in., 2.5 in., or 3.5 in.), and concrete mixture type (normal concrete, concrete with corrosion inhibitor, or concrete with fibers). For specimens subjected to wet-dry cycle test, visual inspection, corrosion potential measurement, electrical resistivity measurement, chloride content analysis and gravimetric study were conducted, as discussed in Section 3.4.1. Results are presented in Sections 4.1.1, 4.3, 4.4, 4.5 and 4.2.1, respectively, to evaluate the effect of the two test variables described in Section 3.2. For specimens subjected to accelerated corrosion test, visual inspection and gravimetric study was conducted as discussed in Section 3.4.2. Results are shown in Sections 4.1.2 and 4.2.2. Based on visual inspection, time from corrosion initiation to corrosion cracking was used to verify the effectiveness of low impressed current in simulating corrosion of prestressing steel reinforcement in concrete. Results from gravimetric study were used to evaluate the effect of the two test variables.

5.1. CONCLUSIONS

Based on results of visual inspection from wet-dry cycle test (Section 4.1.1), corrosion inhibitor added to concrete mixture did not help to enhance resistance to

reinforced concrete specimens against corrosion. On the contrary, specimens with corrosion inhibitor were even more vulnerable to corrosion compared to specimens with normal concrete and fibers. It should be noted, however, that such test results are not representative of the performance of concrete with corrosion inhibitor in service conditions.

Based on results of visual inspection on specimens subjected to accelerated corrosion test (Section 4.1.2), specimens after twelve months of testing period showed much more severe corrosion than those after six months, as expected. In addition, the occurrence of rust, propagation of cracks, and extent of loose concrete were inhibited significantly on the side surfaces with greater concrete cover (i.e. long direction of the cross-section). This indicates that when the dimension of the panel thickness is held constant as in this case (3 in. per the direction of the MoDOT), increasing of side edge distance to reinforcement can improve the corrosion resistance of the bridge deck panel and thus the long term performance in terms of spalling resistance.

Results of gravimetric study of wet-dry cycle test (Section 4.2.1) show that six months may be a too short testing period to cause significant corrosion on specimens.

Results of gravimetric study of accelerated corrosion test (Section 4.2.2) show that Faraday's law can give a reasonable prediction of the mass loss due to corrosion, even though the prediction is not so accurate when the impressed current is much less than the effective range provided by Tamer and Khaled (2003).

Results from corrosion potential measurement (Section 4.3) show that specimens with concrete containing corrosion inhibitor exhibited generally higher corrosion possibility than the other two types of specimens (specimen with normal concrete and specimens of concrete with fibers). These findings are consistent with the visual inspection results of specimens subjected to wet-dry cycle test (Conclusion 1).

Results from electrical resistivity measurement (Section 4.4) show that possibility of corrosion of all specimens decreases with increasing side edge distance, even when panel thickness is held constant.

Results from chloride content measurement and analysis (Section 4.5) show that larger side edge distance can retard the penetration of chloride ions in concrete, even when panel thickness is held constant. These results are consistent with the observation of

electrical resistivity test (Conclusion 6). Secondly, specimens with concrete containing corrosion inhibitor showed relatively higher chloride content than the other two types of specimens with respect to each side edge distance. This result is consistent with observation of the corrosion potential test discussed in Conclusion 5 and Section 4.3.

According to the visual inspection results on specimens subjected to accelerated corrosion test (Section 4.6), EI Maaddawy and Soudki's model can give a reasonable prediction of the time from corrosion initiation to corrosion cracking, considering the complication of the corrosion process itself and despite the relatively low impressed current.

5.2. RECOMMENDATIONS TO MODOT

1. In 3 in. thick precast-prestressed bridge deck panels currently specified by MoDOT, the specified minimum side edge distance to tendon should be increased from the current minimum of 1.5 in.
2. The addition of synthetic fiber and/or corrosion inhibitor to the concrete mixture is not recommended because it did not reduce the deterioration level compared with normal concrete, which is currently specified.

5.3. RECOMMENDATIONS FOR FUTURE STUDIES

1. In addition to the corrosion monitoring techniques used in this test, such as corrosion potential measurement, electrical resistivity measurement, chloride content measurement, and gravimetric study, linear polarization technique could be used to determine corrosion current density and give more accurate data of instantaneous corrosion rate.
2. For the wet-dry cycle test, testing period of more than two years is suggested to cause significantly corrosion in the steel reinforcement.

APPENDIX A

GRAVIMETRIC STUDY OF WET-DRY CYCLE TEST

A. GRAVIMETRIC STUDY OF WET-DRY CYCLE TEST

This appendix provides test results of the gravimetric study on twenty-seven specimens subjected to wet-dry cycle test as described in Section 3.4.1.5 and summarized in Section 4.2.1.

Table A.1. Mass Loss and Corrosion Rate for Specimens Subjected to Wet-dry Cycle Test

Specimens ID	Reinforcement initial mass (g)	Reinforcement final mass (g)	Reinforcement mass loss (g)
SP1-NC-1	142.0	141.1	0.9
SP1-NC-2	142.0	139.3	2.7
SP1-NC-3	142.0	142.0	0.0
SP1-CI-1	142.0	141.5	0.5
SP1-CI-2	140.6	140.6	0.0
SP1-CI-3	142.0	140.6	1.4
SP1-FRC-1	140.6	140.6	0.0
SP1-FRC-2	142.0	142.0	0.0
SP1-FRC-3	140.2	140.2	0.0
SP2-NC-5	140.2	140.0	0.2
SP2-NC-6	142.0	140.6	1.4
SP2-NC-7	140.6	139.3	1.3
SP2-CI-5	141.5	141.1	0.4
SP2-CI-6	141.5	141.5	0.0
SP2-CI-7	141.5	141.5	0.0
SP2-FRC-5	141.5	141.1	0.4
SP2-FRC-6	142.0	141.1	0.9
SP2-FRC-7	141.1	140.2	0.9
SP3-NC-9	140.6	139.7	0.9
SP3-NC-10	142.0	141.1	0.9
SP3-NC-11	140.6	140.6	0.0
SP3-CI-9	141.5	140.6	0.9
SP3-CI-10	142.0	142.0	0.0
SP3-CI-11	140.6	140.6	0.0
SP3-FRC-9	142.0	141.5	0.5
SP3-FRC-10	142.4	141.5	0.9
SP3-FRC-11	141.5	140.6	0.9

APPENDIX B

GRAVIMETRIC STUDY OF ACCELERATED CORROSION TEST

B. GRAVIMETRIC STUDY OF ACCELERATED CORROSION TEST

This appendix provides detailed test results of the eighteen specimens subjected accelerated corrosion test for six months and other eighteen for twelve months as described in Section 3.4.2.2 and summarized in Section 4.2.2.

Table B.1. Mass Loss of Reinforcement in Specimens with Sodium Chloride Content of 3% Subjected to Impressed Current of 0.4 mA for Six Months.

Specimens ID	Reinforcement initial mass (g)	Reinforcement final mass (g)	Measured mass loss (g)	Predicted mass loss (g)
SP1-NC-13	141.52	139.71	1.81	1.86
SP1-NC-14	141.97	139.71	2.26	1.86
SP1-CI-13	140.15	138.80	1.35	1.86
SP1-CI-14	140.15	134.72	5.43	1.86
SP1-FRC-13	141.51	138.80	2.71	1.86
SP1-FRC-14	140.61	138.35	2.26	1.86
SP2-NC-17	140.61	137.89	2.72	1.86
SP2-NC-18	139.70	136.99	2.71	1.86
SP2-CI-17	140.15	136.99	3.16	1.86
SP2-CI-18	140.61	140.16	0.45	1.86
SP2-FRC-17	140.15	135.17	4.98	1.86
SP2-FRC-18	139.70	133.81	5.89	1.86
SP3-NC-21	139.70	138.80	0.90	1.86
SP3-NC-22	141.97	140.62	1.35	1.86
SP3-CI-21	141.97	141.52	0.45	1.86
SP3-CI-22	139.70	138.80	0.90	1.86
SP3-FRC-21	142.42	140.62	1.80	1.86
SP3-FRC-22	141.06	137.44	3.62	1.86

Table B.2. Mass Loss of Reinforcement in Specimens with Sodium Chloride Content of 3% Subjected to Impressed Current of 0.4 mA for Twelve Months

Specimens ID	Reinforcement initial mass (g)	Reinforcement final mass (g)	Measured mass loss (g)	Predicted mass loss (g)
SP1-NC-15	141.97	134.80	7.17	3.72
SP1-NC-16	139.70	139.64	0.10	3.72
SP1-CI-15	140.61	138.71	1.90	3.72
SP1-CI-16	141.97	139.40	2.57	3.72
SP1-FRC-15	139.70	138.80	0.90	3.72
SP1-FRC-16	140.15	136.01	4.14	3.72
SP2-NC-19	140.15	139.73	0.42	3.72
SP2-NC-20	141.06	138.67	2.39	3.72
SP2-CI-19	140.61	139.55	1.11	3.72
SP2-CI-20	140.15	134.52	5.65	3.72
SP2-FRC-19	139.70	136.41	3.30	3.72
SP2-FRC-20	140.15	140.02	0.15	3.72
SP3-NC-23	140.61	138.62	1.99	3.72
SP3-NC-24	141.97	139.64	2.33	3.72
SP3-CI-23	139.70	137.90	1.80	3.72
SP3-CI-24	141.51	140.28	1.31	3.72
SP3-FRC-23	142.42	139.44	2.98	3.72
SP3-FRC-24	140.61	138.33	2.31	3.72

APPENDIX C

CORROSION POTENTIAL MEASUREMENT

C. CORROSION POTENTIAL MEASUREMENT

This appendix provides complete test results of the corrosion potential measurement on the twenty-seven specimens subjected to wet-dry cycle test as described in Section 3.4.1.2 and summarized in Section 4.3.

Table C.1 Corrosion potential measurement (mV)

Specimen ID	Week							
	2				4			
SP1-NC-1	-242	-235	-238.5		-300	-298	-299.0	
SP1-NC-2	-273	-265	-269.0	-252.3	-273	-274	-273.5	-289.0
SP1-NC-3	-254	-245	-249.5		-299	-290	-294.5	
SP1-CI-1	-244	-242	-243.0		-232	-226	-229.0	
SP1-CI-2	-240	-245	-242.5	-242.3	-331	-347	-339.0	-274.3
SP1-CI-3	-243	-240	-241.5		-260	-250	-255.0	
SP1-FRC-1	-351	-337	-344.0		-347	-392	-369.5	
SP1-FRC-2	-346	-329	-337.5	-310.3	-251	-362	-306.5	-308.8
SP1-FRC-3	-253	-246	-249.5		-251	-250	-250.5	
SP2-NC-5	-237	-234	-235.5		-241	-245	-243.0	
SP2-NC-6	-230	-232	-231.0	-226.8	-218	-222	-220.0	-223.8
SP2-NC-7	-215	-213	-214.0		-213	-204	-208.5	
SP2-CI-5	-211	-228	-219.5		-221	-212	-216.5	
SP2-CI-6	-313	-312	-312.5	-248.0	-337	-338	-337.5	-296.3
SP2-CI-7	-212	-212	-212.0		-330	-340	-335.0	
SP2-FRC-5	-254	-257	-255.5		-330	-326	-328.0	
SP2-FRC-6	-221	-222	-221.5	-240.2	-217	-205	-211.0	-259.0
SP2-FRC-7	-244	-243	-243.5		-235	-241	-238.0	
SP3-NC-9	-228	-230	-229.0		-358	-363	-360.5	
SP3-NC-10	-222	-224	-223.0	-229.0	-210	-220	-215.0	-299.2
SP3-NC-11	-237	-233	-235.0		-316	-328	-322.0	
SP3-CI-9	-243	-242	-242.5		-330	-337	-333.5	
SP3-CI-10	-245	-244	-244.5	-228.3	-257	-262	-259.5	-263.2
SP3-CI-11	-196	-200	-198.0		-201	-192	-196.5	
SP3-FRC-9	-215	-216	-215.5		-219	-218	-218.5	
SP3-FRC-10	-229	-223	-226.0	-217.8	-221	-232	-226.5	-226.5
SP3-FRC-11	-212	-212	-212.0		-232	-237	-234.5	

Table C.1 (continued)

Specimen ID	Week							
	6				8			
SP1-NC-1	-250	-246	-248.0	-319.5	-287	-296	-291.5	-320.7
SP1-NC-2	-316	-310	-313.0		-307	-307	-307.0	
SP1-NC-3	-364	-431	-397.5		-343	-384	-363.5	
SP1-CI-1	-219	-235	-227.0	-298.8	-234	-237	-235.5	-340.2
SP1-CI-2	-346	-381	-363.5		-379	-411	-395.0	
SP1-CI-3	-301	-311	-306.0		-378	-402	-390.0	
SP1-FRC-1	-335	-378	-356.5	-317.0	-332	-369	-350.5	-319.8
SP1-FRC-2	-331	-384	-357.5		-364	-401	-382.5	
SP1-FRC-3	-235	-239	-237.0		-228	-225	-226.5	
SP2-NC-5	-231	-234	-232.5	-231.7	-217	-220	-218.5	-253.8
SP2-NC-6	-231	-233	-232.0		-274	-283	-278.5	
SP2-NC-7	-228	-233	-230.5		-263	-266	-264.5	
SP2-CI-5	-202	-190	-196.0	-279.5	-237	-243	-240.0	-285.2
SP2-CI-6	-325	-329	-327.0		-259	-283	-271.0	
SP2-CI-7	-312	-319	-315.5		-341	-348	-344.5	
SP2-FRC-5	-321	-322	-321.5	-291.7	-313	-324	-318.5	-292.5
SP2-FRC-6	-341	-333	-337.0		-338	-348	-343.0	
SP2-FRC-7	-221	-212	-216.5		-217	-215	-216.0	
SP3-NC-9	-344	-362	-353.0	-297.8	-355	-366	-360.5	-306.8
SP3-NC-10	-190	-186	-188.0		-172	-175	-173.5	
SP3-NC-11	-346	-359	-352.5		-379	-394	-386.5	
SP3-CI-9	-405	-434	-419.5	-292.0	-457	-469	-463.0	-325.5
SP3-CI-10	-275	-276	-275.5		-298	-302	-300.0	
SP3-CI-11	-181	-181	-181.0		-215	-212	-213.5	
SP3-FRC-9	-248	-241	-244.5	-251.8	-306	-301	-303.5	-309.8
SP3-FRC-10	-247	-237	-242.0		-275	-279	-277.0	
SP3-FRC-11	-267	-271	-269.0		-347	-351	-349.0	

Table C.1 (continued)

Specimen ID	Week							
	10				12			
SP1-NC-1	-351	-393	-372.0	-378.8	-409	-362	-385.5	-413.7
SP1-NC-2	-392	-429	-410.5		-476	-411	-443.5	
SP1-NC-3	-340	-368	-354.0		-450	-374	-412.0	
SP1-CI-1	-395	-426	-410.5	-418.2	-451	-407	-429.0	-441.5
SP1-CI-2	-396	-438	-417.0		-485	-408	-446.5	
SP1-CI-3	-409	-445	-427.0		-472	-426	-449.0	
SP1-FRC-1	-365	-405	-385.0	-342.0	-412	-368	-390.0	-353.5
SP1-FRC-2	-375	-402	-388.5		-434	-388	-411.0	
SP1-FRC-3	-257	-248	-252.5		-267	-252	-259.5	
SP2-NC-5	-360	-374	-367.0	-337.8	-408	-396	-402.0	-387.8
SP2-NC-6	-328	-340	-334.0		-383	-363	-373.0	
SP2-NC-7	-312	-313	-312.5		-394	-383	-388.5	
SP2-CI-5	-374	-384	-379.0	-386.2	-421	-406	-413.5	-428.8
SP2-CI-6	-391	-423	-407.0		-461	-423	-442.0	
SP2-CI-7	-357	-388	-372.5		-454	-408	-431.0	
SP2-FRC-5	-348	-356	-352.0	-327.2	-356	-345	-350.5	-333.2
SP2-FRC-6	-365	-379	-372.0		-399	-378	-388.5	
SP2-FRC-7	-257	-258	-257.5		-259	-262	-260.5	
SP3-NC-9	-405	-419	-412.0	-337.0	-416	-409	-412.5	-342.3
SP3-NC-10	-195	-204	-199.5		-193	-189	-191.0	
SP3-NC-11	-396	-403	-399.5		-426	-421	-423.5	
SP3-CI-9	-505	-542	-523.5	-399.5	-487	-455	-471.0	-415.8
SP3-CI-10	-387	-405	-396.0		-459	-432	-445.5	
SP3-CI-11	-283	-275	-279.0		-331	-331	-331.0	
SP3-FRC-9	-351	-362	-356.5	-355.7	-354	-349	-351.5	-383.7
SP3-FRC-10	-291	-285	-288.0		-372	-363	-367.5	
SP3-FRC-11	-413	-432	-422.5		-445	-419	-432.0	

Table C.1 (continued)

Specimen ID	Week							
	14				16			
SP1-NC-1	-429	-370	-399.5	-420.2	-430	-370	-400.0	-409.2
SP1-NC-2	-481	-416	-448.5		-431	-390	-410.5	
SP1-NC-3	-447	-378	-412.5		-446	-388	-417.0	
SP1-CI-1	-481	-411	-446.0	-455.2	-507	-426	-466.5	-471.0
SP1-CI-2	-490	-407	-448.5		-488	-422	-455.0	
SP1-CI-3	-491	-451	-471.0		-525	-458	-491.5	
SP1-FRC-1	-446	-394	-420.0	-395.5	-421	-376	-398.5	-338.2
SP1-FRC-2	-421	-384	-402.5		-411	-359	-385.0	
SP1-FRC-3	-372	-356	-364.0		-235	-227	-231.0	
SP2-NC-5	-482	-431	-456.5	-435.3	-479	-433	-456.0	-418.2
SP2-NC-6	-394	-374	-384.0		-342	-333	-337.5	
SP2-NC-7	-493	-438	-465.5		-488	-434	-461.0	
SP2-CI-5	-480	-442	-461.0	-454.7	-451	-424	-437.5	-444.2
SP2-CI-6	-493	-435	-464.0		-485	-435	-460.0	
SP2-CI-7	-465	-413	-439.0		-452	-418	-435.0	
SP2-FRC-5	-392	-371	-381.5	-388.8	-408	-392	-400.0	-327.2
SP2-FRC-6	-469	-431	-450.0		-419	-392	-405.5	
SP2-FRC-7	-339	-331	-335.0		-185	-167	-176.0	
SP3-NC-9	-438	-414	-426.0	-352.2	-443	-415	-429.0	-307.2
SP3-NC-10	-203	-206	-204.5		-161	-160	-160.5	
SP3-NC-11	-439	-413	-426.0		-341	-323	-332.0	
SP3-CI-9	-559	-501	-530.0	-471.5	-503	-469	-486.0	-417.7
SP3-CI-10	-502	-462	-482.0		-400	-357	-378.5	
SP3-CI-11	-406	-399	-402.5		-389	-388	-388.5	
SP3-FRC-9	-354	-351	-352.5	-398.7	-375	-362	-368.5	-395.2
SP3-FRC-10	-425	-407	-416.0		-440	-418	-429.0	
SP3-FRC-11	-441	-414	-427.5		-396	-380	-388.0	

Table C.1 (continued)

Specimen ID	Week							
	18				20			
SP1-NC-1	-452	-380	-416.0	-322.0`	-357	-425	-391.0	-404.2
SP1-NC-2	-258	-227	-242.5		-352	-365	-358.5	
SP1-NC-3	-318	-297	-307.5		-449	-477	-463.0	
SP1-CI-1	-524	-441	-482.5	-457.0	-499	-470	-484.5	-471.5
SP1-CI-2	-491	-385	-438.0		-490	-445	-467.5	
SP1-CI-3	-496	-405	-450.5		-426	-499	-462.5	
SP1-FRC-1	-378	-344	-361.0	-372.0	-495	-415	-455.0	-401.2
SP1-FRC-2	-423	-360	-391.5		-392	-355	-373.5	
SP1-FRC-3	-376	-351	-363.5		-360	-390	-375.0	
SP2-NC-5	-261	-261	-261.0	-369.5	-492	-430	-461.0	-427.8
SP2-NC-6	-349	-342	-345.5		-360	-358	-359.0	
SP2-NC-7	-529	-475	-502.0		-477	-450	-463.5	
SP2-CI-5	-448	-420	-434.0	-445.3	-455	-416	-435.5	-446.8
SP2-CI-6	-478	-428	-453.0		-474	-436	-455.0	
SP2-CI-7	-477	-421	-449.0		-480	-420	-450.0	
SP2-FRC-5	-447	-423	-435.0	-441.3	-450	-438	-444.0	-430.3
SP2-FRC-6	-470	-420	-445.0		-443	-391	-417.0	
SP2-FRC-7	-448	-440	-444.0		-424	-436	-430.0	
SP3-NC-9	-382	-365	-373.5	-358.2	-354	-364	-359.0	-355.0
SP3-NC-10	-229	-218	-223.5		-244	-242	-243.0	
SP3-NC-11	-507	-448	-477.5		-490	-436	-463.0	
SP3-CI-9	-491	-441	-466.0	-350.2	-456	-401	-428.5	-449.0
SP3-CI-10	-326	-280	-303.0		-487	-486	-486.5	
SP3-CI-11	-288	-275	-281.5		-443	-421	-432.0	
SP3-FRC-9	-381	-380	-380.5	-328.5	-387	-386	-386.5	-419.3
SP3-FRC-10	-468	-424	-446.0		-474	-473	-473.5	
SP3-FRC-11	-166	-152	-159.0		-388	-408	-398.0	

Table C.1 (continued)

Specimen ID	Week							
	22				24			
SP1-NC-1	-375	-470	-422.5	-399.3	-351	-393	-372.0	-378.8
SP1-NC-2	-377	-335	-356.0		-392	-429	-410.5	
SP1-NC-3	-379	-460	-419.5		-340	-368	-354.0	
SP1-CI-1	-424	-379	-401.5	-420.2	-395	-426	-410.5	-418.2
SP1-CI-2	-470	-397	-433.5		-396	-438	-417.0	
SP1-CI-3	-463	-388	-425.5		-409	-445	-427.0	
SP1-FRC-1	-490	-448	-469.0	-445.2	-365	-405	-385.0	-342.0
SP1-FRC-2	-441	-505	-473.0		-375	-402	-388.5	
SP1-FRC-3	-375	-412	-393.5		-257	-248	-252.5	
SP2-NC-5	-489	-416	-452.5	-427.7	-360	-374	-367.0	-337.8
SP2-NC-6	-384	-375	-379.5		-328	-340	-334.0	
SP2-NC-7	-479	-423	-451.0		-312	-313	-312.5	
SP2-CI-5	-413	-485	-449.0	-425.0	-374	-384	-379.0	-386.2
SP2-CI-6	-487	-448	-467.5		-391	-423	-407.0	
SP2-CI-7	-440	-277	-358.5		-357	-388	-372.5	
SP2-FRC-5	-470	-465	-467.5	-440.8	-348	-356	-352.0	-327.2
SP2-FRC-6	-397	-465	-431.0		-365	-379	-372.0	
SP2-FRC-7	-417	-431	-424.0		-257	-258	-257.5	
SP3-NC-9	-366	-382	-374.0	-376.3	-405	-419	-412.0	-337.0
SP3-NC-10	-275	-266	-270.5		-195	-204	-199.5	
SP3-NC-11	-519	-450	-484.5		-396	-403	-399.5	
SP3-CI-9	-392	-443	-417.5	-374.0	-505	-542	-523.5	-399.5
SP3-CI-10	-478	-405	-441.5		-387	-405	-396.0	
SP3-CI-11	-271	-255	-263.0		-283	-275	-279.0	
SP3-FRC-9	-393	-392	-392.5	-408.7	-351	-362	-356.5	-355.7
SP3-FRC-10	-463	-421	-442.0		-291	-285	-288.0	
SP3-FRC-11	-381	-402	-391.5		-413	-432	-422.5	

APPENDIX D

ELECTRICAL RESISTIVITY MEASUREMENT

D. ELECTRICAL RESISTIVITY MEASUREMENT

This appendix provides complete test results of the electrical resistivity measurement on the twenty-seven specimens subjected to wet-dry cycle test as described in Section 3.4.1.3 and summarized in Section 4.4.

Table D.1. Electrical resistivity measurement (kΩ-cm)

Specimen ID	Week					
	2		4		6	
SP1-NC-1	5.80	10.33	19.00	22.00	13.00	11.67
SP1-NC-2	5.00		11.00		11.00	
SP1-NC-3	12.00		36.00		11.00	
SP1-CI-1	14.00	10.33	19.00	15.00	8.60	11.20
SP1-CI-2	7.00		14.00		14.00	
SP1-CI-3	10.00		12.00		11.00	
SP1-FRC-1	9.00	8.37	8.50	7.80	8.10	7.30
SP1-FRC-2	9.00		5.80		6.50	
SP1-FRC-3	7.10		9.10		7.30	
SP2-NC-5	17.00	15.00	16.00	15.33	29.00	20.67
SP2-NC-6	15.00		12.00		14.00	
SP2-NC-7	13.00		18.00		19.00	
SP2-CI-5	10.00	16.33	12.00	14.33	11.00	14.00
SP2-CI-6	21.00		18.00		16.00	
SP2-CI-7	18.00		13.00		15.00	
SP2-FRC-5	10.00	12.33	14.00	14.67	11.00	11.50
SP2-FRC-6	12.00		15.00		12.00	
SP2-FRC-7	15.00		15.00		14.00	
SP3-NC-9	18.00	16.33	23.00	20.33	25.00	25.33
SP3-NC-10	16.00		20.00		28.00	
SP3-NC-11	15.00		18.00		23.00	
SP3-CI-9	20.00	17.33	17.00	18.33	24.00	23.00
SP3-CI-10	15.00		18.00		25.00	
SP3-CI-11	17.00		20.00		20.00	
SP3-FRC-9	12.00	14.00	16.00	18.33	27.00	21.67
SP3-FRC-10	15.00		21.00		19.00	
SP3-FRC-11	15.00		18.00		19.00	

Table D.1 (continued)

Specimen ID	Week					
	8		10		12	
SP1-NC-1	14.00	18.00	31.00	20.00	34.00	18.67
SP1-NC-2	17.00		14.00		11.00	
SP1-NC-3	19.00		15.00		11.00	
SP1-CI-1	17.00	18.00	9.30	7.37	12.00	8.17
SP1-CI-2	20.00		6.40		5.80	
SP1-CI-3	17.00		6.40		6.70	
SP1-FRC-1	15.00	16.00	6.30	9.10	6.60	8.57
SP1-FRC-2	18.00		11.00		9.10	
SP1-FRC-3	15.00		10.00		10.00	
SP2-NC-5	32.00	31.00	17.00	16.67	16.00	15.67
SP2-NC-6	28.00		19.00		17.00	
SP2-NC-7	33.00		14.00		14.00	
SP2-CI-5	19.00	22.33	19.00	15.00	16.00	13.00
SP2-CI-6	25.00		14.00		12.00	
SP2-CI-7	23.00		12.00		11.00	
SP2-FRC-5	21.00	22.67	14.00	12.67	15.00	12.67
SP2-FRC-6	21.00		11.00		11.00	
SP2-FRC-7	26.00		13.00		12.00	
SP3-NC-9	37.00	39.00	18.00	23.00	22.00	21.00
SP3-NC-10	45.00		27.00		23.00	
SP3-NC-11	35.00		24.00		18.00	
SP3-CI-9	29.00	30.33	17.00	18.67	15.00	17.33
SP3-CI-10	30.00		20.00		18.00	
SP3-CI-11	32.00		19.00		19.00	
SP3-FRC-9	27.00	28.33	19.00	19.00	15.00	16.00
SP3-FRC-10	29.00		18.00		15.00	
SP3-FRC-11	29.00		20.00		18.00	

Table D.1 (continued)

Specimen ID	Week					
	14		16		18	
SP1-NC-1	19.00		54.00		19.00	
SP1-NC-2	13.00	13.67	20.00	30.00	8.20	12.40
SP1-NC-3	9.00		16.00		10.00	
SP1-CI-1	9.70		14.00		12.00	
SP1-CI-2	5.50	7.83	9.50	11.83	4.80	9.60
SP1-CI-3	8.30		12.00		12.00	
SP1-FRC-1	8.00		13.00		8.00	
SP1-FRC-2	9.80	9.60	22.00	17.33	9.30	10.43
SP1-FRC-3	11.00		17.00		14.00	
SP2-NC-5	20.00		29.00		21.00	
SP2-NC-6	21.00	19.00	31.00	28.00	17.00	17.00
SP2-NC-7	16.00		24.00		13.00	
SP2-CI-5	22.00		30.00		21.00	
SP2-CI-6	14.00	16.00	19.00	22.00	11.00	15.00
SP2-CI-7	12.00		17.00		13.00	
SP2-FRC-5	16.00		21.00		13.00	
SP2-FRC-6	13.00	14.67	19.00	20.33	13.00	13.00
SP2-FRC-7	15.00		21.00		13.00	
SP3-NC-9	22.00		33.00		17.00	
SP3-NC-10	24.00	23.67	44.00	34.67	18.00	18.67
SP3-NC-11	25.00		27.00		21.00	
SP3-CI-9	19.00		24.00		17.00	
SP3-CI-10	20.00	20.67	30.00	30.33	20.00	21.67
SP3-CI-11	23.00		37.00		28.00	
SP3-FRC-9	20.00		35.00		16.00	
SP3-FRC-10	18.00	19.33	27.00	31.00	12.00	15.00
SP3-FRC-11	20.00		31.00		17.00	

Table D.1 (continued)

Specimen ID	Week					
	20		22		24	
SP1-NC-1	20.00	14.33	18.00	13.67	54.00	28.33
SP1-NC-2	10.00		11.00		20.00	
SP1-NC-3	13.00		12.00		11.00	
SP1-CI-1	11.00	8.33	10.00	9.00	14.00	11.50
SP1-CI-2	3.00		5.00		8.50	
SP1-CI-3	11.00		12.00		12.00	
SP1-FRC-1	7.00	9.33	9.00	11.33	13.00	17.33
SP1-FRC-2	8.00		10.00		22.00	
SP1-FRC-3	13.00		15.00		17.00	
SP2-NC-5	20.00	16.00	21.00	15.67	29.00	28.00
SP2-NC-6	16.00		15.00		31.00	
SP2-NC-7	12.00		11.00		24.00	
SP2-CI-5	20.00	14.33	18.00	13.67	30.00	22.00
SP2-CI-6	12.00		13.00		19.00	
SP2-CI-7	11.00		10.00		17.00	
SP2-FRC-5	13.00	11.67	14.00	11.00	21.00	20.33
SP2-FRC-6	12.00		10.00		19.00	
SP2-FRC-7	10.00		9.00		21.00	
SP3-NC-9	15.00	18.00	18.00	17.67	33.00	34.67
SP3-NC-10	19.00		17.00		44.00	
SP3-NC-11	20.00		18.00		27.00	
SP3-CI-9	18.00	21.00	17.00	21.00	24.00	30.33
SP3-CI-10	19.00		21.00		30.00	
SP3-CI-11	26.00		25.00		37.00	
SP3-FRC-9	14.00	13.00	15.00	13.33	35.00	31.00
SP3-FRC-10	10.00		9.00		27.00	
SP3-FRC-11	15.00		16.00		31.00	

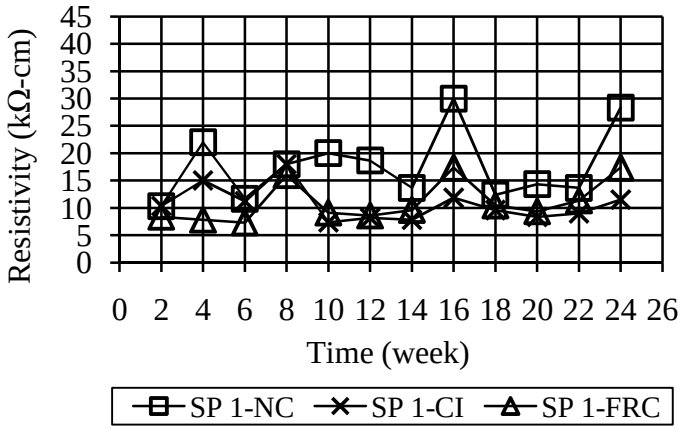

1. 1.5 in. side edge distance

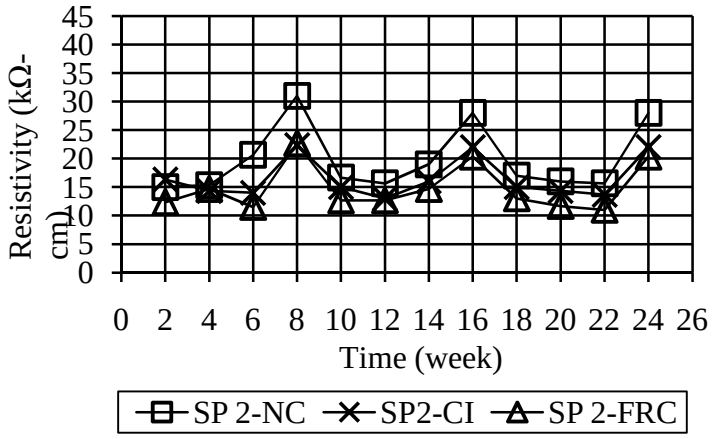

2. 2.5 in. side edge distance

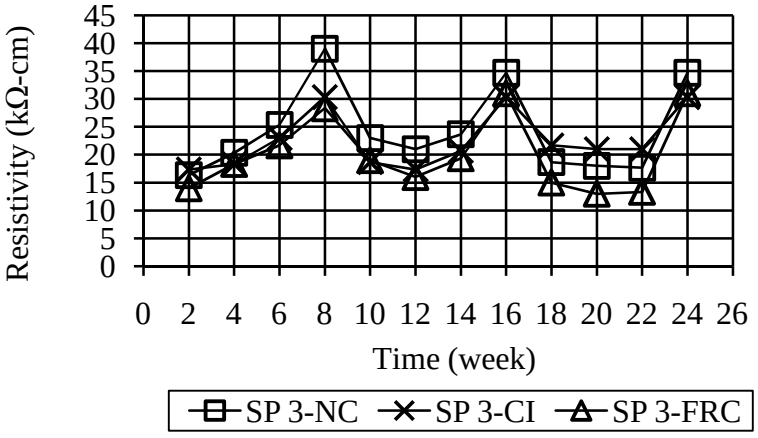

c. 3.5 in. side edge distance

Figure D.1. Electrical resistivity vs. time curve for specimens with different side edge distances

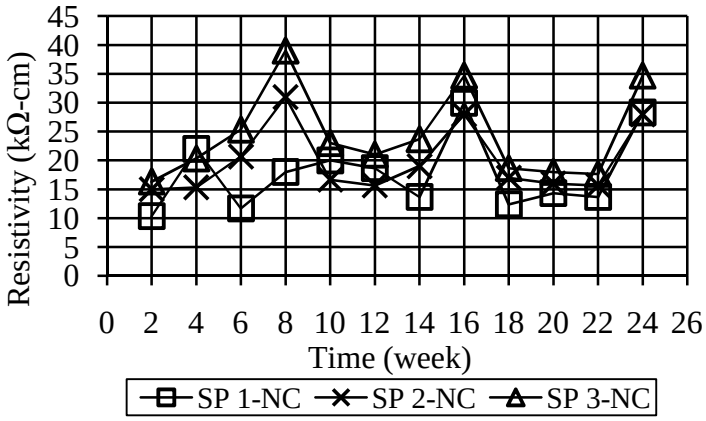

1. Normal Concrete

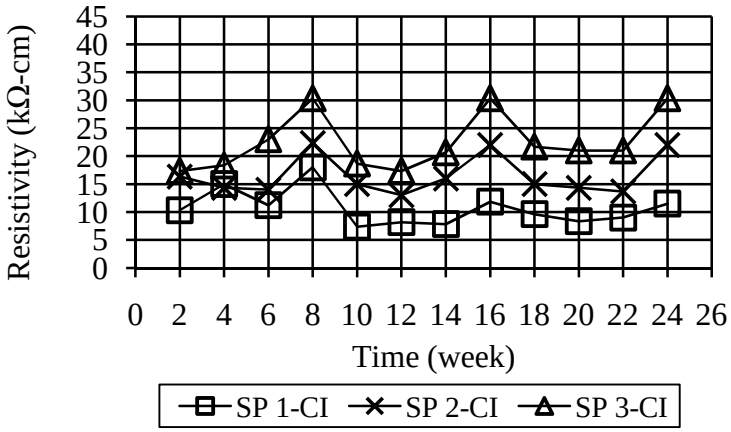

2. Concrete with Corrosion Inhibitor

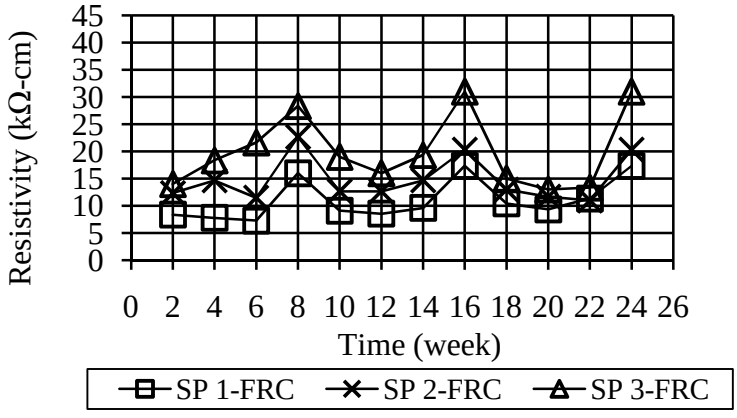

3. Concrete with Fibers

Figure D.2. Electrical Resistivity vs. Time Curve for Specimens with different Concrete Materials

BIBLIOGRAPHY

ACI Committee 222, 2001. “Protection of metals in concrete against corrosion (ACI 222R),” *Guide*, American Concrete Institute, September.

ACI Committee 549, 2004. “Report on Thin Reinforced Cementitious Products (ACI 549.2R),” *Guide*, American Concrete Institute, May.

American Standard Test Method (ASTM) G 1, 2003. “Standard Practice for Preparing, Cleaning, and Evaluating Corrosion Test Specimens,” *Standard*, ASTM International, West Conshohocken, PA.

American Standard Test Method (ASTM) C 1218, 2008. “Standard Test Method for Water-Soluble Chloride in Mortar and Concrete,” *Standard*, ASTM International, West Conshohocken, PA.

American Standard Test Method (ASTM) C 876, 2009. “Standard Test Method for Corrosion Potentials of Uncoated Reinforcing Steel in Concrete,” *Standard*, ASTM International, West Conshohocken, PA.

American Standard Test Method (ASTM) C 1152, 2004. “Standard Test Method for Acid-Soluble Chloride in Mortar and Concrete,” *Standard*, ASTM International, West Conshohocken, PA.

American Standard Test Method (ASTM) G 109, 2007. “Standard Test Method for Determining Effects of Chemical Admixtures on Corrosion of Embedded Steel Reinforcement in Concrete Exposed to Chloride Environments,” *Standard*, ASTM International, West Conshohocken, PA.

American Standard Test Method (ASTM) A 416, 2010. “Standard Specification for Steel Strand, Uncoated Seven-Wire for Prestressed Concrete,” *Standard*, ASTM International, West Conshohocken, PA.

Bazant, Z. P., 1979, “Physical Model for Steel Corrosion in Concrete Sea Structures-Theory,” Journal of the Structural division, American Society of Civil Engineers, Volume. 105, No. 6, pp. 1137–1153.

Barneyback, R. S., and Diamand S., 1981, “Expression and Analysis of Pore Fluids from Harden Cement Pastes and Mortars,” Cement Concrete Research, volume.11.

Bhaskara, M.V., and Maheshwari, R. K., 1987, “A Review of the Investigation and Evaluation of Corrosion in Concrete Structures,” Indian Highways, pp. 22-33.

Byfors, K., Hansson, C. M., and Tritthart, J., 1986, “Pore Solution Expression as a Method to Determine the Influence of Mineral Additives on Chloride Binding,” Cement and Concrete Research, volume. 16, pp. 760-770.

Cady, P.D., and Gannon, E.J., 1992, “Condition Evaluation of Concrete Bridges Relative to Reinforcement Corrosion,” Volume 8: Procedural Manual, Strategic Highway Research Program SHRP-S/FR-92-110, National Research Council, Washington, DC.

Cady, P.D., and Weyers, R.E., 1983, “Chloride Penetration and the Deterioration of Concrete Bridge Decks,” Cement, Concrete and Aggregates, volume. 5, No. 2, pp. 81-87.

Canadian Standards Association, 1994, “Design of concrete structures,” Rexadle, ON, Canada, A23.3-94.

EI Maaddawy, T., Soudki, K., 2003, “Effectiveness of Impressed Current Technique ot Simulate Corrosion of Steel Reinforcement in Concrete,” Journal of Materials in Civil Enginerring, pp.41-47.

EI Maaddawy, T., Soudki, K., 2007, “A model for prediction of time from corrosion initiation to corrosion cracking,” Cement and Concrete Composites Volume 29, Issue 3, pp.168-175.

Hamid, A., 2004, “A TEM Study of the Oxide Scale Development in Ni-Cr Alloys,” Anti-Corrosion Methods and Materials, Volume. 51, Issue. 3, pp. 216 – 222.

Jones, and Denny, A., 1992, “Principles and Prevention of Corrosion,” Macmillan Publishing Company, New York, NY.

K.C. Clear, 1989, "Measuring Rate of Corrosion of Steel in Field Concrete Structures," Transportation Research Record, pp.2-20.

Klieger, Paul, Joseph F. Lamond (Eds.), 1994, “Significance of Tests and Properties of Concrete and Concrete-Making Materials,” ASTM STP 169C.

Liu, Y., 1996, “Modeling the time-to-corrosion cracking in chloride contaminated reinforced concrete structures,” Ph.D thesis, Virginia Polytechnic Institute and State University.

Mehta, P. K., 1993, "Concrete Structure, Properties, and Materials," Prentice-Hall, Inc., Englewood Cliffs, N.J. 07632.

Mehta, P. K., 1984, “Mineral Admixtures,” Concrete Admixtures Handbook, Properties Science and Technology, Ed. V.S. Ramachandran.

Mehta, P. K., and Manmohan D., 1980, Proceedings of the 7th International Congress on Chemistry of Cement, Paris.

Missouri Department of Transportation (MoDOT), 2004, "2004 Missouri Standard Specification Book for Highway Construction," Missouri Department of Transportation, Jefferson City, MO.

Morinaga, S., 1988, "Prediction of service lives of reinforced concrete buildings based on rate of corrosion of reinforcing steel," Report No. 23, Shimizu Corp., Japan, 82.

Tuutti K., 1980, "Service life of structures with regard to corrosion of embedded steel," ACI Volume. 65, pp. 223–236.

Newhouse, Charles D., 1993, "Corrosion Rates and the Time to Cracking of Chloride Contaminated Reinforced Concrete Bridge Components," M.S. Thesis, Virginia Polytechnic Institute and State University.

NRMCA, 1994, "Synthetic Fibers in Concrete," Concrete in practice (CIP)-24, National Ready Mixed Concrete Association, 900 Spring Street, Silver Spring, MD

Proceo SA, 2007, "Canin+ Corrosion analyzing instrument for the measurement of corrosion potential and electrical resistivity operating instruction."

Smith, J.L., and Virmani, Y.P., 2000, "Materials and Methods for Corrosion Control of Reinforced and Prestressed Concrete Structures in New Construction," FHWA Report No. 00-081, Federal Highway Administration, Virginia, pp.82.

Sneed, L., Belarbi, A., and You, Y., 2010, "Spalling Solution of Precast-Prestressed Bridge Deck Panels," Report for Missouri Department of Tranportation, pp.108.

Sohanghpurwala, A.A, 2006, "Manual on Service Life of Corrosion-Damaged Reinforced Concrete Bridge Superstructure Elements," NCHRP Report 558, National Cooperative Highway Research Program, Washington D.C., pp.72.

Sorensen, Birgit, "Penetration Rate of Chloride in Marine Concrete Structures," Nordic Concrete Research, n. 1, December 1982, pp.24.1-24.18.

Stern, M., and Geary A. L., 1957, "Electrochemical Polarization No. 1: Theoretical Analysis of the Shape of Polarization Curve," Journal of Electrochemical Society, volume. 104, pp.56- 63.

Thoft-Christensen, P., 2000, "Stochastic modelling of the crack initiation time for reinforced concrete structures," ASCE Structures Congress, Philadelphia, pp. 8.

Weyers,R. 1998, "Service life model for concrete structures in chloride laden environments," ACI Vol. 95, Issue 4, pp. 445–53.

Zemajtis, J., 1998, “Modeling the Time to Corrosion Initiation for Concretes with Mineral Admixtures and/or Corrosion Inhibitors in Chloride-Laden Environments,” Ph.D. Thesis, Civil Engineering Department, Virginia Polytechnic Institute and State University.

VITA

Dayi Zhang graduated from Zhengzhou No.1 High School located in Zhengzhou, Henan, in June 2005. Following high school, he attended Tianjin Institute of Urban Construction for four years and obtained his Bachelor of Science in Civil Engineering.

Immediately following his undergraduate studies, Dayi continued his education at Missouri University of Science and Technology attaining his Master of Science in Civil Engineering with an emphasis in structural engineering in August 2011.